

MASTER

Damping in high-rise : Verification of the energy flow analysis method as identification tool for damping in high-rise buildings

Talib, I.

Award date:
2019

[Link to publication](#)

Disclaimer

This document contains a student thesis (bachelor's or master's), as authored by a student at Eindhoven University of Technology. Student theses are made available in the TU/e repository upon obtaining the required degree. The grade received is not published on the document as presented in the repository. The required complexity or quality of research of student theses may vary by program, and the required minimum study period may vary in duration.

General rights

Copyright and moral rights for the publications made accessible in the public portal are retained by the authors and/or other copyright owners and it is a condition of accessing publications that users recognise and abide by the legal requirements associated with these rights.

- Users may download and print one copy of any publication from the public portal for the purpose of private study or research.
- You may not further distribute the material or use it for any profit-making activity or commercial gain

DAMPING IN HIGH-RISE.

Verification of the energy flow analysis as identification
tool for damping in High-Rise Buildings



Master Thesis Report

Verification of the energy flow analysis method as identification tool for damping in High-Rise Buildings

By
Ikram Talib

Master Thesis Report for the final graduation project of the Master variant Structural Design of the master 'Architecture, Building and Planning' at Eindhoven University of Technology

26th April 2019

Graduation committee:

First faculty supervisor prof.dr.ir. A.S.J. Suiker TU Eindhoven, Structural Design
Applied Mechanics and Design

Second faculty supervisor prof.ir. S.N.M. Wijte TU Eindhoven, Structural Design
Sustainment of Concrete Structures

Daily supervisor: ir. A.J. Bronkhorst TNO Delft, Structural Dynamics

Supervisor: ir. J.P. Pruiksma TNO Delft, Structural Dynamics

Cover: This photo captures the content of this thesis; a verification of a new method as identification tool for soil damping for high-rise buildings on typical Dutch soil. Akkerdijksche polder. (photo: Jan Parie)

“In every branch of knowledge the progress is proportional to the amount of facts on which to build, and therefore to the facility of obtaining data.” ~ James Clerk Maxwell

Preface

This thesis has been written as a final work in partial fulfilment for the degree of Master of Science for the master Architecture, Building and Planning and specialization in Structural Design at the Eindhoven University of Technology. The subject of this research was formed in cooperation with TNO, the Dutch Organisation for applied scientific research, and specifically the department of Structural Dynamics in Delft.

I would like to thank my graduation committee for their guidance and support throughout the development of my research. I am very grateful for the guidance I received from Akke Suiker. His knowledge, encouragement and motivation were incredibly helpful during this research. Special thanks goes to Okke Bronkhorst for his critical view and for providing me with helpful remarks on my thesis on more than one occasion. I would also like to thank Jitse Pruiksmá for helping me get familiar with Python and the subject of damping and soil-structure interaction. Simon Wijte for pushing me in the right direction towards the chair '*Applied Mechanics*' and a collaboration with TNO that resulted in a very special and unique adventure.

Furthermore, I would like to take this opportunity to express my sincere gratitude to Sergio Sánchez Gómez for supporting me with his knowledge on Structural Dynamics and especially Thermodynamics. Special thanks goes to Johan Kraus, not only for his technical help but also for being a friend during the tough moments. I am grateful for the colleagues and fellow interns at TNO for their cooperative attitude and the many informative and enjoyable conversations we had. Pim Peters, even though he was not part of this work, he was the one who first awakened my interest for research in this topic and encouraged me to take this path. Bart Leclercq, Andy Mak and Andy Davids from Aurecon in Dubai, for inviting me and inspiring me with their endless energy and passion for tall buildings.

Lastly, I would like to thank my friends and family for their support throughout my studies, and especially this last year. It has been a very inspiring year in which I have been working on an interesting subject with pride and dedication.

Towards an accurate identification of damping in high-rise buildings!

Ikram Talib
Utrecht, April 2019

Abstract

High-rise buildings are becoming more slender and lighter, which makes them more sensitive to wind induced vibrations. These vibrations can be uncomfortable for people in the building, and in the worst case can cause motion sickness and anxiety. Damping is an important parameter in the calculation of vibrations in high-rise buildings. Current damping measurement methods only determine the overall damping of a structure. Little is known about the damping contribution of the different parts of a high-rise building, such as the contribution of the foundation or the main load-bearing structure.

Recently, an Energy Flow Analysis (EFA) technique was developed in the field of structural analysis, which allows for the determination of the damping contribution of different parts of a structure. The EFA is an energy-based approach and computes the energy flow through a system. The first results of this technique are promising and indicate the potential of EFA for the identification of damping.

However, the damping values obtained with the EFA technique applied on a high-rise building were based on a relatively small set of sensor positions and limited information on the wind loading. To what extent this lack of information influences the accuracy of the damping prediction with the EFA technique is unknown. Without information on these uncertainties, the reliability of the outcome of in-situ measurements is low. Before the EFA based measurement technique can be applied successfully in future monitoring and measurement campaigns, the uncertainties in this technique need to be assessed.

The objective of this research is to assess the influence of the lack of information on the accuracy of the soil damping prediction of a high-rise building with the EFA technique. The focus of this study lies on the influence of a lack of data on the dynamic behaviour of the building and the wind load. To eliminate experiment-related uncertainties, the study is performed in a controlled FEM environment. Several cases were investigated to gain insight in the EFA method and quantify the influences of different parameters. For every case the applied soil damping value in FEM and the identified damping value due to the energy method were compared.

From the study it can be concluded that the EFA allows for an accurate identification of energy dissipation by using all data needed for the EFA method. For the quantification of two damping mechanism with the EFA technique, an accurate determination of the energy flux is needed. The energy flux describes the amount of energy that flows from the building towards the foundation. The interaction between soil and structure energy dissipation can be better understood by a better qualification of the structure damping.

The approach of including analytical expressions for the mode shape does give information about the dynamic behaviour of the building, but this precise determination is not needed for identification of the soil energy dissipation. Determining the energy balance at the bottom of the building resulted in an accurate identification of the soil damper value. Solving the energy balance in the bottom part of the building is possible if the curvature, rotational velocity at the base and the soil stiffness are determined well. However, validation of these parameters can be done by determining the mode shapes belonging to the dynamic behaviour of the building.

This research has shown that with a realistic wind load the EFA allows for an accurate identification of the soil energy dissipation. Reducing the amount of wind data has shown that applying the EFA method to identify the soil energy dissipation, an accurate knowledge of the wind load distribution over the building is not directly needed. The amount of energy that flows towards the soil is taken into account by the energy flux which implicitly involves the load that acts on the building. However, the distribution of the wind load is needed for accurately knowing what the structural energy dissipation distribution is in the building.

Contents

PREFACE	3
ABSTRACT	4
CONTENTS.....	5
SYMBOLS AND ABBREVIATIONS	7
1 INTRODUCTION.....	9
1.1 RELEVANCE OF HIGH-RISE BUILDINGS.....	9
1.2 DAMPING IN HIGH-RISE BUILDINGS	11
1.3 STATE OF THE ART - DAMPING PREDICTORS FOR HIGH-RISE BUILDINGS	12
1.4 DAMPING MEASUREMENT TECHNIQUES	17
1.5 STRUCTURAL DYNAMICS.....	20
1.6 ENERGY FLOW ANALYSIS.....	29
1.7 FORMULATION OF THE PROBLEM	35
1.8 RESEARCH OBJECTIVE.....	35
2 METHODOLOGY	36
2.1 INTRODUCTION	36
2.2 RESEARCH FOCUS.....	36
2.3 RESEARCH STRATEGY.....	38
2.4 RESEARCH LIMITATIONS	42
2.5 CASE STUDIES	42
3 WIND LOAD.....	49
3.1 INTRODUCTION	49
3.2 WIND LOADING CHAIN.....	49
3.3 DETERMINATION OF THE BASIC WIND VELOCITY.....	53
3.4 DETERMINATION OF THE MEAN WIND VELOCITY.....	54
3.5 DETERMINATION OF THE FULL SCALE PRESSURE BY USING WIND TUNNEL MEASUREMENT DATA.....	55
4 BUILDING CASE AND FEM MODELLING	60
4.1 INTRODUCTION – NEW ERASMUS MEDICAL CENTRE.....	60
4.2 FINITE ELEMENT MODELLING.....	61
4.3 DETERMINATION OF THE FOUNDATION PROPERTIES	63
4.4 DETERMINATION OF BEAM MODEL	64
4.5 STRUCTURAL VERSUS SOIL DAMPING	65
4.6 MESH SENSITIVITY STUDY	68
4.7 SENSITIVITY ANALYSIS ROTATIONAL SOIL STIFFNESS VERSUS BUILDING STIFFNESS	69
5 RESULTS AND DISCUSSION	71
5.1 CASE 1 - ONLY SOIL DAMPING	72
5.2 CASE 2 - SOIL AND STRUCTURAL DAMPING	81
5.3 CASE 3 - ONLY SOIL DAMPING - REDUCED NODE INFORMATION	92
5.4 CASE 4 – ONLY SOIL DAMPING WITH WIND LOAD	99
5.5 CASE 5 - STRUCTURAL AND SOIL DAMPING WITH WIND LOAD.....	108
5.6 CASE 6 – REDUCED WIND INFORMATION WITH ONLY SOIL DAMPING	119
5.7 OVERVIEW RESULTS	125
6 CONCLUSIONS	126
6.1 ASSESSMENT OF THE ACCURACY OF THE EFA METHOD	126
6.2 ASSESSMENT OF THE INFLUENCE OF LACK OF INFORMATION DUE TO LIMITED SENSOR POSITIONS.....	128

6.3	ASSESSMENT OF THE INFLUENCE OF LACK OF INFORMATION ON THE WIND LOAD	129
7	RECOMMENDATIONS	130
8	BIBLIOGRAPHY	131
APPENDIX A.....		134
	DETERMINE NATURAL FREQUENCIES AND MODE SHAPES OF CONTINUOUS MODEL FOR A FLEXIBLE SYSTEM	134
APPENDIX B.....		137
	WIND LOAD.....	137
APPENDIX C.....		141
	RESULTS CASE 2 – IDENTIFICATION OF SOIL DAMPING IN FREQUENCY DOMAIN	141

Symbols and abbreviations

List of Latin symbols

Sign	Description	unit
A	Area	m^2
C_r	Rotational damping value	Nms/rad
E	Young's modulus	N/m^2
$E(t)$	Energy change obtained by the summation of the potential and kinetic energy	Nm
I	Area moment of inertia	m^4
M	Base bending moment over time	Nm/s
Q	Base shear force	
$S(x, t)$	Energy flux [power]	J/s
$w_{ext}(t)$	Rate of power introduced by the wind over length of building	J/s
$w_{diss}(t)$	Rate of dissipated power	J/s
c_p	Pressure coefficient	
h	Height	m
k_r	Rotational spring stiffness	Nm/rad
l	Length	m
$v_{ref, h}$	Wind velocity at reference height	m/s
z_0	Roughness length in full scale	

$$1 \text{ Nm/s} = 1 \text{ J/s}$$

$w(x, t)$	Displacement over time	m
$\frac{\partial w(x, t)}{\partial x}$	Rotational displacement: first derivative over space	rad
$\frac{\partial^2 w(x, t)}{\partial x^2}$	Curvature: second derivative over space	m^{-1}
$\frac{\partial w(x, t)}{\partial t}$	Velocity: first derivative over time	m/s
$\frac{\partial^2 w(x, t)}{\partial t^2}$	Acceleration: second derivative over time	m/s^2
$\frac{\partial^2 w(x, t)}{\partial x \partial t}$	Rotational velocity: first derivative over space and time	rad/s

List of Greek symbols

Sign	Description	unit
α	Mass proportional constant to achieve desired damping ratio by using Rayleigh damping	
β	Stiffness proportional constant to achieve desired damping ratio by using Rayleigh damping	
δ	Logarithmic decrement of damping	
ζ_n	Damping as a fraction of the critical damping	
ν	Poisson's ratio	
ρ	Mass density	kg/m ³
ρ_{air}	Air density	kg/m ³
ω_n	The circular frequency	rad/s

List of abbreviations

Abbreviation	Description
ABL	Atmospheric boundary layer
EFA	Energy flow analysis
FEM	Finite element method

1 Introduction

1.1 Relevance of High-rise buildings

Humans have always attempted to build higher and higher. In the Bible a story of the Tower of Babylon is told, the Egyptians created the pyramids, the Muslims built minarets and the Mayans built the temples of Tikal, see Figure 1. The motivation behind their construction was primarily for creating monumental rather than human habitats.



Figure 1 - Example of a couple of building in history.

The constructing philosophy has changed tremendously over the years. Contemporary high-rise buildings are nowadays a response to the demand of commercial activities and they often form distinctive landmarks in the cities centres as prestige symbols for corporate organizations. Figure 2 shows the tallest buildings at the moment. The tallest building in the world is the Burj Khalifa 828m in Dubai followed by the Shanghai tower in Shanghai with a height of 632m.

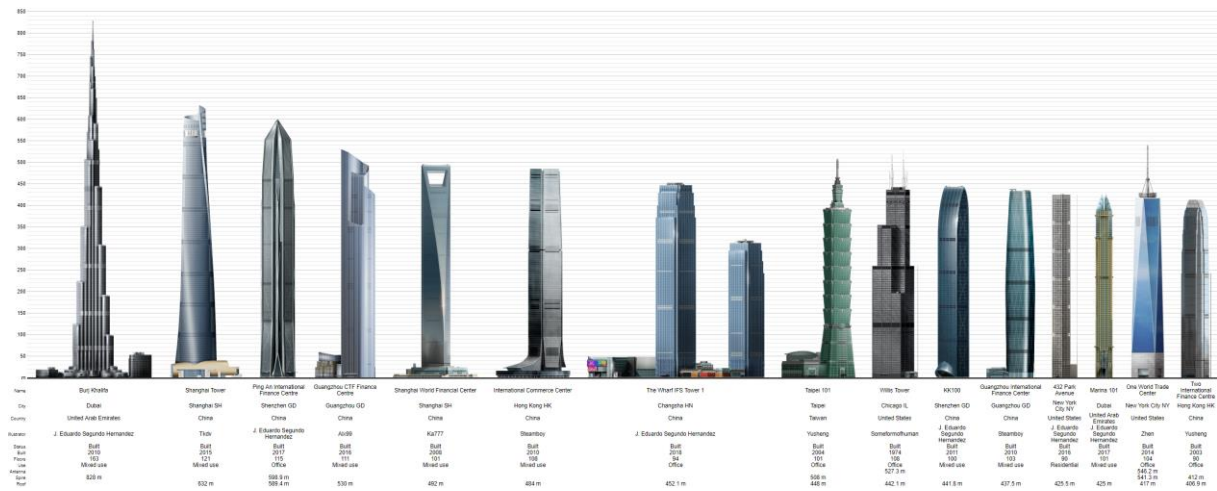


Figure 2- Timeline of highest buildings in the world [Skyscraperpage,2019]

High rise buildings in the Netherlands have currently a maximum height of approximately 160 m, as shown in Figure 3. The Dutch government has published its vision on the development of the Randstad region in the Netherlands in 2040 [1]. A solution to accommodate 500.000 new dwellings in 2040 is to increase the density of the urban areas. High-rise buildings can give an interesting and inspiring interpretation to urban densification. The government, real estate developers and engineers are therefore challenged by this new perspective.

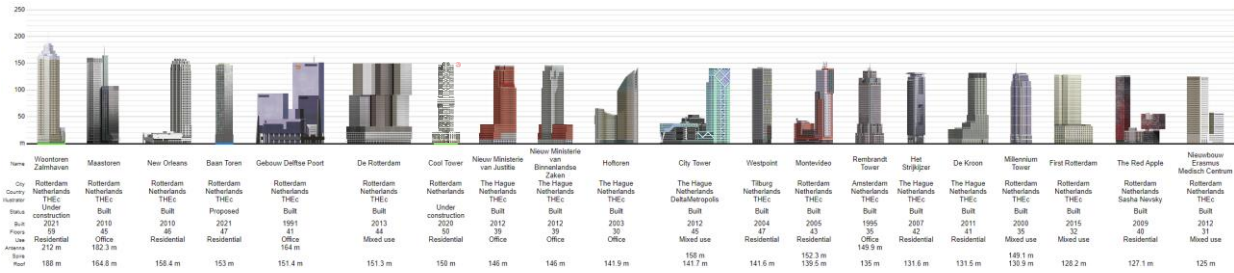


Figure 3 - Tallest 20 buildings in the Netherlands. The Zalmhaventoren (212m) is the tallest building under construction in the Netherlands. [skyscraperpage,2019]

The large increase in height make buildings more sensitive to dynamic loads such as wind. Strong wind gusts make tall buildings oscillate. This phenomenon is commonly referred to as wind-induced vibrations. These vibrations can be uncomfortable for people in the building, and in the worst case can cause motion sickness and anxiety. The building parameters that affect the vibrations are the mass of the building, the stiffness of the building and the damping. The mass and stiffness of the building determine its natural frequency. If the wind loading on a building matches the natural frequency of the building, resonance will occur. Damping is the most important factor to reduce the amplitude of vibration at resonance, see Figure 4. Buildings are generally light damped structures. Damping has as a positive influence on vibrations, hence structural designers would like to design buildings with enough damping to limit the amplitude of wind-induced vibrations. But damping in high-rise buildings is a complex phenomenon. Where stiffness and mass can be determined quite accurately during the design phase of a building, particularly by using FEM programs, is it for damping not yet possible to give an accurate prediction in the design phase.

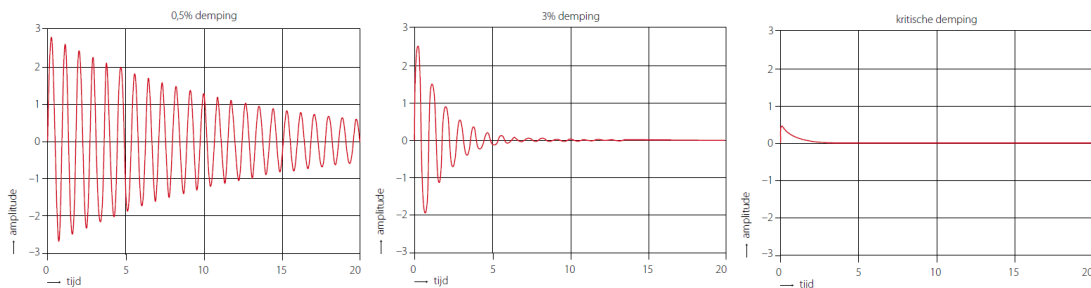


Figure 4 - Free vibration: underdamped, overdamped and critical damped [2]

1.2 Damping in High-Rise Buildings

Energy dissipation sources in buildings may be governed by one or more damping mechanisms as shown in Figure 5. The main load bearing structure (MLBS) dissipates energy at material level caused by the deformation of the material. The same behaviour is expected from the non-structural elements (NSE) and joints, at low vibrations amplitudes these elements help to dissipate energy in the structure by simple deformation. However when vibration amplitudes are sufficiently large non-linear behaviour caused by friction between surfaces is expected. In the soil-structure interaction (SSI), two main mechanisms of energy dissipation can be distinguished. The wave radiation, where waves travel from the building to the soil, and the material damping, which consists of dissipating energy from the friction between the soil particles. The aerodynamic damping (Aero) is introduced by the wind surrounding the structure.

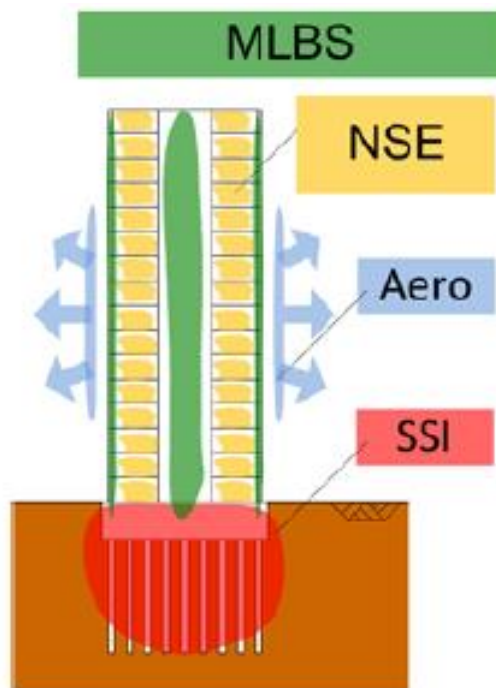


Figure 5 - Energy dissipation in buildings [3]

1.3 State of the art - Damping predictors for High-rise buildings

In this section methods to prescribe damping values to buildings in the design stage are presented. A brief description of the background of these models is given. This section finishes with a comparison of the damping predictor models with measurements on Dutch buildings performed by TNO.

1.3.1 Eurocode and NEN6702

The damping values that are made available in European building code EN 1991-1-4 [4] are obtained by field experiments on high-rise buildings, mostly foreign buildings. The values given are independent on building method, the soil properties, slenderness ratio of the building and the amount of material used. The Eurocode prescribes the logarithmic decrement as:

$$\delta = \delta_s + \delta_a + \delta_d \quad (1.1)$$

The logarithmic decrement of damping is estimated by the summation of the structural damping δ_s , the aerodynamic damping δ_a and the additional damping due to tuned mass dampers and other special devices δ_d . The approximated values for the structural damping are given for the first fundamental mode, dependent on construction material and construction type as shown in Table 1.

Structural type	structural damping, δ_s
reinforced concrete buildings	0,10
steel buildings	0,05
mixed structures concrete + steel	0,08
reinforced concrete towers and chimneys	0,03

Table 1 - Logarithmic decrement according to EN 1991-1-4

The Dutch guideline NEN6702 [5] also gives values for damping in terms of percentage of critical damping D. The following values are given:

0.01	For steel structures
0.02	For concrete structures
0.05	For timber structures

Table 2 - critical damping D values from NEN6702

The relation between δ and D is given by:

$$\delta = 2\pi D \quad (1.2)$$

1.3.2 Empirical estimator for damping by Jeary

Jeary has developed an empirical formula based on observed damping values for reinforced concrete buildings in Great Britain [6] [7] [8]. Figure 6 shows the relation between the damping ratio and the amplitude of response of the measurements. Jeary distinguished three regions: the 0-amplitude plateau region, the non-linear region and the High amplitude region as can be seen in Figure 6.

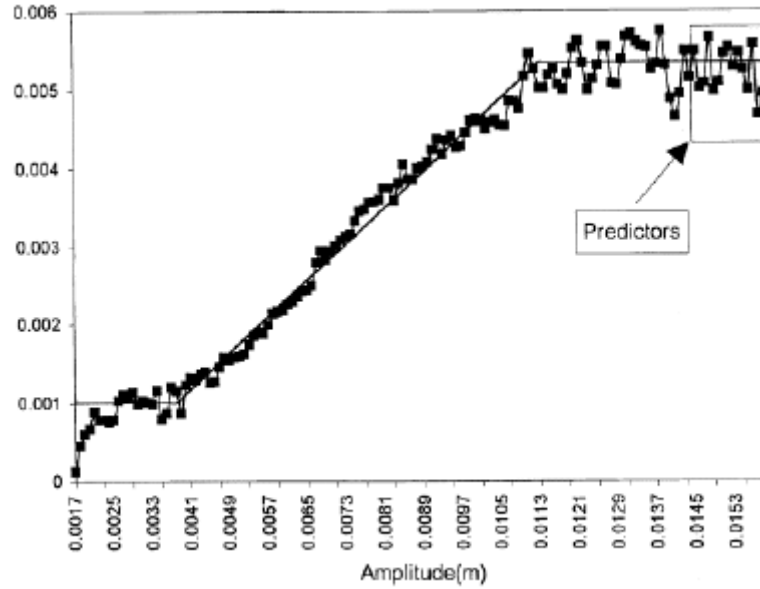


Figure 6 - Results of forced vibration test by Jeary. Lower and higher amplitude plateau according to Jeary. [9]

Jeary describes damping by two damping regimes:

- 0-amplitude regime (ξ_0); According to Jeary, damping is constant for very low amplitudes of vibration. Jeary states that the damping at low amplitudes are caused by the construction material, given that the material behaves elastically within this amplitude regime. The dissipated energy is caused by the strain in the material and an interesting relation is made with the fundamental frequency. Jeary used the empirical formula derived by Ellis [10] for estimating the natural frequency and describes the 0-amplitude regime as:

$$\xi_0 = f_n = 0.01 \frac{46}{H} \quad (1.3)$$

- Amplitude-dependent regime (ξ_I); Jeary defines the amplitude-dependent regime as the non-linear region caused by formation and rapid elongation of the micro-cracks in the material. the work done in elongating represents energy dissipation. Therefore this area involves friction damping.

The damping predictors develop by Jeary is described as:

$$\xi_{Jeary} = \xi_0 + \xi_I = 0.01 f_n + 10 \frac{\sqrt{D}}{2} \frac{x}{H} \quad (1.4)$$

Jeary states that in the high amplitude plateau all possible mechanisms are activated and even for increasing amplitudes the energy dissipation remains constant. Friction is assumed to be the dominant mechanism in this regime and suggests that in very high amplitude response “smoothing” of rubbing surfaces will eventually lead to a reduction in damping.

1.3.3 Empirical estimators for damping by Tamura et al.

In 2003 Sakate and Tamura et al. proposed a damping predictor based on full-scale data of buildings in Japan in the small amplitude region [11]. Sakate and Tamura et al. have investigated several building types (such as reinforced concrete(RC), steel-framed and steel-framed reinforced concrete(SRC)) and the influence of foundation type/depth on the damping ratio, see Figure 7 and Figure 8.

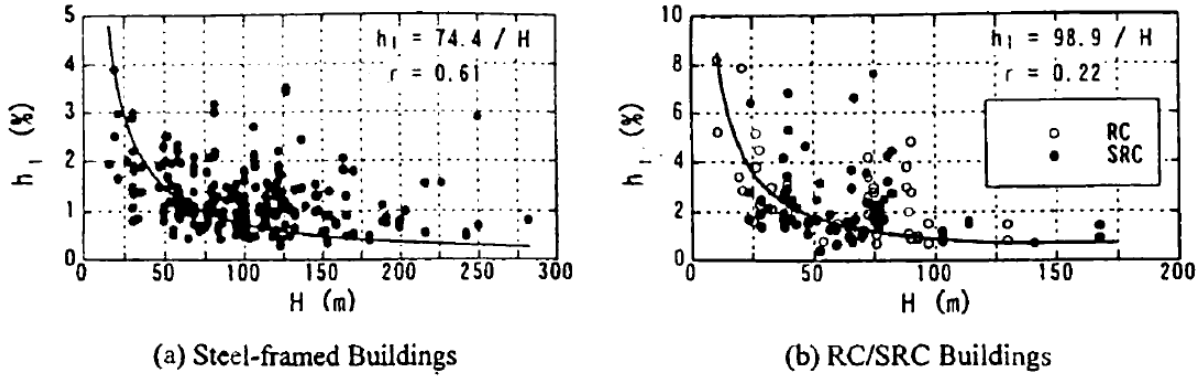


Figure 7 – Damping ratio h_1 in the translational first-mode for steel and concrete buildings related to building height H [11]

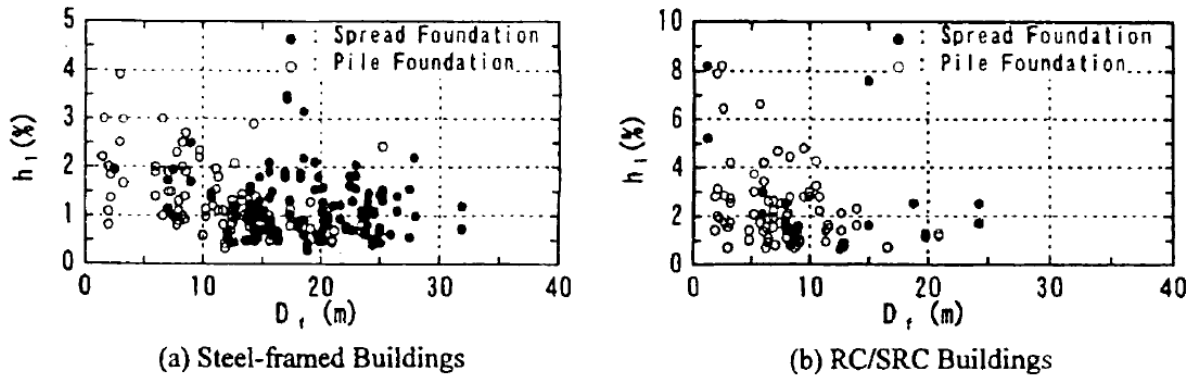


Figure 8 - Damping ratio h_1 in the translational first-mode for steel and concrete buildings related to foundation depth D_f [11]

The damping predictor developed by Tamura are described as:

$$\xi_{Tamura} = 0.014 f_n + 470 \frac{x}{H} - 0.0018 \quad \text{for RC buildings} \quad (1.5)$$

$$\xi_{Tamura} = 0.013 f_n + 400 \frac{x}{H} - 0.0029 \quad \text{for steel-framed buildings} \quad (1.6)$$

Figure 9 the fundamental natural period T_1 is plotted against the damping ratio and a comparison is made between the proposed model and the measured damping values. It can be noticed that a large scatter is found between the proposed model and the measurements. However, it is questionable if the buildings with a low period ($T < 3$ s) can be considered as slender building that are sensitive to dynamic loads such as wind.

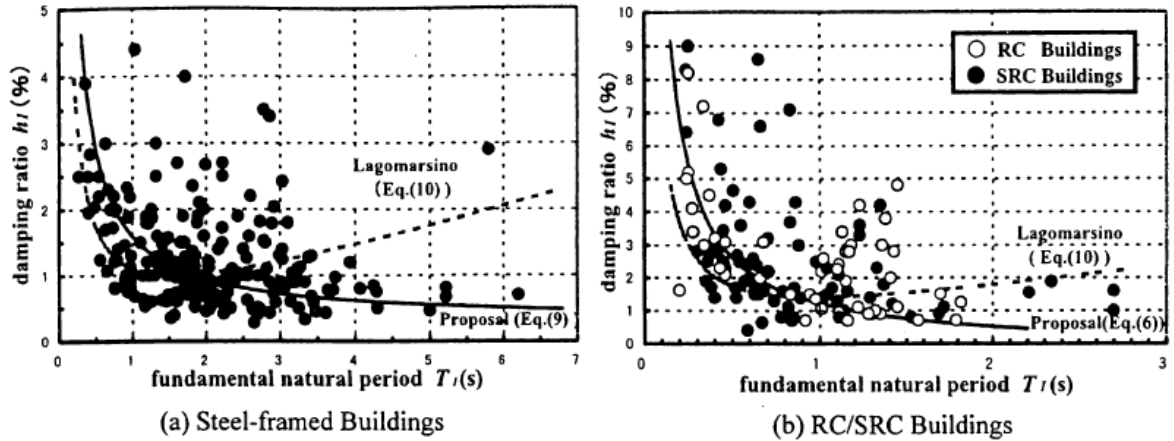


Figure 9 - Comparison of full-scale damping ratios in Japanese database and proposed predictor, and Lagomarsino's predictor

1.3.4 Empirical estimators for damping by Lagomarsino

Lagomarsino collected data from full-scale tests on 185 buildings. For ductile materials, the material damping seems to be principally due to viscous phenomena. Lagomarsino states that for brittle materials, which have a microstructure with cracks, the stresses are caused both deformations and sliding between the crack faces. Lagomarsino's predictor describes Rayleigh damping and does not depend on the vibration amplitude:

$$\xi_{Lago} = \alpha f_n + \frac{\beta}{f_n} \quad (1.7)$$

Where f_n is the fundamental frequency (Hz), α and β are material-dependent constants:

$$\alpha = 0.0072, \beta = 0.0070 \quad \text{for reinforced concrete buildings} \quad (1.8)$$

$$\alpha = 0.0032, \beta = 0.0078 \quad \text{for steel-framed buildings} \quad (1.9)$$

1.3.5 Comparison of the empirical estimators for damping

TNO has obtained measurements on Dutch high-rise buildings [12]. Figure 10 shows damping ratio values of 12 Dutch high-rise buildings obtained with measurements and the damping estimators. The first 8 buildings have a concrete structure, the Montevideo and EWI faculty have a mixed structure, and the Kennedytoren and La Fenetre have a steel structure. The height of the load-bearing part of the building structure is specified between brackets excl. antennas or masts.

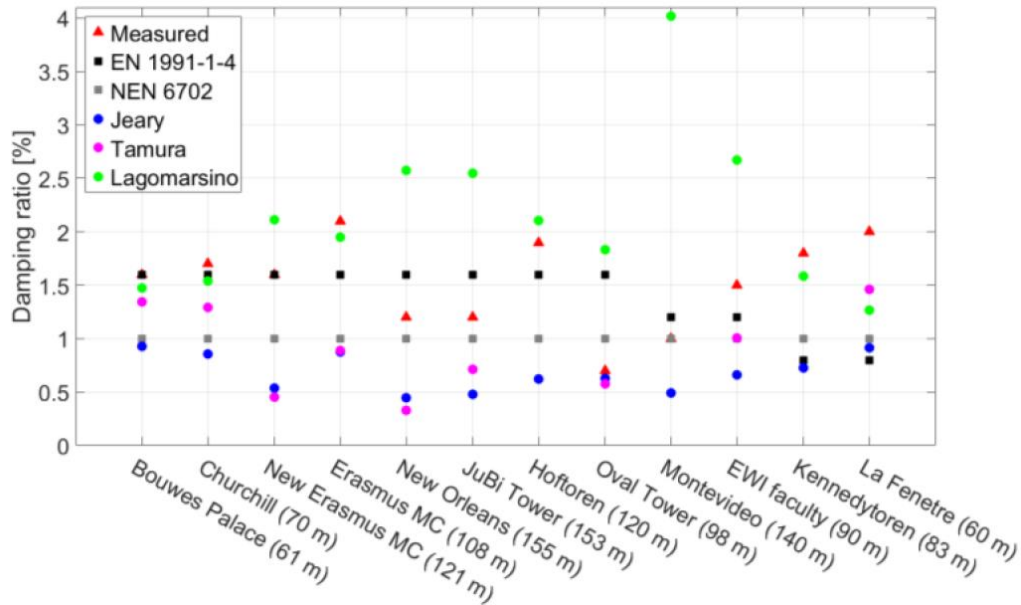


Figure 10 - Predicted and measured damping for 12 high-rise buildings in the Netherlands. [12]

The figure shows a large variation between the measured and predicted values. For 4 cases the values derived with the Eurocode seems to be larger than the measured values. The separation of materials, which is made by the Eurocode, Tamura and Lagomarsino is not clearly recognizable by the measured damping values.

Part of the research of TNO on damping in high-rise buildings, is carried out by PhD-student, Sergio Sanchez Gomez, at TU Delft. Gomez [3] showed that the Dutch soil conditions are such that the foundation plays a large role in the total damping. The current damping formulas do not take this into account, since they are based on measurements on foreign buildings with generally stiffer soil conditions than in the Netherlands. In order to validate this statement based on theoretical data, measurements on Dutch high-rise buildings need to be performed. A sufficient measurement technique that makes it possible to identify the damping due to the Dutch soil conditions is needed. In section 1.5 the Energy flow analysis is discussed which enables the separation of multiple damping mechanisms in buildings. In the next section, common used measurement techniques to identify damping in buildings are discussed.

1.4 Damping measurement techniques

In this section the principles of the common used damping identification techniques are given. Starting with the logarithmic decrement method, followed by the half power band with method and the random decrement method.

1.4.1 Logarithmic decrement method

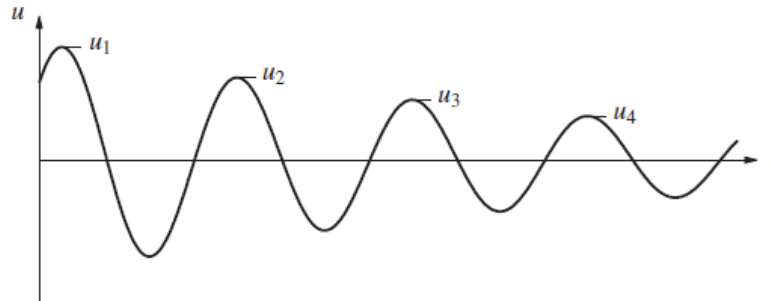


Figure 11 - Free vibration with decay of the amplitude. [13]

The logarithmic decrement is defined as the natural log of the ratio between two successive peaks:

$$\delta = \frac{1}{n} \ln \frac{u(t)}{u(t+nT)} \quad (1.10)$$

Where $u(t)$ is the amplitude at time t and $u(t+nT)$ is the amplitude of the peak n periods away, where n is any integer number of successive, positive peaks. The damping ratio is then found from the logarithmic decrement by:

$$\zeta = \frac{1}{\sqrt{1 + \left(\frac{2\pi}{\delta}\right)^2}} \quad (1.11)$$

1.4.2 Half Power Bandwidth method

With the half power bandwidth method the determination of damping involves assessing the form of the resonance peak as shown in Figure 12.

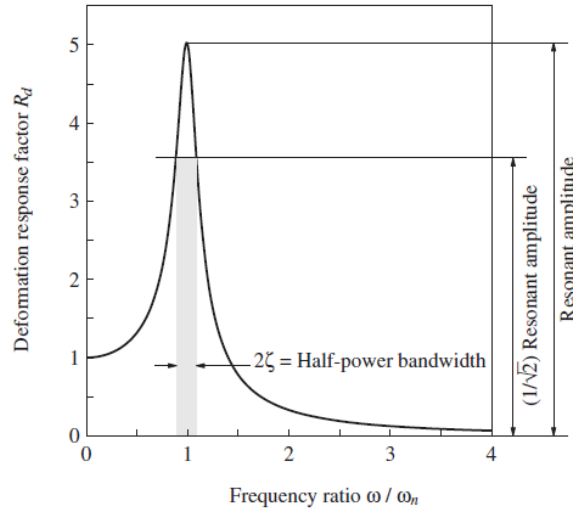


Figure 12 - Definition of half-power bandwidth [13]

By assuming that the damping ratio ξ is small and that the frequency of maximum amplitude is approximately equal to the undamped natural frequency ω_n , the damping ratio can be calculated with:

$$\xi = \frac{\omega_b - \omega_a}{2\omega_n} \quad (1.12)$$

Where ω_a and ω_b are half-power frequencies. Jeary states that the HPB method is accurate for systems with a damping ratio less than 1% [6].

1.4.3 Random Decrement Technique

The Random Decrement Technique (RDT) was developed by Cole and was first proposed as an integrity monitoring exercise for space craft [14]. The method is based on the observation that the response of a linear system at any time instant is the result of the linear superposition of initial displacement, initial velocity at the initial time. therefore, the dynamic response of a linear system can be described in the following form:

$$x(t) = x_{x_0}(t) + x_{\dot{x}_0}(t) + x_e(t) \quad (1.13)$$

In order to apply the RDT, uniform time segments of the response signal are chosen from a measured response time history. Together with the triggering conditions t_n as well as the length of the observation window are crucial parameters for successful identification of the damping. and the level crossing are selected. At those points in time where the signal crosses a predefined level (either upward or downwards) the time traces of a specific segment are averaged and overlapped as shown in Figure 13.

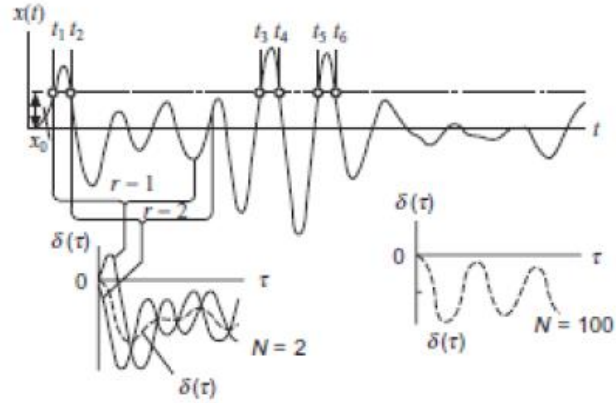


Figure 13 - Time segments of a random response signal

As of the number of averages N increases, the part of the response corresponding to the initial velocity as well as the random part at each segment will be minimized such that the remaining part of the signal will be an exponentially decaying function. This is demonstrated in Figure 14.

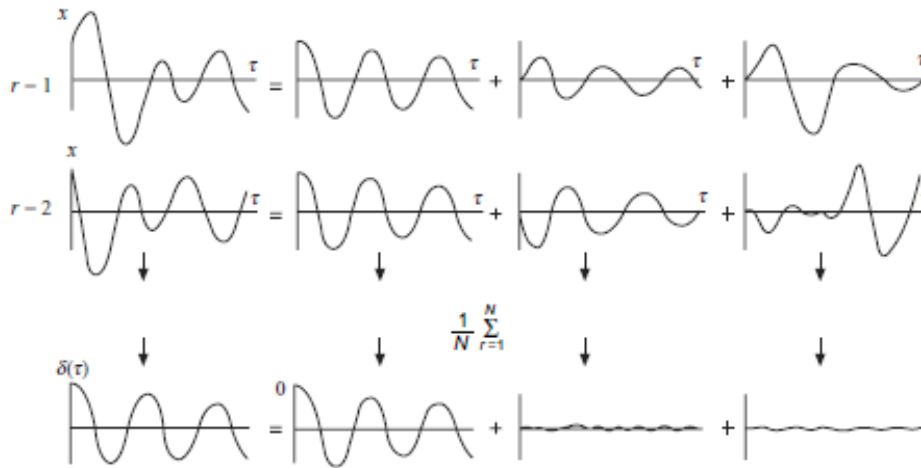


Figure 14 - Averaged time segments of a random response signal

An equivalent viscous damping ratio can be evaluated from the exponential decay function by means of the following expression:

$$\xi = \frac{1}{\sqrt{1 + \left(\frac{2\pi}{\ln(x_0 / x_1)} \right)^2}} \quad (1.14)$$

Where x_0 and x_1 represents the amplitude of two successive peaks.

1.5 Structural dynamics

The analysis and design of structures subject to time dependent forces constitute the field of structural dynamics. In this section the dynamic behaviour is analytically analysed for a continuous system which is used through this research. This section starts with the derivation of the equation of motion for the continuous system. Followed by the free vibration and the derivation of the eigen frequencies and mode shapes. Knowledge on this topic is gained by studying the lecture notes of A. Metrikine [15] and the book "Engineering vibration" by Daniel J. Inman [16].

1.5.1 Continuous system and the equation of motion

A continuous system can be defined as a system which is discretized to an infinity many masses to have continuous properties along the system. Vibrations in the direction perpendicular to its length are often called transverse vibrations, or flexural vibrations because they move across the length of the beam. Figure 15 illustrates a cantilevered beam with the transverse direction of vibration indicated. The beam is of rectangular cross section $A(x)$ with width h_y , thickness h_z , and length l .

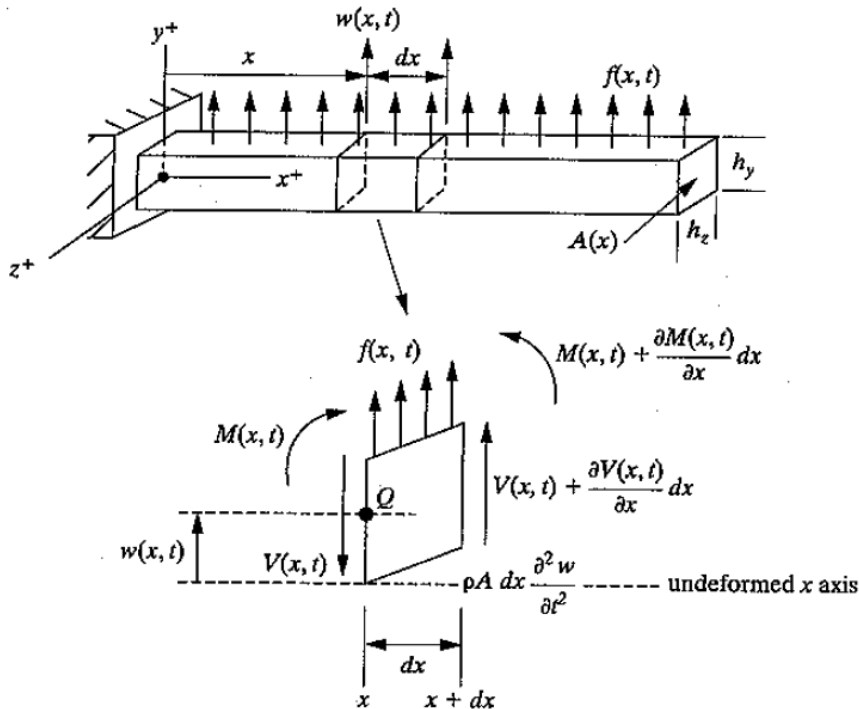


Figure 15 - Simple beam in transverse vibration and a free-body diagram of a small element of the beam as it is deformed [16]

Also associated with the beam is a flexural bending stiffness $EI(x)$, where E is Young's elastic modulus for the beam and $I(x)$ is the cross-sectional area of inertia about the z -axis. From mechanics of materials, the beam sustains a bending moment $M(x,t)$, which is related to the beam deflection $w(x,t)$ by:

$$M(x,t) = EI(x) \frac{\partial^2 w(x,t)}{\partial x^2} \quad (1.15)$$

Flexural vibration can be derived from examining the force diagram of an infinitesimal element of the beam as indicated in Figure 15. Assuming the deformation to be small enough such that the shear deformation is much smaller than $w(x,t)$, a summation of forces un the y direction yields:

$$(V(x,t) + \frac{\partial V(x,t)}{\partial x} dx) - V(x,t) + f(x,t)dx = \rho A(x)dx \frac{\partial^2 w(x,t)}{\partial t^2} \quad (1.16)$$

Where:

- $V(x,t)$ is the shear force at the left end of the element dx .
- $V(x,t) + V_x(x,t)dx$ is the shear force at the right end of the element dx .
- $f(x,t)$ is the total external force applied to the element per unit length.
- $\rho A(x)dx \frac{\partial^2 w(x,t)}{\partial t^2}$ is the inertial force of the element.

The assumption of small shear deformation used in the force balance of (1.16) is true if $l/h_z \geq 10$ and $l/h_y \geq 10$ (i.e., for long slender beams). The moment acting on the element dx about the z-axis through point Q are summed and yields as:

$$\left[M(x,t) + \frac{\partial M(x,t)}{\partial x} dx \right] - M(x,t) + \left[V(x,t) + \frac{\partial V(x,t)}{\partial x} dx \right] dx + [f(x,t)dx] \frac{dx}{2} = 0 \quad (1.17)$$

Here the left-hand side of the equation is zero since it is also assumed that the rotary inertia of the element dx is negligible. Simplifying this expression yields

$$\left[\frac{\partial M(x,t)}{\partial x} + V(x,t) \right] dx + \left[\frac{\partial V(x,t)}{\partial x} + \frac{f(x,t)}{2} \right] (dx)^2 = 0 \quad (1.18)$$

Since dx is assumed to be very small, $(dx)^2$ is assumed to be almost zero, so that this moment expression gives

$$V(x,t) = -\frac{\partial M(x,t)}{\partial x} \quad (1.19)$$

This states that the shear force is proportional to the spatial change in the bending moment. Substitution of this expression for the shear force into equation (1.16) gives

$$-\frac{\partial^2}{\partial x^2} [M(x,t)] dx + f(x,t)dx = \rho A(x)dx \frac{\partial^2 w(x,t)}{\partial t^2} \quad (1.20)$$

Further substitution of equation (1.15) into (1.20) and dividing by dx results in the classic Euler-Bernouli equation:

$$\rho A(x) \frac{\partial^2 w(x,t)}{\partial t^2} + \frac{\partial^2}{\partial x^2} \left[EI(x) \frac{\partial^2 w(x,t)}{\partial x^2} \right] = f(x,t) \quad (1.21)$$

Now that the equation of motion is derived, the free vibration is investigated to determine the natural frequencies. For structural dynamics it is known that a system vibrates in a specific way dependent on the natural frequencies of the system. The natural frequencies are dependent on the mass and stiffness of the system. Each natural frequency is related to specific vibration shape i.e. shape mode. Dependent on the configuration of the system, analytical expressions can be made of the mode shapes.

1.5.2 Free Vibration

The free vibration represents the dynamic behaviour of the non-loaded bending beam; this vibration is described by means of the homogeneous partial differential equation (equation of motion):

$$EI \frac{\partial^4 w(x,t)}{\partial x^4} + \rho A \frac{\partial^2 w(x,t)}{\partial t^2} = 0 \quad (1.22)$$

This function can be solved by the separation of variables method, in which $w(x,t)$ is decomposed into a product of two unknown functions of x and t . Assumed is a synchronic harmonic motion as a homogeneous solution. This means that the response can be written as the product of an unknown space function $W(x)$ and a harmonic time function $w(t) = \sin(\omega t + \varphi)$:

$$w(x,t) = W(x) \sin(\omega_n t + \varphi) \quad (1.23)$$

ω_n is called the natural frequency of the system. Without any external loading, the system will vibrate in the natural frequency, because for vibrating in this frequency the least amount of energy is needed. φ is the phase angle. To check whether the assumed solution is correct, it is substituted into the homogeneous differential equation:

$$\left(EI \frac{\partial^4 W(x)}{\partial x^4} - \rho A \omega^2 W(x) \right) \sin(\omega_n t + \varphi) = 0 \quad (1.24)$$

The time function is not equal to zero at any time, therefore the term between brackets of the left-hand side should be equal to zero:

$$EI \frac{\partial^4 W(x)}{\partial x^4} - \rho A \omega^2 W(x) = 0 \quad (1.25)$$

This differential equation is also called the eigenvalue problem. The solution $W(x)$ of the eigenvalue problem is called the eigenfunction. When determining the eigenfunction $W(x)$ it will be shown that the frequency ω can only adopt specific values. These frequencies are called the natural frequencies. For convenience purpose, the eigenvalue problem will be noted in a simpler fashion:

$$\frac{d^4W(x)}{dx^4} - \beta^4W(x) = 0 \quad (1.26)$$

With

$$\beta^4 = \frac{\rho A}{EI} \omega^2 \quad (1.27)$$

An assumed solution of the eigen value problem is chosen:

$$W(x) = \sum_{k=1}^4 C_k e^{\lambda_k x} \quad (1.28)$$

This function is substituted into the equation of motion which results in the following equation:

$$\sum_{k=1}^4 C_k (\lambda_k^4 - \beta^4) e^{\lambda_k x} = 0 \quad (1.29)$$

This gives the characteristic equation and the roots of it:

$$\lambda_k^4 - \beta^4 = 0 \rightarrow \lambda_1 = \beta, \lambda_2 = -\beta, \lambda_3 = i\beta, \lambda_4 = -i\beta \quad (1.30)$$

The solution $W(x)$ consist of four contributions. The general solution reads:

$$W(x) = C_1 e^{\beta x} + C_2 e^{-\beta x} + C_3 e^{i\beta x} + C_4 e^{-i\beta x} \quad (1.31)$$

This equation can also be written as:

$$W(x) = A \cosh \beta x + B \sinh \beta x + C \cos \beta x + D \sin \beta x \quad (1.32)$$

This expression for the eigenfunction applies to any (prismatic) bending beam. The precise characters is however highly dependent on the choice of the constants A, B, C, D and β . β is related to the unknown frequency ω . The values of the five constants are dependent on the applied boundary conditions.

1.5.3 The boundary conditions

Every structure has a finite length and is fixed or attached to another structure at its ends. Describing mathematically the conditions at the ends of the structure is needed to predict the mechanical behaviour of a structure. This is done with the so called boundary conditions.

There are two types of boundary conditions, namely: kinematic and dynamic. Often, these are also referred to as essential and natural. A boundary condition is called kinematic or essential if the kinematic characteristics of the structure are prescribed at its ends such as displacement, angles or slopes. A boundary condition is called dynamic or natural if the forces or moments are prescribed at the ends. The number of the boundary conditions, which have to be formulated at an end of the structure, depends on the equation of motion. The number of required conditions is determined by the highest order derivative in each independent variable. For example, if the equation of motion contains of a fourth order equation, at least 4 boundary conditions are needed in order to be able to solve the equation.

The kinematic boundary conditions of a fixed-free system are stated as:

$$W|_{x=0} = 0 \quad (1.33)$$

$$\left. \frac{\partial W}{\partial x} \right|_{x=0} = 0 \quad (1.34)$$

Assumed is a fixed connection which means that at the bottom of the system, $x = 0$, the transverse deflection and slope are equal to zero.

The dynamic boundary conditions are stated as:

$$EI \left. \frac{\partial^2 W}{\partial x^2} \right|_{x=L} = 0 \quad (1.35)$$

$$EI \left. \frac{\partial^3 W}{\partial x^3} \right|_{x=L} = 0 \quad (1.36)$$

At the top of the system $x = L$ the system is assumed to have a free end which results in the dynamic boundary conditions that the moment and shear force are equal to zero.

Substitution of the four boundary conditions into the expression for the eigenfunction $W(x)$, gives the following set homogeneous system of algebraic equations:

$$W|_{x=0} = 0 \rightarrow A + C = 0 \quad (1.37)$$

$$\frac{\partial W}{\partial x} \Big|_{x=0} = 0 \rightarrow B + D = 0 \quad (1.38)$$

$$EI \frac{\partial^2 W}{\partial x^2} \Big|_{x=L} = 0 \rightarrow EI \beta^2 \{ A \cosh(\beta L) + B \sinh(\beta L) - C \cos(\beta L) - D \sin(\beta L) \} = 0 \quad (1.39)$$

$$EI \frac{\partial^3 W}{\partial x^3} \Big|_{x=L} = 0 \rightarrow EI \beta^3 \{ A \sinh(\beta L) + B \cosh(\beta L) + C \sin(\beta L) - D \cos(\beta L) \} = 0 \quad (1.40)$$

Simplify eq. (A.9) by dividing by EI and β^2 :

$$EI \frac{\partial^2 W}{\partial x^2} \Big|_{x=L} = 0 \rightarrow A \cosh(\beta L) + B \sinh(\beta L) - C \cos(\beta L) - D \sin(\beta L) = 0 \quad (1.41)$$

Simplify eq. (A.10) by dividing by EI and β^3 :

$$EI \frac{\partial^3 W}{\partial x^3} \Big|_{x=L} = 0 \rightarrow A \sinh(\beta L) + B \cosh(\beta L) + C \sin(\beta L) - D \cos(\beta L) = 0 \quad (1.42)$$

The eq.(1.37), (1.38), (1.39) and (1.40) can be written as a coefficient matrix:

$$\begin{bmatrix} 1 & 0 & 1 & 0 \\ 0 & 1 & 0 & 1 \\ \cosh(\beta L) & \sinh(\beta L) & -\cos(\beta L) & -\sin(\beta L) \\ \sinh(\beta L) & \cosh(\beta L) & \sin(\beta L) & -\cos(\beta L) \end{bmatrix} \begin{bmatrix} A \\ B \\ C \\ D \end{bmatrix} = 0 \quad (1.43)$$

1.5.4 Natural Frequencies of continuous model

The homogeneous system shown at eq. (1.43) has a non-trivial solution if the determinant of the coefficient matrix is equal to zero. The determinant of this matrix gives an equation dependent on β . These β 's contain the natural frequencies of the system.

However, in this case, it is more convenient to first reduce the system to solve the problem partially. For the first and second equation of the homogeneous system it follows that:

$$\begin{aligned} C &= -A; \\ D &= -B \end{aligned} \quad (1.44)$$

With these relations, the third and fourth equation can be rewritten:

$$\begin{aligned} A\beta^2(\cosh \beta L + \cos \beta L) + B\beta^2(\sinh \beta L + \sin \beta L) &= 0 \\ A\beta^3(\sinh \beta L + \sin \beta L) + B\beta^3(\cosh \beta L + \cos \beta L) &= 0 \end{aligned} \quad (1.45)$$

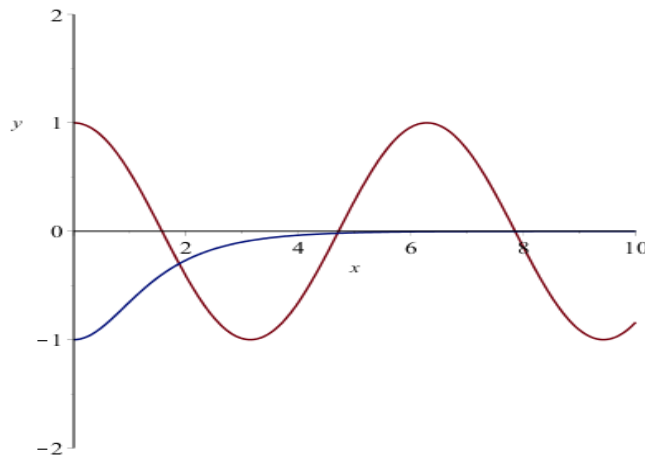
The determinant of the (2x2) coefficient matrix leads to the following result:

$$\cosh \beta L * \cos \beta L + 1 = 0 \quad (1.46)$$

$$\cos \beta L = \frac{-1}{\cosh \beta L} \quad (1.47)$$

Solving eq. (1.47) gives the following values:

$$\begin{aligned} \beta_1 L &\approx 1.875104069 \approx 0.6\pi \\ \beta_2 L &\approx 4.694091133 \approx \frac{3}{2}\pi \\ \beta_3 L &\approx 7.854757438 \approx \frac{5}{2}\pi \end{aligned} \quad (1.48)$$



With these values of the weighted frequencies $\beta_n L$, the individual frequencies of vibration can be calculated:

$$\omega_i = \frac{(\beta_i L)^2}{2\pi L^2} \left(\frac{EI}{\rho A} \right)^{1/2} \quad (1.49)$$

1.5.5 Mode Shapes of continuous model

For the determination of the corresponding principal modes, the earlier derived reduced system of algebraic equations (1.45) is used. Solving this set of equations results in expressions for the coefficients A and B. Both equations are dependent, so arbitrarily the first function is chosen:

$$A_n \beta_n^2 (\cosh \beta_n L + \cos \beta_n L) + B_n \beta_n^2 (\sinh \beta_n L + \sin \beta_n L) = 0 \quad (1.50)$$

For the constant B it then follows:

$$B_n = -A_n \frac{\cosh \beta_n L + \cos \beta_n L}{\sinh \beta_n L + \sin \beta_n L} \quad (1.51)$$

Substitution of this result into the expression for the eigenfunction:

$$W_n(x) = A_n (\cosh \beta_n x - \cos \beta_n x) + B_n (\sinh \beta_n x - \sin \beta_n x) \quad (1.52)$$

Insert eq. (1.51) in eq. (1.52) gives:

$$W_n(x) = A_n (\cosh \beta_n x - \cos \beta_n x) - A_n \frac{\cosh \beta_n L + \cos \beta_n L}{\sinh \beta_n L + \sin \beta_n L} (\sinh \beta_n x - \sin \beta_n x) \quad (1.53)$$

By setting:

$$w_n(x) = W_n(x) / A_n \quad (1.54)$$

The eigenfunction can now be written as:

$$w_n(x) = \cosh \beta_n x - \cos \beta_n x - \sigma_n (\sinh \beta_n x - \sin \beta_n x) \quad (1.55)$$

With:

$$\sigma_n = \frac{\cosh \beta_n L + \cos \beta_n L}{\sinh \beta_n L + \sin \beta_n L} \quad (1.56)$$

Which is the weighting constant associated with each mode.

Notice that the bending beam appears to have an infinite number of natural frequencies. However, the differential equation merely applies to slender beams and low frequencies, this as a result of neglecting the shear deformation and the rotation inertia. In accordance to this we may expect that the formula derived here for the natural frequencies, have a reliable result for only low values of n . In *Figure 16* the first three normalized mode shapes of the fixed-free system are plotted.

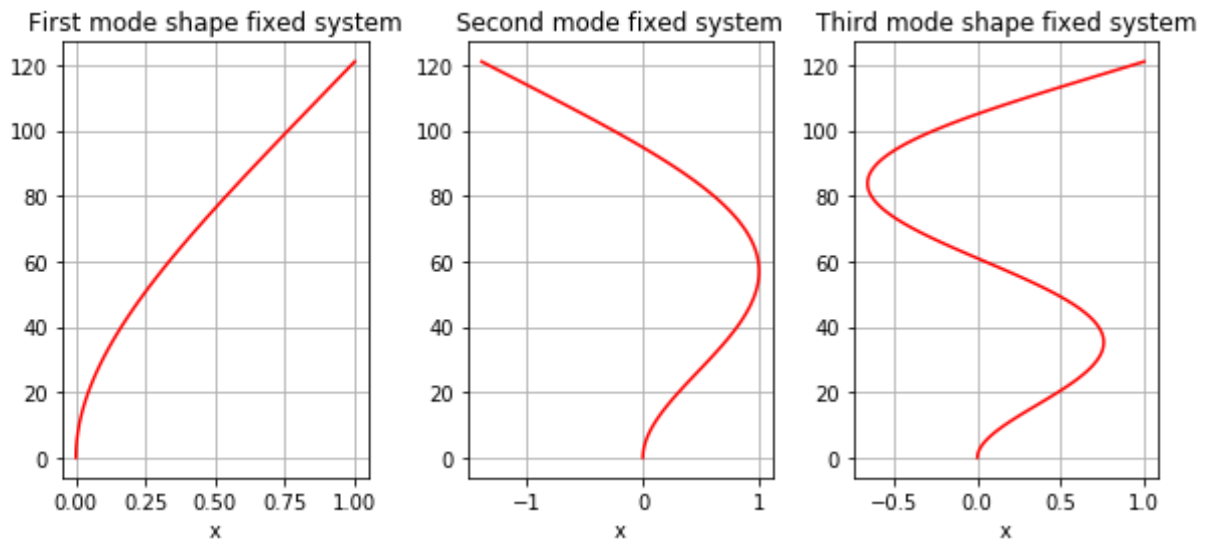


Figure 16 - first three mode shapes of a fixed-free system

1.6 Energy flow analysis

Energy flow analysis (EFA) is an analytical tool for response prediction of structural/acoustic systems [17], [18], [19], [20] and [21]. It is an energy-based approach based on the first law of thermo dynamics. The first law of thermodynamics for closed systems can be simply states as:

“The amount of energy gained by the system must be exactly equal to the amount of energy lost by the surroundings. [22]

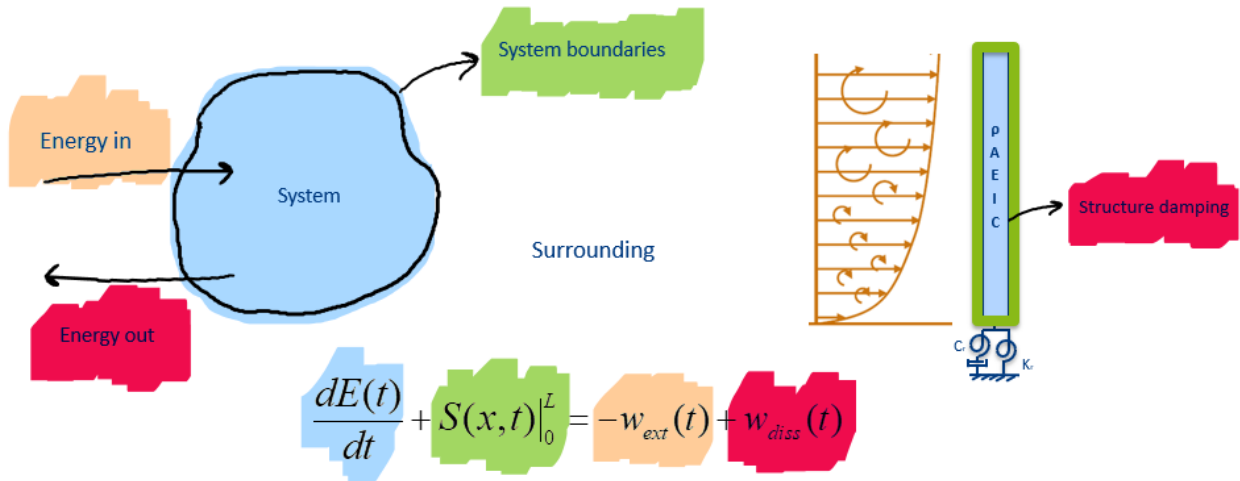


Figure 17 - A system in its surrounding.

The concept of energy conservation is expressed in an energy balance, see Figure 17. A system is that part of the universe on which people focus their attention. The rest of the universe is the surrounding. The interaction between the system and the surrounding is determined by the system boundaries (whether material or not) that encloses the system. Interaction in the form of heat and work exist only at the boundaries when considering a closed system. This concept is applied on a continuous beam model where the properties of the energy balance are given, see Figure 17. The variation of energy within the system can be derived by the equations that govern the energy contained in the structural elements. The derivation of the transfer of energy through the boundaries is called the energy flux of the system $S(x,t)$. The external power added to the system due to the wind load is given with $w_{ext}(t)$. Last, the amount of energy dissipation (losses) is comprised by the power dissipation term $w_{diss}(t)$. The EFA will be applied on a continuous beam model to demonstrate the derivation of the needed equations.

The energy of the system can be described as the summation of the potential and kinetic energy within the system.

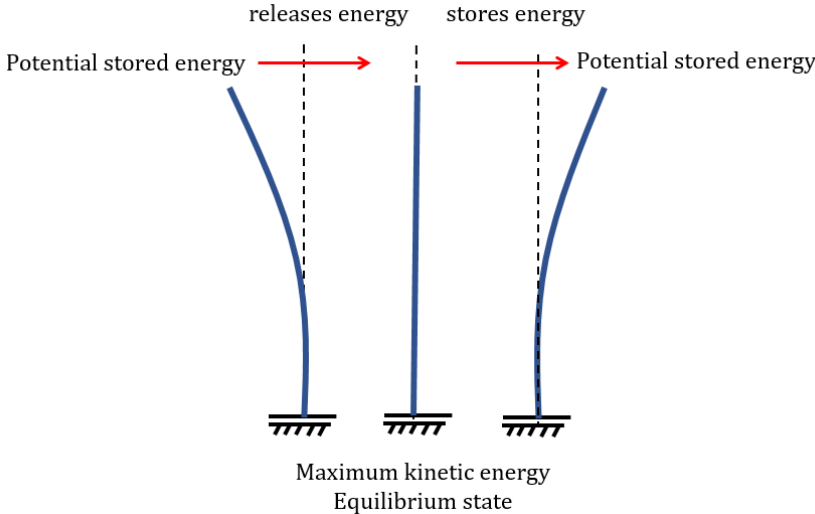


Figure 18 - Conservation of energy

Potential energy is stored in the beam when an external load is set and gives the system an certain displacement. The beam contains gravitational potential energy when it is removed from the equilibrium position. When the beam is released, from the external force, it wants to return to its equilibrium position. This gravitational energy is transferred to kinetic energy.

1.6.1 Derivation of the potential energy of a continuous system

Potential energy E_{pot} is proportional to the energy stored in the system not in motion. This energy can be determined as the work done by the bending moment $M(x)$ undergoing a small angular displacement $d\theta$. For small displacements the following kinematic relations can be described:

$$\frac{dw}{dx} = \theta \tag{1.57}$$

$$\frac{d^2w}{dx^2} = \kappa = \frac{d\theta}{dx} \tag{1.58}$$

In which $w(x,t)$ is the function describing the displacement of the motion corresponding to the free end of the beam. The relation between bending stiffness and curvature can be written as the constitutive relation:

$$M = EI\kappa \tag{1.59}$$

- E = Young's modulus of the beam [N/m²]
- I = Second moment of area of the beam [m⁴]

Combining (1.57) -(1.59) gives:

$$\frac{d^2w}{dx^2} = \frac{d\theta}{dx} = \frac{M(x)}{EI} \quad (1.60)$$

or

$$d\theta = \frac{M(x)}{EI} dx \quad (1.61)$$

and plotting the bending moment with respect to the curvature gives the following graph for linear elastic systems:

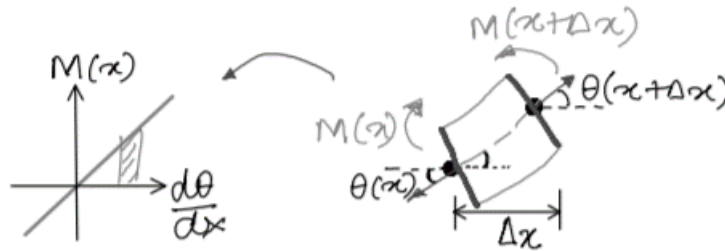


Figure 19 - relation between bending moment and curvature

Since $dw/dx = \theta$, where θ , being assumed small, is taken as the slope of the elastic curve. Consequently, the potential energy is given by

$$E_{pot} = \int_0^L M(x) d\theta \quad (1.62)$$

Utilizing eq. (1.60) and (1.61) into (1.62) and taking the integral results in the following equation:

$$E_{pot} = \frac{1}{2} EI \left(\frac{d^2w}{dx^2} \right)^2 \quad (1.63)$$

1.6.2 Derivation of the kinetic energy of a continuous system

As mentioned before, the kinetic energy is related to speed and describes the motion energy. For the continuous system considered in Figure 17 we can compute the kinetic energy as:

$$E_{kin} = \frac{1}{2} \rho A \left(\frac{\partial w}{\partial t} \right)^2 \quad (1.64)$$

Where

$w(x,t)$	=	is the function describing the displacement of the motion corresponding to the free end of the beam	[m]
ρ	=	mass density of the beam material	[N]
$\frac{\partial w}{\partial t}$	=	velocity of the motion	[m/s]

1.6.3 Energy density of the system

The total energy of the system can be described as:

$$E(t) = E_{kin} + E_{pot} = \frac{1}{2} \rho A \left(\frac{\partial w}{\partial t} \right)^2 + \frac{1}{2} EI \left(\frac{\partial^2 w}{\partial x^2} \right)^2 \quad (1.65)$$

By the chain rule the derivative of E over t become:

$$\frac{\partial E(t)}{\partial t} = \rho A \frac{\partial^2 w}{\partial t^2} \frac{\partial w}{\partial t} + EI \frac{\partial^2 w}{\partial x^2} \frac{\partial^2 w}{\partial x^2} \frac{\partial w}{\partial t} \quad (1.66)$$

In eq. (1.66) the energy density of the beam has been determined. Note that when no energy dissipation occurs in the system, the variation of energy over time is zero.

1.6.4 Energy flux

Energy flux is the rate of energy transfer through a surface. For determination of the energy flux, the Euler- Bernoulli model is used. The Euler-Bernoulli equation describes the relationship between the beam's deflection and the external applied force.

$$\rho A \frac{\partial^2 w}{\partial t^2} + EI \frac{\partial^4 w}{\partial x^4} = q_z \quad (1.67)$$

The first term describes the deflection due to the dynamic behaviour of the structural element. The second term, is the classic static beam equation. q_z represent the external force. To get the energy density of the beam, the Euler- Bernoulli equation has to be multiplied with the velocity. This gives:

$$\rho A \frac{\partial^2 w}{\partial t^2} \frac{\partial w}{\partial t} + EI \frac{\partial^4 w}{\partial x^4} \frac{\partial w}{\partial t} = q_z \quad (1.68)$$

Subtraction of Eq.(1.68) from eq. (1.66) gives the variation in energy in the system.

$$\begin{aligned} & \rho A \frac{\partial^2 w}{\partial t^2} \frac{\partial w}{\partial t} + EI \frac{\partial^2 w}{\partial x^2} \frac{\partial^2 w}{\partial x^2} \frac{\partial w}{\partial t} - \rho A \frac{\partial^2 w}{\partial t^2} \frac{\partial w}{\partial t} - EI \frac{\partial^4 w}{\partial x^4} \frac{\partial w}{\partial t} = \\ & EI \frac{\partial^2 w}{\partial x^2} \frac{\partial^2 w}{\partial x^2} \frac{\partial w}{\partial t} - EI \frac{\partial^4 w}{\partial x^4} \frac{\partial w}{\partial t} = \\ & EI \left(\frac{\partial^2 w}{\partial x^2} \frac{\partial^2 w}{\partial x^2} \frac{\partial w}{\partial t} - \frac{\partial^4 w}{\partial x^4} \frac{\partial w}{\partial t} \right) \end{aligned} \quad (1.69)$$

Substitute eq. (1.69) into the energy balance gives:

$$EI \left(\frac{\partial^2 w}{\partial x^2} \frac{\partial^2 w}{\partial x^2} \frac{\partial w}{\partial t} - \frac{\partial^4 w}{\partial x^4} \frac{\partial w}{\partial t} \right) + \frac{\partial s}{\partial x} = w_{diss} \quad (1.70)$$

The energy dissipation terms do not incorporate with the flux in the system. Therefore, these terms are cancelled for deriving the energy flux in the system. The energy flux through the structural element, which in this case, is only through the beam element and can be determined by taken the integral of s over x ;

$$\begin{aligned}
s &= \int EI \left(\frac{\partial^2 w}{\partial x^2} \frac{\partial^2 w}{\partial x^2} \frac{\partial w}{\partial t} - \frac{\partial^4 w}{\partial x^4} \frac{\partial w}{\partial t} \right) dx \\
s &= EI \left[\int \left(\frac{\partial^2 w}{\partial x^2} \frac{\partial^2 w}{\partial x^2} \frac{\partial w}{\partial t} \right) dx - \frac{\partial^3 w}{\partial x^3} \frac{\partial w}{\partial t} \right] \\
s &= EI \left[\frac{\partial^2 w}{\partial x^2} \left(\frac{\partial w}{\partial x} \frac{\partial w}{\partial t} \right) - \int \left(\left(\frac{\partial w}{\partial x} \frac{\partial w}{\partial t} \right) \frac{\partial^3 w}{\partial x^3} \right) dx - \frac{\partial^3 w}{\partial x^3} \frac{\partial w}{\partial t} \right] \\
s &= EI \left[\frac{\partial^2 w}{\partial x^2} \left(\frac{\partial w}{\partial x} \frac{\partial w}{\partial t} \right) - \frac{\partial^3 w}{\partial x^3} \frac{\partial w}{\partial t} + \int \left(\frac{\partial^4 w}{\partial x^4} \frac{\partial w}{\partial t} \right) dx - \frac{\partial^3 w}{\partial x^3} \frac{\partial w}{\partial t} \right] \\
s &= EI \left[\frac{\partial^2 w}{\partial x^2} \left(\frac{\partial w}{\partial x} \frac{\partial w}{\partial t} \right) - \frac{\partial^3 w}{\partial x^3} \frac{\partial w}{\partial t} + \frac{\partial^3 w}{\partial x^3} \frac{\partial w}{\partial t} - \frac{\partial^3 w}{\partial x^3} \frac{\partial w}{\partial t} \right] \\
s &= EI \left[\frac{\partial^2 w}{\partial x^2} \left(\frac{\partial w}{\partial x} \frac{\partial w}{\partial t} \right) - \frac{\partial^3 w}{\partial x^3} \frac{\partial w}{\partial t} \right]
\end{aligned} \tag{1.71}$$

The energy flux found in eq. (1.71) can be written as

$$s = M \left(\frac{\partial w}{\partial x} \frac{\partial w}{\partial t} \right) - Q \frac{\partial w}{\partial t} \tag{1.72}$$

1.6.5 Power dissipation

This term describes the energy dissipation by the dashpot damping which is included in this system.

$$w_{diss} = \delta(x-l)c \frac{\partial x}{\partial t} \tag{1.73}$$

Multiplying with velocity gives the power dissipated density of the damper

$$w_{diss} = \delta(x-l)c \left(\frac{\partial x}{\partial t} \right)^2 \tag{1.74}$$

1.6.6 Application of the EFA in structural analysis

Gomez applied the Energy Flow Analysis to determine the damping of a high-rise building [23]. First he investigated the capability by demonstrating the energy flow method in identification of damping in the joints of a lab-scale structure [24]. This research is explained stepwise in Figure 20.

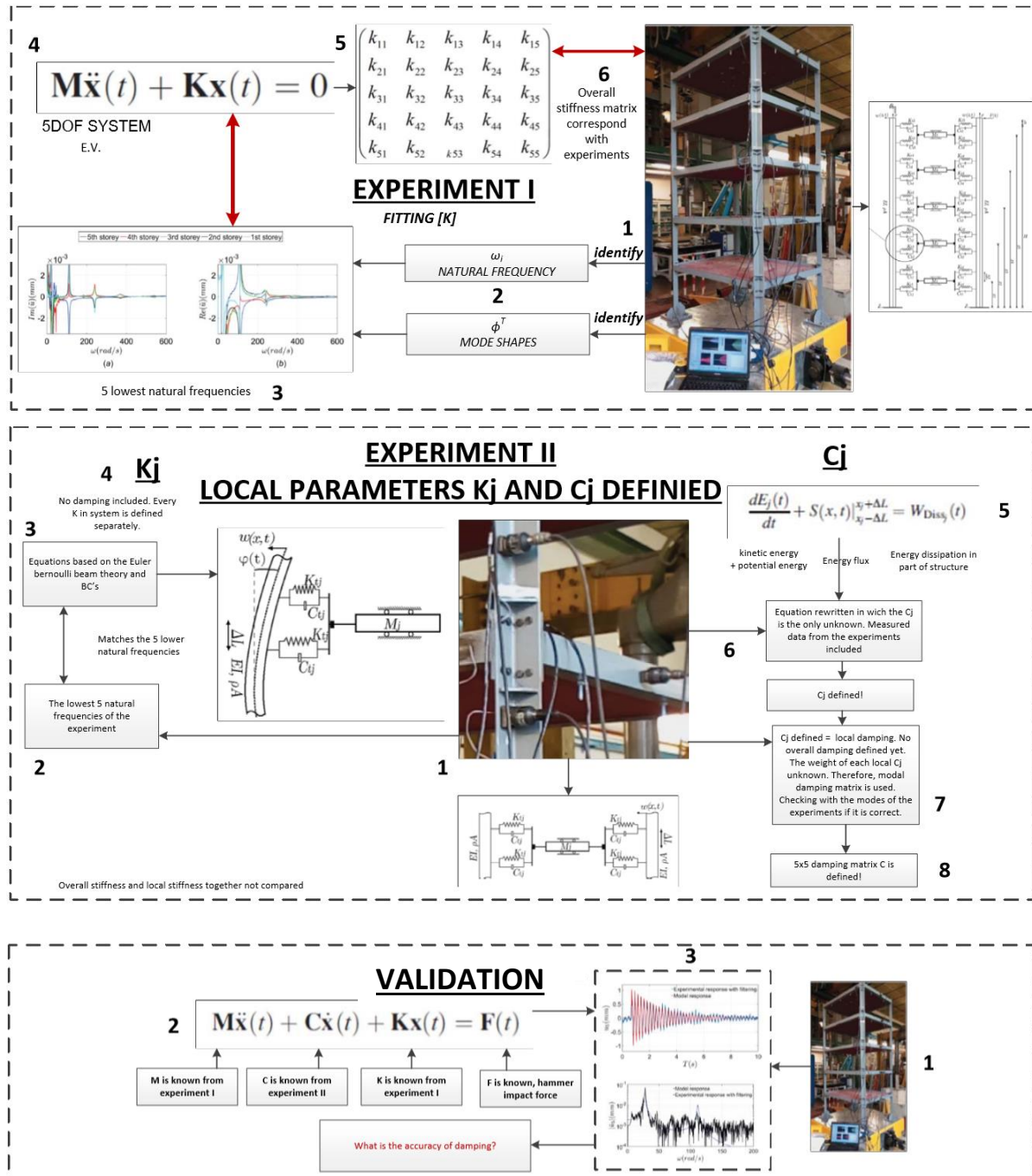


Figure 20 - Visualization of the procedure to identify the damping in the joints of a lab-scale structure

1.7 Formulation of the problem

A large amount of research has been performed on the overall damping of high-rise buildings. The empirical damping predictors which were proposed by different researchers are based on large sets of full-scale measurements on buildings. These empirical formulas have large dissimilarities. The cause of these dissimilarities is the difference in soil and building methods between the datasets on which the formulas were based. Little is known about the damping contribution of these different parts, such as the contribution of the foundation and load-bearing structure of a high rise building.

Recently an Energy Flow Analysis (EFA) technique was developed in the field of structural analysis, which allows for the determination of the damping contribution of different parts of a structure. This technique has been applied in combination with measurements performed on a model building on a shaking table, and on a high-rise building excited by wind loading. The results of these studies are promising and indicate the potential of EFA for the identification of damping.

To provide designers with reliable predictions of the damping distribution in high-rise buildings, the EFA based measurement technique needs to be developed in a reliable method for the quantification of damping.

The values obtained with the EFA based measurement method are based on a significant number of assumptions, especially in the case of in-situ measurements.

Without information on these uncertainties, the reliability of the outcome of in-situ measurements is low. Before the EFA based measurement technique can be applied successfully in future monitoring and measurement campaigns, these uncertainties in this technique need to be assessed.

1.8 Research objective

The objective of this Master's thesis is to assess the influence of some of the assumptions and simplifications in the EFA based measurement method. The focus in this study lies on the assumptions and simplifications needed to accommodate for the lack of information typically present in (in-situ) measurements. To eliminate experiment-related uncertainties (e.g. faulty calibration, improper sensor placement, disturbance sources, etc.), the study will be performed in a controlled FEM environment. The examination will be done by reversed engineering by means of using damping values which are known by beforehand. With this information an accurate assessment can be made of the error with which the energy method quantifies the damping contribution of a structural component. The applied damping values in FEM and the identified damping due to the energy method will be compared. This can be translated in the following main question:

With what accuracy can the energy method predict the damping contribution of the foundation of a high-rise building during in-situ experiments?

This main question is subdivided into research phases to build up an understanding of the question, the context of the research and the answer itself. This is further explained in Chapter 2.

2 Methodology

2.1 Introduction

In this chapter the research methodology of this thesis is explained. First the main research focus and what it adds to previous research is discussed in 2.2. In 2.3 the research strategy is described which gives insight in the uncertainties accounted for and the uncertainties which cannot be assessed with this strategy are described in 2.4. In 2.5 the case studies are introduced which accommodate for giving insight in the uncertainties described in 2.3. The application of the energy flow method is explained for every case study.

2.2 Research focus

The EFA technique has been recently applied in the field of structural engineering in the work of [3]. Two experiments were performed in which a combination with measurements on a model building on a shaking table was performed. This research demonstrated the capability of the EFA technique in identification of damping in the joints of the lab-structure. The second experiment was a demonstration of the applicability of the EFA technique on a high-rise building excited by wind loading. The results of these studies are promising and indicate the potential of EFA for the identification of damping.

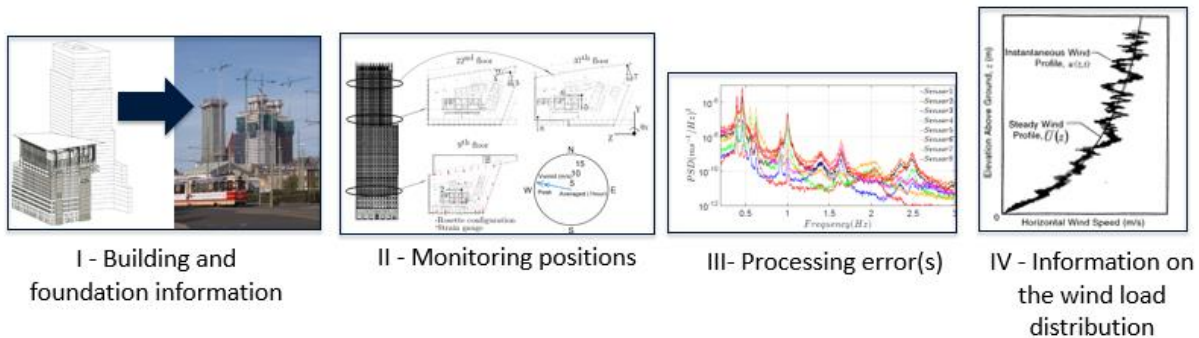


Figure 21 - Illustration of uncertainties typically presented in measurement campaigns.

During these two researches several assumptions are done. These assumptions results in uncertainties within the EFA technique. Figure 6 depicted the uncertainties typically presented in measurement campaigns, such as:

- I. Uncertainty due to inaccurate building and foundation information (e.g. mass, soil, and stiffness properties); these parameters have influence on the dynamic behaviour of the building and cannot be predicted accurately on the basis of available design calculations.
- II. Uncertainty due to a limited number of sensors; during field measurements a measurement strategy is used to collect the needed information. This measurement strategy is consists of a limited number of sensors which is a fraction of the total behaviour of the building.
- III. Uncertainty due to processing error(s); the measured data undergoes a post-processing process which involves filtering of data.
- IV. Uncertainty due to lack of information on the wind load distribution; During in-situ measurements the full wind load distribution over the façade is desired. However, in previous research (Gomez 2018) no wind sensors were installed and therefore the needed data is not explicitly collected. The wind pressure is assumed

by using the procedure described in the Eurocode and the KNMI database is used for assuming the wind velocity.

Without information on these uncertainties, the reliability of the outcome of in-situ measurements is low. Before the EFA based measurement technique can be applied successfully in future monitoring and measurement campaigns, the uncertainties in this technique need to be assessed. An overview of the focus of this research and what it adds to previous research is displayed in Figure 22. Assessing the uncertainties results in a reliable measurement technique. This gives insight in the contribution of different energy dissipation mechanisms to the total energy dissipation in tall buildings. With accurate measurement data, future damping prediction models can be validated and be provided to designers.

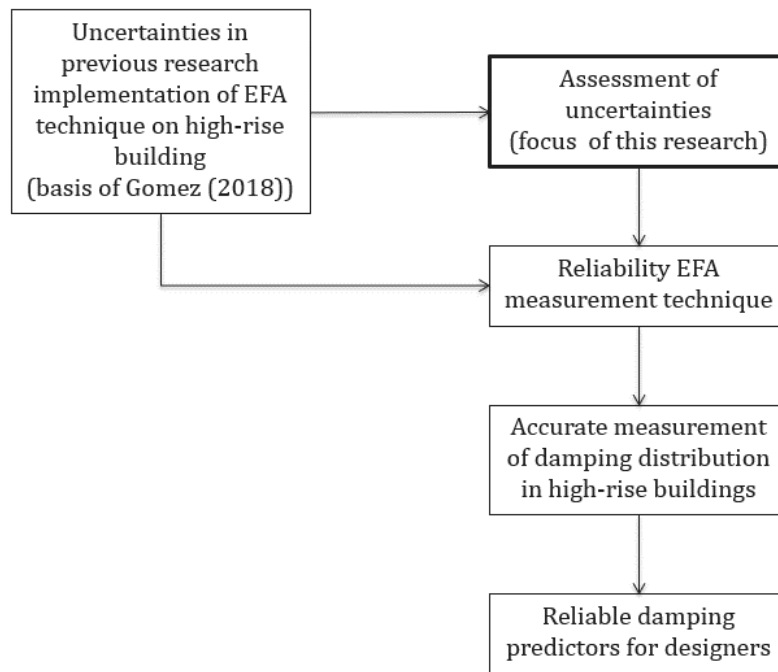


Figure 22 - Overview of the focus of this research

The objective of this Master's thesis is to assess the influence of some of the assumptions and simplifications in the EFA based measurement method. The focus in this study lies on the assumptions and simplifications needed to accommodate for the lack of information typically present in (in-situ) measurements. The research question comprising the research objective can be formulated as followed:

With what accuracy can the Energy Flow Analysis method predict the damping contribution of the foundation of a high-rise building during in-situ experiments?

This main question is divided into three research phases to build up an understanding of the question, the context of the research and the answer itself:

1. Assessment of the accuracy of the energy flow analysis as damping identification method.
2. Assessment of the influence of lack of information due to limited sensor positions on the identification of damping.

- Assessment of the influence of lack of information on the wind load on the identification of damping.

2.3 Research Strategy

The assessment procedure developed in this research should be able to determine the influence of some of the assumptions and simplifications needed for the quantification of the distribution of damping in high-rise buildings with the EFA technique. The study will be performed in a controlled FEM environment which eliminates experiment-related uncertainties. This is in contrast with the method by [3] which uses experimental in-situ data and combines it with a semi analytical model. The developed procedure in this research links the uncertainties in limited number of sensors and lack of information on the wind load distribution. Before assessing these uncertainties, the accuracy of the EFA is investigated.

2.3.1 Accuracy of EFA computation to determine the soil damper using all variable model output

For evaluating the influence of limited number of sensors on the identification of damping, first the energies which accommodate for the EFA, needs to be assessed. The amount of other uncertainties must be reduced, therefore the high-rise building is reduced to a 1D beam model and is excited by an initial displacement. The focus is placed on the foundation and structural damping in which aerodynamic damping is neglected. In Chapter 4 the model used in this research is explained in detail. The procedure to determine the accuracy with which the EFA method computes the damper value is shown in Figure 23.

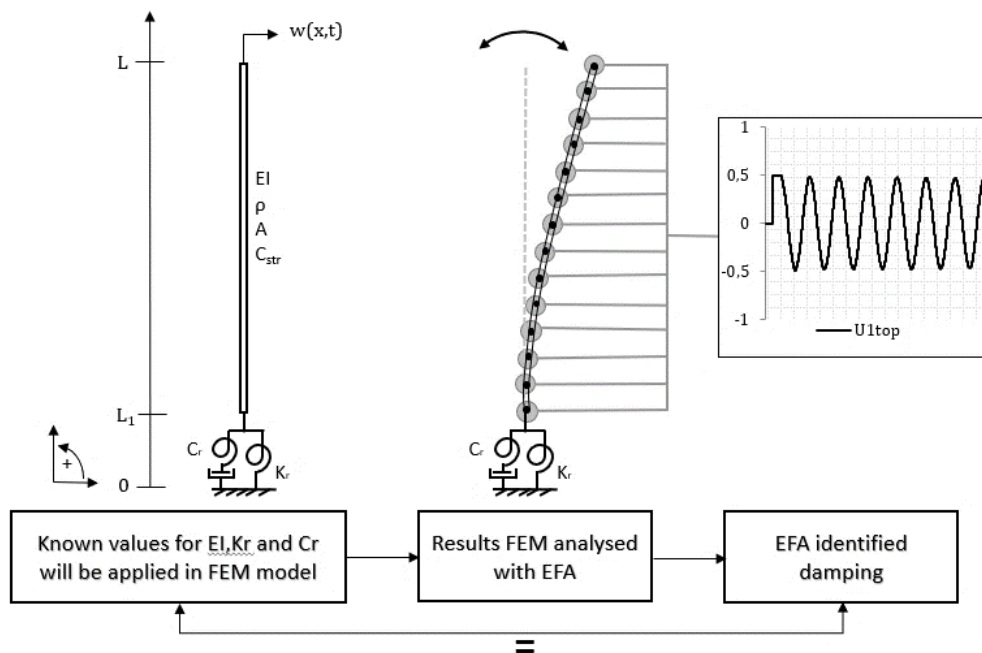


Figure 23 - General assessment procedure to identify damping by using the EFA

First the FEM model is modelled with parameters such as the bending stiffness of the building, building mass and building dimensions which are based on a case study explained in Chapter 4. The results of the dynamic analysis in FEM are used in the EFA. The following analysis steps are performed with the data from the FEM model:

- The computed timeseries for the displacement, velocities and curvatures of every node in the FEM model are used as input in the EFA method. The curvature timeseries are used to

compute the potential energy of the beam, the displacement and velocity timeseries are used to compute the kinetic energy.

2. After computing all the needed energies for the energy balance, the energies are compared to the energy module of FEM, which also calculates the energy quantities.
3. The energy dissipation is computed from the potential and kinetic energy and is compared with the dissipation computed by the energy module in FEM.
4. The damping value is computed from the energy dissipation. A comparison is made between the input damping value and the damping value obtained with the EFA method. The difference is expressed as percentage which quantifies the error with which the EFA method computes the damping value.

With this reversed engineering method, an accurate assessment can be made of the error with which the energy method quantifies the damping contribution of a structural component were all information available is used.

2.3.2 Uncertainty due to limited number of sensors

The amount of information will be reduced by using a minimal number of sensors which are represented by the nodes in the FEM model. The procedure to determine the accuracy with which the EFA method computes the damper value by reducing the amount of information, is shown in Figure 24.

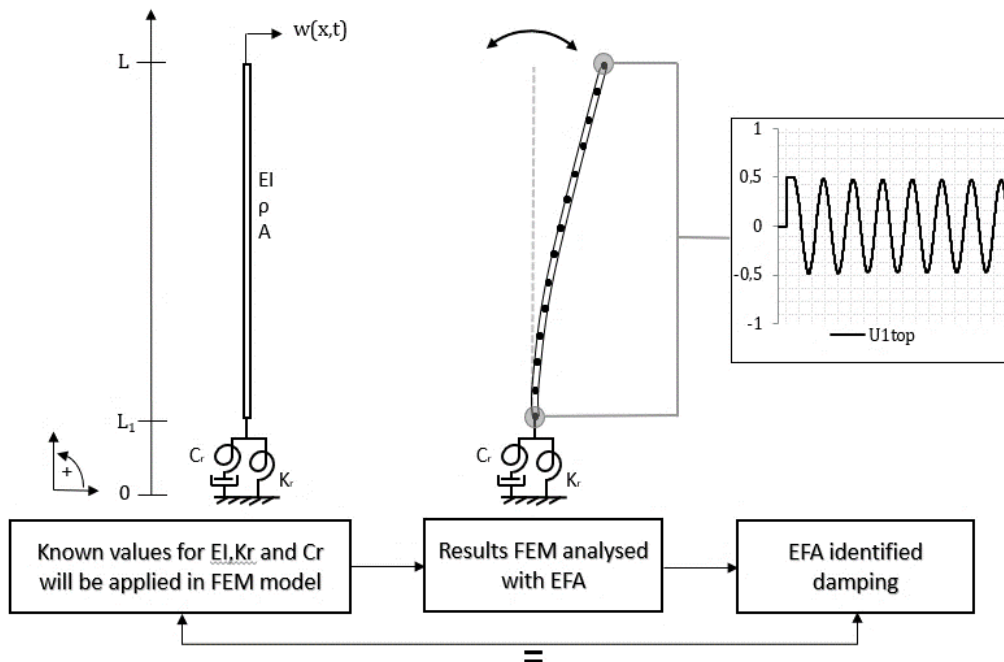


Figure 24 - Assessment procedure to identify damping with the EFA by using limited amount of information.

The following analysis steps are performed to assess the influence on the identification of damping using a reduced amount of information from the FEM model:

1. To compensate for the lack of information, analytical expressions for the mode shapes of the beam model are made and used to predict the dynamic behaviour of the intermediate building area where no FEM model data is used.
2. Time series can be computed by combining the mode shapes with the extracted data from the FEM model. Only at the top and bottom of the beam data is extracted from the FEM model. The computed timeseries for the displacement, velocities and

curvature at the location of every node are used for computing the kinetic and potential energy of the beam.

3. After computing all the needed energies for the energy balance, the energies are compared to the energy module of FEM, which also calculates the energy quantities.
4. The energy dissipation is computed from the potential and kinetic energy and is compared with the dissipation computed by the energy module in FEM.
5. The damping value is computed from the energy dissipation. A comparison is made between the input damping value and the damping value obtained with the EFA method. The difference is expressed as percentage which quantifies the error with which the EFA method computes the damping value.

2.3.3 Uncertainty due to lack of information on the wind load distribution

Assessing the influence of a lack of information on the wind load distribution is done by using wind tunnel data. This data made it possible to mimic a full scale wind profile along the building façade. In practice the wind load distribution on every location on the building is not precisely known. Hereby the external work added to the building is hard to determine accurately. Therefore, the influence of having insufficient wind load information on the identification of damping in buildings is investigated. First the accuracy of the EFA method is tested. This is done by applying a full wind profile and using all information needed for the assessment. Combining this wind profile with the general assessment of identifying the energy dissipation displayed in Figure 25 gives insight in the error with which the energy method quantifies the damping contribution of structural components were all information available is used.

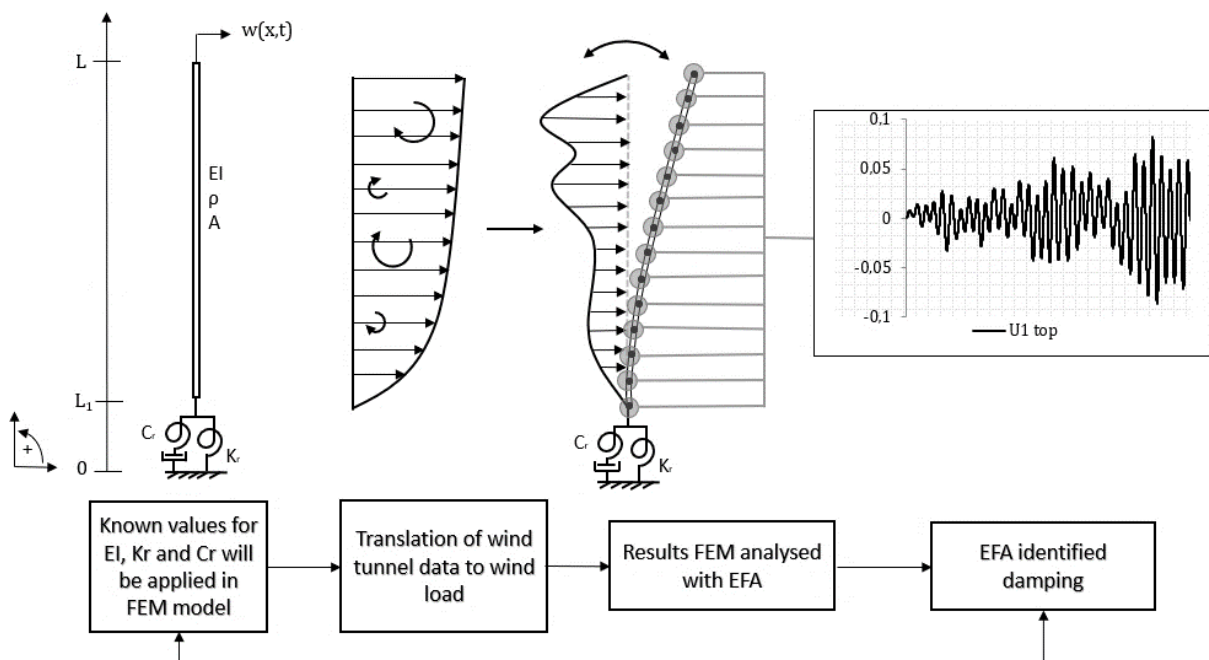


Figure 25 - Assessment procedure of the determination the influence of a full wind profile on the identification of damping with the EFA.

The following analysis steps are performed to assess the influence of using a full scale wind load distribution realistic wind load on the identification of damping using data from the FEM model:

1. First the FEM model needs to be adjusted. The mimic a full scale wind loading, the wind tunnel data is transformed to wind load time series for every node on the beam model. In chapter 3 a detailed explanation is presented of the translation from wind tunnel data to full scale wind load. For every node a wind signal is determined and applying in the FEM model. Note that the illustration of the wind distribution in Figure 25 is representing a single time moment. Over time the wind profile changes. This is taken into account in the wind load time series.
2. Further, the computed timeseries for the displacement, velocities and curvatures of every node in the FEM model are used as input in the EFA method. The curvature timeseries is used to compute the potential energy of the beam, the displacement and velocity timeseries are used to compute the kinetic energy.
3. After computing all the needed energies for the energy balance, the energies are compared to the energy module of FEM, which also calculates the energy quantities.
4. The energy dissipation is computed from the potential and kinetic energy and is compared with the dissipation computed by the energy module in FEM.
5. The damping value is computed from the energy dissipation. A comparison is made between the input damping value and the damping value obtained with the EFA method. The difference is expressed as percentage which quantifies the error with which the EFA method computes the damping value.

With this method, an accurate assessment can be made of the error with which the energy method quantifies the damping contribution of a structural component where all information available is used. After this, the preciseness of the wind load on the beam will be reduced by using the top wind load time series only. This wind load over time is introduced to the FEM model by using it on all the nodes. The procedure to determine the accuracy with which the EFA method computes the damper value by reducing the amount of wind information, is shown in Figure 26. The steps above are also applicable for this case.

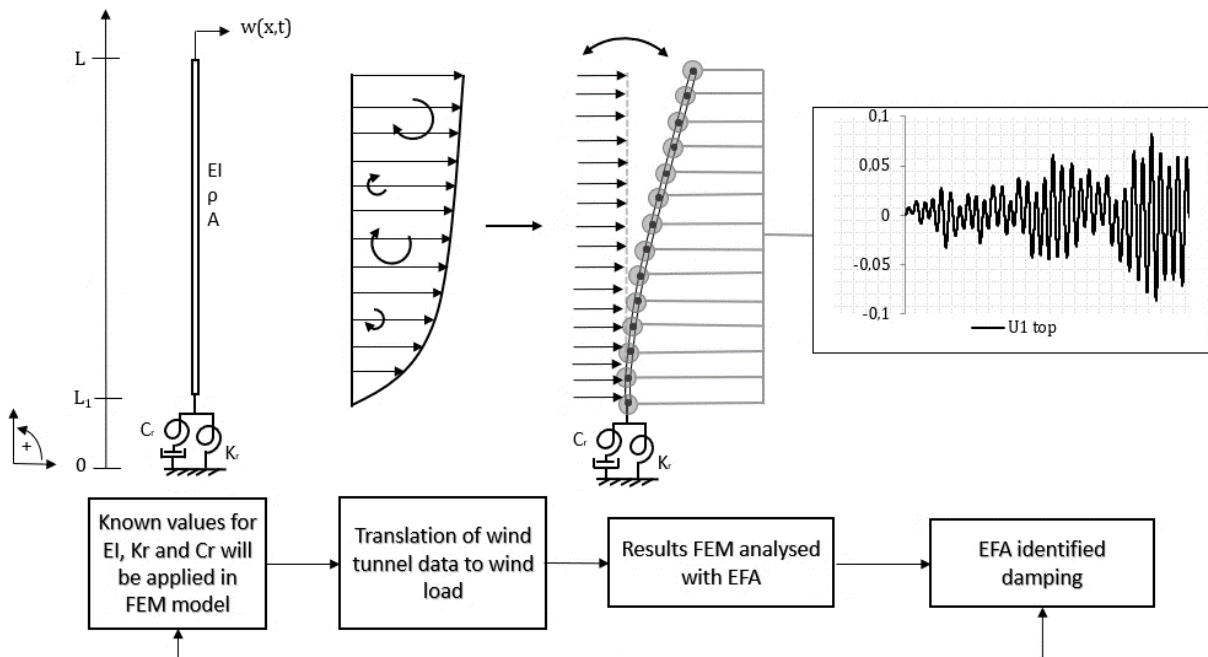


Figure 26 - Assessment procedure of the determination of the influence of a reduced amount of wind information on the identification of damping with the EFA.

2.4 Research limitations

The uncertainties which are not taken into account explicitly in this research are listed below:

1. This research does not give insight in experiment-related uncertainties (e.g. faulty calibration, improper sensor placement, disturbance sources, etc). Experiment-related uncertainties can be investigated through lab scale validation studies were test are done in a controlled environment.
2. Secondly, this research does not give insight in the physical modelling errors introduced by the deliberate simplification on the model. This can be investigated by making a more detailed FEM model and comparing this with a simplified model. Finally, calibrating these models with accurate in-situ measurement results of the considered high rise building.
3. Uncertainties due to incorporation of inaccurate building and foundation information (e.g. mass, soil and stiffness properties). Investigating this uncertainty can be done by performing accurate in-situ measurements on the considered high rise building.
4. Does not give insight in processing error(s) by means of filtering data.

2.5 Case studies

The assessment procedure developed in this research is further divided into six cases. With these cases the accuracy and the influence of the discussed assumptions on the identification of damping with the EFA method can be investigated. The following six cases are introduced, all having a soil damper at the base:

1. The first case was used to determine appropriate settings for the setup of the model and check the EFA routines by introducing a single damping mechanism. The system within this case is excited by an initial displacement at the top. Data is obtained from all model nodes.
2. The second case is introduced to assess the error in which the EFA quantifies soil and structural damping separately. Rayleigh damping is introduced as structural damping in the beam. The system is excited by an initial displacement at the top. Data is obtained from all model nodes.
3. The third case is computed to determine the error with which the EFA quantifies a single damping mechanism when a reduced amount of information of the building motion is available. The system is excited by an initial displacement at the top. Data is only obtained from the top and bottom node of the beam and expanded with the use of analytical expressions of the mode shapes.
4. In the fourth case wind tunnel was introduced to assess the error in which the EFA quantifies a single damping in case of a stochastic wind loading. The system is excited by wind loading. Data is obtained from all model nodes.
5. The fifth case was used to assess the error with which the EFA quantifies soil and structural damping separately in case of a stochastic wind load. Rayleigh damping is introduced as structural damping in the beam. The system is excited by wind load. Data is obtained from all model nodes.
6. In this case an assessment was done on the identification of soil damping with a reduced amount of information on the wind load on the building by using the top wind load time series only.

In the following sections, the outline of the theory of EFA and its application to all cases is discussed in detail. To perform the EFA, the energy balance of the system needs to be set up. The general expression of the energy balance is shown in eq. 4.1.

$$\frac{dE(t)}{dt} + S(x,t)|_0^L = w_{diss}(t) + w_{ext}(t) \tag{2.1}$$

With $E(t)$ describing the energy of the system comprising the kinetic and potential energy. The energy flux $S(x,t)$ describes the energy flow over a specific boundary. The external power $w_{ext}(t)$ depends on the external loads applied on the system, and the power dissipation term $w_{diss}(t)$ is dependent of the damping in the system. With eq. 2.1 and information on the various terms, the dissipated energy can be identified. Assuming a certain damping mechanism, this dissipated energy can be used to estimate the damper value of the system.

2.5.1 Case 1 – Only soil damping

The aim of this case study is to provide insight in the identification of energy dissipation by the EFA when only rotational soil damping is introduced by means of a dashpot damper at the bottom of the system, see Figure 27. The first strategy of 2.3.1 is used to accomplish this goal.

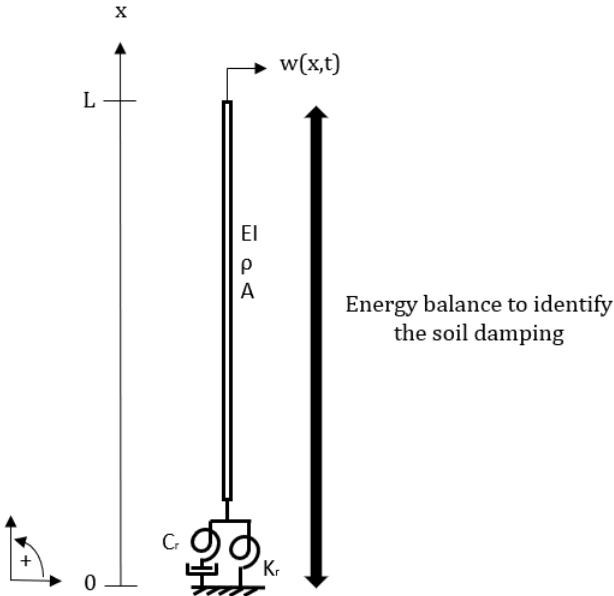


Figure 27 - Case 1. This system consists of a beam model supported by a rotational spring at the bottom. Damping is introduced by the dashpot at the bottom which mimic the rotational soil damping.

The boundaries of the system are defined at the top and the bottom of the beam. At these boundaries the energy flux is zero. This means the energy flux term $S(x,t)$ is zero and for that reason left out of the energy balance in eq. 2.1. The system is excited by an initial displacement which means that the external energy effects are equal to zero. The general energy balance belonging to this case is reduced to:

$$\frac{\partial E(t)}{\partial t} = w_{diss}(t) \tag{2.2}$$

The system is modelled as a Euler-Bernoulli beam with attached rotational spring/dashpot for the foundation. Then the energy of the system $E(t)$ comprising the kinetic and potential energy stored in the beam and in the spring can be written as:

$$E(t) = \int_0^L \frac{1}{2} \left[\underbrace{EI \left(\frac{\partial^2 w(x,t)}{\partial x^2} \right)^2}_I + \underbrace{\rho A \left(\frac{\partial w(x,t)}{\partial t} \right)^2}_{II} + \underbrace{k_r \left(\frac{\partial w(0,t)}{\partial x} \right)^2}_{III} \right] dx \quad (2.3)$$

The first term (I) describes the potential energy of the beam. The second term (II) describes the kinetic energy of the beam with ρ the mass density of the building and A the cross sectional area of the building. These values are used from available design calculations described in Chapter 4. The third term (III) describes the potential energy of the rotational spring by k_r being the rotational spring stiffness explained in Chapter 4. The rotational displacement of the spring at the bottom of the model $\left. \frac{\partial w(x,t)}{\partial x} \right|_{x=0}$ is extracted from the FEM model.

The power dissipation term which is introduced as a viscous elastic dashpot can be written as in eq. 2.4.

$$w_{diss}(t) = C_r \left(\frac{\partial^2 w(0,t)}{\partial x \partial t} \right)^2 \quad (2.4)$$

In order to identify the damping coefficient C_r , it is instrumental to compute a cumulative dissipated energy within a time period t . This can be done by integration of the energy variation eq. 2.2 as shown in eq. 2.5.

$$E(t) \Big|_{t_0}^{t_0+t} = \int_{t_0}^{t_0+t} w_{diss}(t) dt \quad (2.5)$$

Where $E(t)$ is given by eq. 2.3 and $w_{diss}(t)$ by eq. 2.4. Therefore, from eq. 2.4 and eq. 2.5, C_r can be computed as:

$$C_r = \frac{E(t) \Big|_{t_0}^{t_0+t}}{\int_{t_0}^{t_0+t} \left(\frac{\partial^2 w(0,t)}{\partial x \partial t} \right)^2 dt} \quad (2.6)$$

With these equations and the first procedure described in 2.3.1. an assessment of the error in which the energy method quantifies a single damping mechanism can be investigated.

2.5.2 Case 2 - Soil and structural damping

In this case a combination of a structural and soil damper is considered, see Figure 28. An accurate assessment of the error in which the energy method quantifies several damping mechanisms can be investigated. Insight will be gained in the separation of multiple damping mechanisms. The first strategy of 2.3.1 is used to accomplish this goal.

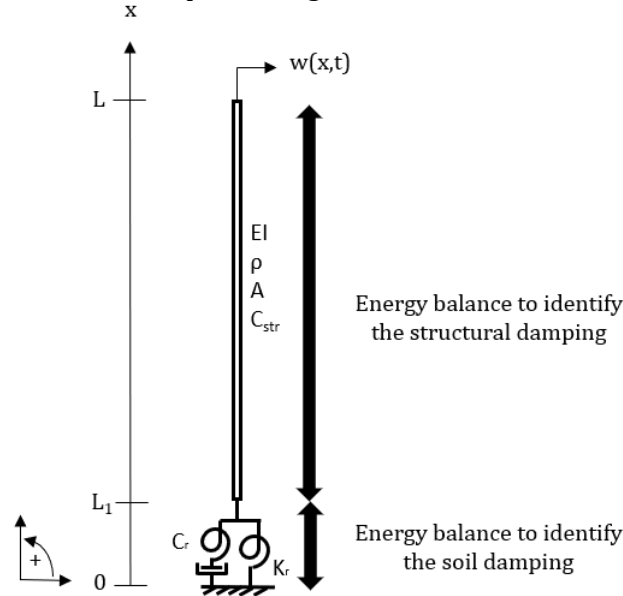


Figure 28 - Case 2. This system consists of a beam model supported by a rotational spring at the bottom. Damping is introduced by the dashpot at the bottom and by structural damping.

2.5.2.1 Energy balance to identify the structural damping

To determine the power dissipation of the structure, the energy balance is set up from the top L of the system until just above the spring and dashpot L_1 . Therefore, an energy flux is present at the bottom which contains of the energy flow towards the foundation. The energy dissipation term will represent the dissipation by means of the structural damping. This results in the following equation:

$$\frac{\partial E(t)}{\partial t} + S(x,t)|_{L_1}^L = w_{diss_str}(t) \quad (2.7)$$

With $E(t)$ describing the energy of the system comprising the kinetic and potential energy stored in the beam and leads to the following expression:

$$E(t) = \int_{L_1}^L \frac{1}{2} \left[EI \left(\frac{\partial^2 w(x,t)}{\partial x^2} \right)^2 + \rho A \left(\frac{\partial w(x,t)}{\partial t} \right)^2 \right] dx \quad (2.8)$$

Note that the potential energy stored in the rotational spring is not taken into account in this part of the energy balance explicitly. The spring energy is a part of the energy flux that flows towards the soil.

The energy flux $S(x, t)$ can be described as the energy that crosses the boundaries:

$$S(x, t) \Big|_{L_1}^L = M \frac{\partial^2 w(x, t)}{\partial x \partial t} \Big|_{L_1}^L \quad (2.9)$$

With M being the bending moment. Therefore, the energy flux is computed as the bending moment multiplied by the time rate of the rotation velocity.

The energy dissipation present in the structure can be described by the energy balance in eq. 2.7 being the unknown term in the equation. Expressing the structural damping into a damping value is difficult since there is no damper operator yet which describes the dissipated energy due to Rayleigh damping into a damping constant. However, not having an accurate operator to validate the identified structural damping, another work method is computed which gives some reliability in the identification. In order to compare the identified structural damping with a known dissipated energy, the energy dissipation due to the soil is first identified. This identified soil energy dissipation can be checked with the eq. 2.4 since the damping value of the soil is known. After that, the energy dissipation due to the soil is subtracted from the total energy dissipation that Abaqus generates. The remaining energy dissipation should be the energy dissipation due to structural damping since no other form of damping is included in the system.

2.5.2.2 *Energy balance to identify the soil damping*

In order to compute the energy dissipation of the soil, equilibrium must be found in the bottom part of the building. Therefore the energy balance is set up for the lower part of the system, which in this case is the bottom node with the attached rotational spring and dashpot. This results in the following equation:

$$\frac{\partial E(t)}{\partial t} - S(x, t) \Big|_0^{L_1} = w_{diss_soil}(t) \quad (2.10)$$

The energy $E(t)$ in this system comprises the potential energy in the spring.

$$E(t) = \frac{1}{2} k_r \left(\frac{\partial w(0, t)}{\partial x} \right)^2 \quad (2.11)$$

The energy flux $S(x, t)$ is the energy flow from the superstructure towards the foundation and consists in theory of the Kelvin-Voigt model comprises a spring in parallel with a dashpot. This means that the energy flux can also be expressed as the summation of the bending moments due to the spring and damper, as stated in eq. (2.13).

$$S(x, t) \Big|_0^{L_1} = M \frac{\partial^2 w(x, t)}{\partial x \partial t} \Big|_0^{L_1} = k_r \frac{\partial w(x, t)}{\partial x} \frac{\partial^2 w(x, t)}{\partial x \partial t} + C_r \left(\frac{\partial^2 w(x, t)}{\partial x \partial t} \right)^2 \Big|_0^{L_1} \quad (2.12)$$

The power dissipated term can be written as eq. 2.4.

The energy dissipation is computed cumulative.

$$E(t)|_{t_0}^{t_0+t} - \int_{t_0}^{t_0+t} S(x,t)|_0^{L_1} dt = \int_{t_0}^{t_0+t} w_{diss_soil}(t)dt \quad (2.13)$$

And can be used to identify the damper value:

$$C_r = \frac{E(t)|_{t_0}^{t_0+t} - \int_{t_0}^{t_0+t} S(x,t)|_0^{L_1} dt}{\int_{t_0}^{t_0+t} \left(\frac{\partial^2 w(0,t)}{\partial x \partial t} \right)^2 dt} \quad (2.14)$$

2.5.3 Case 3 - Reduced information with only soil damping

In this case the amount of information extracted from the FEM model is reduced. An accurate assessment of the error in which the energy method quantifies a single damping mechanism when a reduced amount of information is available can be investigated with this case. The equations described in 2.5.1 Case 1 are applicable since the energy balance does not change. The analysis procedure of the FEM model is described in 2.3.1.

2.5.4 Case 4 - Only soil damping with wind load

Within this case wind tunnel data is introduced to the FEM model. An accurate assessment of the error in which the energy method quantifies a single damping mechanism when all information available can be investigated with this case. The energy balance described in 2.5.2.2. to identify the soil damper can be used for this case. The energy flux implicitly involves the influence of the wind load. Comparing this case with case 1 gives insight in what the influence of wind load is on the identification of the soil damping. The analysis procedure of the data from the FEM model is described in 2.3.3.

2.5.5 Case 5 - Structural and soil damping with wind load

In this case a combination of a structural and soil damper is considered. An accurate assessment of the error in which the energy method quantifies several damping mechanisms can be investigated. Insight will be gained in the separation of multiple damping mechanisms and the influence of wind load. The strategy of 2.3.3 is used to accomplish this goal and the equations of 2.5.2.2. are used for identification of soil damping. The energy flux implicitly involves the influence of the wind load. However, the identification of the energy dissipation of the structure is different since external power due to wind must be taken into account.

So, the equation in Case 4 (energy balance to identify the structural damping) can be applied again but now with adding the external work due to wind. This results in the following energy balance for the identification of structural damping:

$$\frac{\partial E(t)}{\partial t} + S(x,t)|_{L_1}^L = w_{diss_str}(t) + w_{ext}(t) \quad (2.15)$$

The determination of $E(t)$ describing the energy of the system and the energy flux $S(x, t)$ remain the same as in eq. 2.8 and eq. 2.9. The external power due to wind can be calculated by:

$$w_{ext}(t) = \int_0^L f_w(x, t) \frac{\partial w(x, t)}{\partial t} dx \quad (2.16)$$

With $p(x, t)$ being the distributed wind load in space and time determined by the wind tunnel data and applied in the FEM model. This distributed load is calculated by:

$$p(x, t) = \frac{1}{2} \rho_{air} v_{ref, h}^2 c_p(x, t) c_{fs/wt} \quad (2.17)$$

Where:

ρ_{air} = Air density

$v_{ref, h}$ = Wind velocity at reference height

c_p = Pressure coefficient

$c_{fs/wt}$ = correction of the building width

The wind load is further discretized and applied to the FEM model.

2.5.6 Case 6 – Reduced wind information with only soil damping

The amount of information processed to determine the wind load along the beam will be reduced by using the top wind load time series only. This wind load over time is introduced to the FEM model by using it on all the nodes. The equations of case 4 are valid for this case and the procedure described in 2.3.3 is used.

3 Wind load

3.1 Introduction

Wind loads are the result of the interaction between the wind in the atmospheric boundary layer and a building. There are numerous factors that have an influence on the magnitude of the wind loads. Davenport [25] described the calculation and assessment of the wind load on a structure as a chain of links consisting of the wind climate, terrain characteristics, the building aerodynamics, the structural properties and behaviour, and the criteria to assess the acceptability of certain loads and load effects. This wind loading chain is visualized in Figure 29. The parameters in the figure are the ones used in EN 1991-1-4 [4] to determine the wind loads on a structure.



Figure 29 - Davenport wind loading chain

This chapter first gives a qualitative explanation of the various links in the wind loading chain started with the nature of wind. Second, the determination of the wind velocity and the assumptions made with the Eurocode are explained. Finally, pressure coefficient time series of the high-rise building model are determined with data from a wind tunnel experiment on a high-rise building model with approximately the same shape as the high-rise building model used in this study. These pressure coefficients are combined with the wind velocity calculated with the Eurocode to obtain load time series that are applied on the FEM model.

3.2 Wind loading chain

3.2.1 Wind climate

Wind is defined by the meteorological phenomena that occur in the earth's atmosphere due to the solar radiation. Solar radiation gives rise to temperature and pressure fields that are responsible for the displacement of air masses. The earth is warmed by the sun and the atmosphere return the received energy by thermal radiation. The lowest atmospheric layer immediately next to the principal heat source, i.e. land masses, retains higher amounts of heat, giving rise to a vertical profile of the mean temperature value T . As shown the mean temperature decreases approximately linearly with respect to height z .

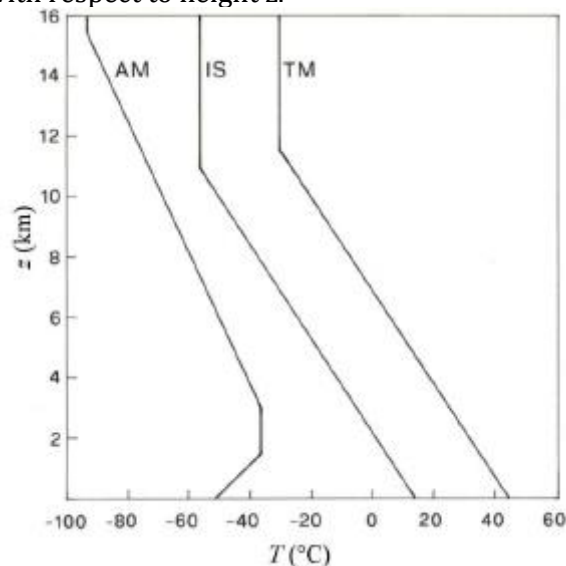


Figure 30 - Mean vertical profiles of atmospheric temperature. (TM: Tropical Maximum, IS: Average terrestrial temperature, AM: Arctic Minimum) [26].

The difference between energy received and energy emitted by the earth-atmosphere system varies mainly in accordance with the different angle of the sun with respect to the horizon, which results in the highest radiation levels in tropical-equatorial regions and the minimum radiation levels at the poles.

If the temperature were unaffected, air would circulate in each hemisphere in accordance with a single cell running from the pole to equator, see Figure 31. But the uneven distribution of the earth surface, causes the formation of a sub-tropical high-pressure belt and of a sub-polar low-pressure belt. This leads to a tricellular circulation system in each hemisphere as shown in Figure 31.

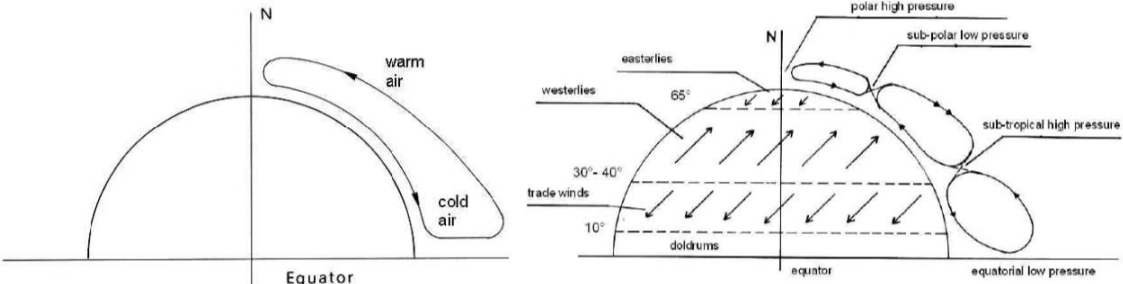


Figure 31 - (left) air circulate with a single cell running from the pole to equator. (right) tricellular circulation system caused by distribution of the earth surface [26].

3.2.2 Influence of the terrain

In Figure 32 a section is considered which illustrates an instantaneous profile of the wind velocity near the surface of the earth. Figure 32 shows that the wind velocity near the earth’s surface has a turbulent, fluctuating nature. This can be divided in two velocity components, namely the mean wind velocity and the fluctuations. Both the mean velocity and the fluctuations are affected by the ground friction, as can be seen in Figure 33. The gradient height is defined as the height z_g above which the wind is no longer affected by the ground friction force. This height depends on the wind velocity and on the roughness length of the terrain, which is expressed by a roughness parameter z_0 . The atmosphere between the earth surface and the gradient height is denoted as atmospheric boundary layer. The area above the gradient height is called free atmosphere.

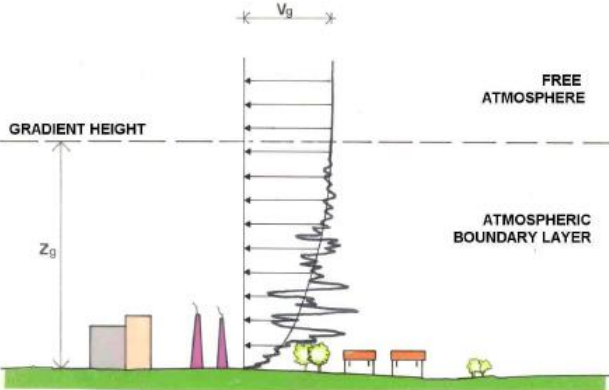


Figure 32 - Mean wind velocity and atmospheric turbulence profile [26].

The influence of the different terrains and their impact on the wind properties near the earth's surface are shown in Figure 33.

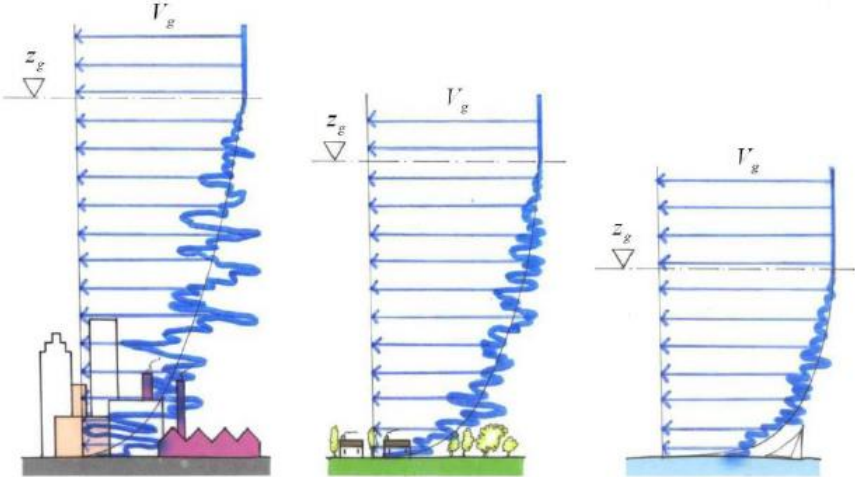


Figure 33 - profiles of mean wind velocity over different terrain types [26].

Several factors that influence the wind characteristics within the ABL are:

- Atmospheric instabilities
- The roughness of the upwind terrain
- The terrain orography
- The effect of neighbouring structures

In the Eurocode the influence of the roughness and the height of the terrain are accounted for with a roughness factor, see section 3.4.

3.2.3 Building aerodynamics - pressure coefficient

The aerodynamic pressure coefficients are defined as the ratio between the local mean or peak pressure measured at the façade and the dynamic wind pressure q in front of the façade. They vary for every location on the building's façade and depend on the type of flow around the building, see Figure 34.

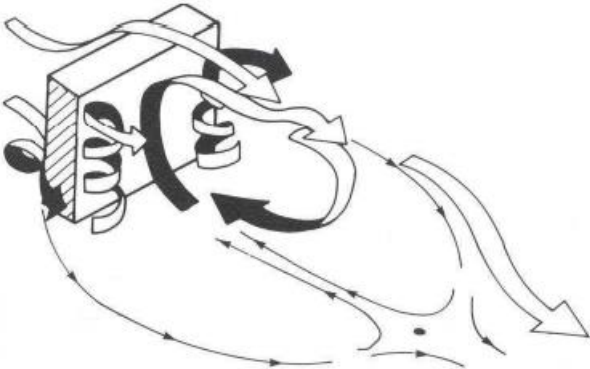


Figure 34 - Three-dimensional body in a wind field [26].

Pressure coefficient are generally not determined for every point on the façade, but they are assumed to have a constant value over a certain area A_{ref} . Peak pressures are not found simultaneously at all locations on the building. Therefore the pressure coefficient contains a space-averaging effect for considered A_{ref} . Where at one point on a larger façade element a large pressure is present, at other locations a lower pressure will be found. This lack of correlation

between pressures at different locations on the building façade results in a lower pressure coefficient for a larger A_{ref} . Pressure coefficients also depend on the averaging time considered. The load duration is very important in the field of wind loading, as the largest peaks have very short durations. Therefore the pressure coefficients for larger duration will be smaller than the coefficients for short duration peaks.

3.2.4 *Structural response*

Davenport [25] turned to structural dynamics and random vibration theory to describe the global wind-induced loads and the structural response, which is summarized in Figure 35.

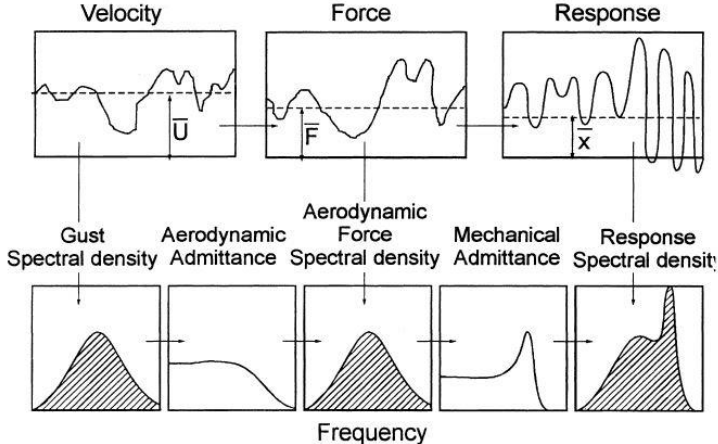


Figure 35 - Davenport's random vibration approach for the wind-induced response of buildings and structures [25]

The response (the top right plot in Figure 35) can be divided in a mean response and a fluctuating response. The fluctuating response is strongly dependent on the natural frequency and damping of a structure. When structures have low natural frequencies and low damping, the fluctuating wind velocities may cause resonant vibrations of the structure. This becomes more significant in taller and more slender structures. The effect of the natural frequency of a structure on the response has been visualized by Holmes [27] in Figure 36.

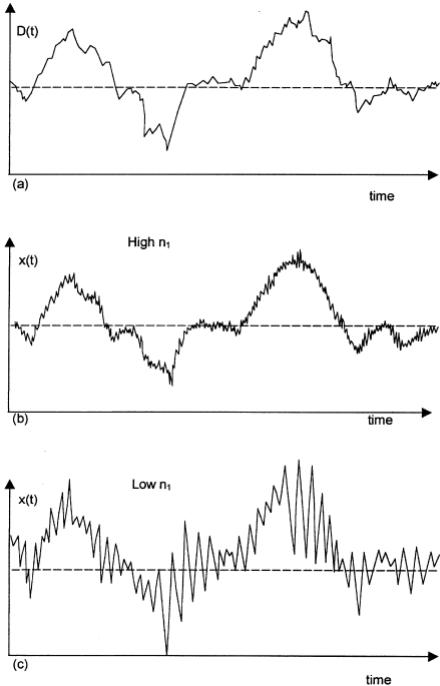


Figure 36- Time histories of: (a) wind force, (b) response of a structure with a high natural frequency and (c) response of a structure with a low natural frequency.

3.3 Determination of the basic wind velocity

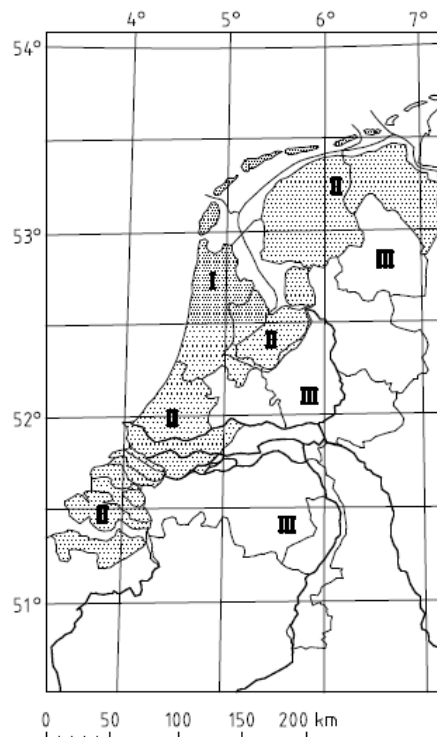
The wind load on a building depends on the wind velocity. A higher wind velocity produces a higher pressure, and thus higher loads. The Eurocode describes a method in which the wind velocity can be determined. This method starts with the calculation of the basic wind velocity:

$$v_b = c_{dir} \cdot c_{season} \cdot c_{prob} \cdot v_{b,0} \quad (3.1)$$

The parameters in eq. 3.1 will be briefly discussed below.

Fundamental basic wind velocity $v_{b,0}$:

The fundamental basic wind velocity $v_{b,0}$ is the characteristic 10 minutes mean wind velocity, irrespective of wind direction and time of year, at 10 m above ground level in open country terrain (terrain category II). The characteristic value has a reference period of 50 years. The values for the fundamental basic wind velocity are given in the National Annex of each country. In the Dutch National Annex three wind areas are distinguished. The wind velocities belonging to these wind areas are given in Table 3.



Wind area	I	II	III
$v_{b,0}$ [m/s]	29.5	27.0	24.5

Table 3 - Fundamental basic wind velocity in the Dutch National Annex

Directional factor c_{dir} :

c_{dir} accounts for wind directionality. The directional factor is defined as the ratio between the characteristic wind velocity within a certain direction and the characteristic wind velocity irrespective of wind direction. The value of the wind direction is given for different wind directions in the National annex. The recommended value is 1.0.

Seasonal factor c_{season} :

c_{season} depends on the season which the structure is designed for. This is particularly important for temporary structures or structures in the construction phase. $c_{season} = 1$ is recommended and this value is considered normative for Dutch design purposes.

Probability factor c_{prob} :

If the design life of the structure is less or more than 50 years, this should be accounted for with the probability factor c_{prob} . For the assessment of the impact of human comfort in buildings the reference period is 1 year. This means that the fundamental basic wind velocity needs to be adjusted by introducing the probability factor:

$$c_{prob} = \left(\frac{1 - K \ln(-\ln(1-p))}{1 - K \ln(-\ln(0.98))} \right)^n \quad (3.2)$$

With:

- K = is the shape parameter depending on the coefficient of variation of the distribution of the extreme values. Recommended value is 0.2
 n = is the exponent. Recommended value is 0.5

See Appendix B for the full calculation of the basic wind velocity used for the cases in this research.

3.4 Determination of the mean wind velocity

The influence of the roughness and the height of the terrain are introduced by determining the mean wind velocity. The mean wind velocity at reference height being the top of the building is defined by:

$$v_m(z) = c_r(z) \cdot c_o(z) \cdot v_b \quad (3.3)$$

The parameters in eq. 3.3 will be briefly discussed below.

Roughness factor $c_r(z)$

The roughness factor accounts for the change of the mean wind velocity with height above ground. This change is dependent on the ground roughness upstream of the structure. Where the basic wind velocity belongs to a height of 10 m above ground, the roughness factor corrects for the profile of the mean wind speed with height z . The basic wind velocity is defined for terrain category II with roughness length $z_{0,II} = 0.05$ m, so the roughness factor also corrects for different terrain categories. The roughness factor is defined by:

$$c_r(z) = k_r \ln \left(\frac{h}{z_0} \right) = 0.19 \left(\frac{z_0}{z_{0,II}} \right) \ln \left(\frac{h}{z_0} \right) \quad (3.4)$$

Where:

- k_r = Terrain factor depending on roughness length z_0
 h = Reference height of the building
 z_0 = Roughness length
 $z_{0,II}$ = Reference roughness length (terrain category II in EN1991-1-4): 0.05m

Orography factor $c_0(z)$

Terrain orography, like hills and cliffs, can increase the mean wind velocity considerably. Therefore when relevant this effect has to be taken into account by the orography factor. This effect can be considered negligible when the slope of the upwind terrain is less than 3° . The terrain orography is set to $c_0(z) = 1.0$.

3.5 Determination of the full scale pressure by using wind tunnel measurement data

For the derivation of the pressure coefficients wind tunnel measurement data is used from the study by La Gasse [28]. Below will be explained what the starting points were for the used study and how this data was made usable for this research.

3.5.1 Case study building

The wind tunnel measurements were performed for a non-existing high-rise building, see Figure 37. The case study building has a rectangular plan of 30x30m and a height of 120m. The building is assumed to be in wind area II in the Netherlands, in an urban environment with a terrain roughness of 0.8 m.

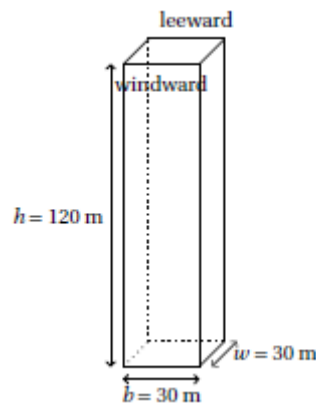


Figure 37 - Case Study building [28]

3.5.2 Wind tunnel data

For the derivation of the load coefficients, pressure measurements are used from the open-circuit atmospheric boundary layer wind tunnel of TNO. According to La Gasse [28] the raw measurement data were determined following the CUR 103 guidelines. For this wind tunnel measurement a static wooden building model was used with geometric scale $\lambda_g = 1:250$. For the terrain roughness a full scale roughness length $z_0 = 0.8 \text{ m}$ was used; the roughness applied in the wind tunnel had a roughness length of 3.2 mm.

88 pressure taps were distributed across the windward, leeward and top face of the building model. The measurements from the top face taps are not used in this study. An overview of the distribution of the pressure taps is shown in Figure 38.

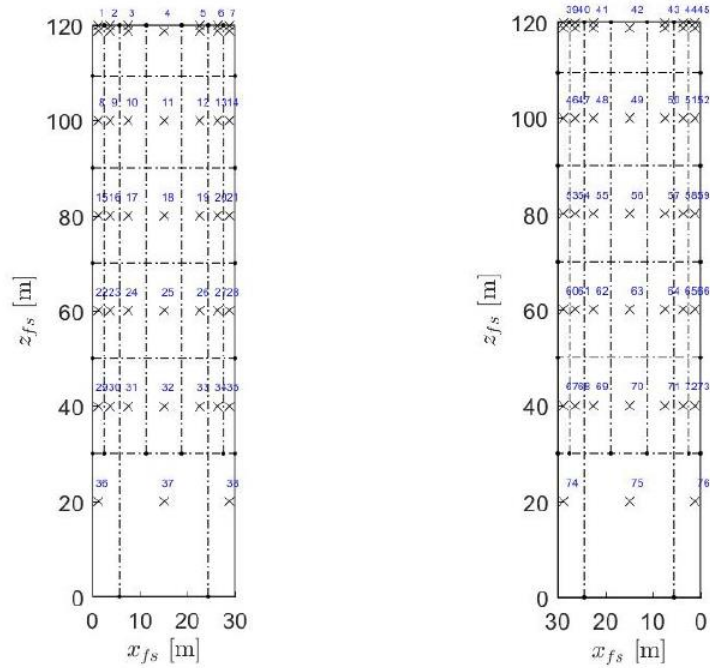


Figure 38 -86 pressure taps are distributed across the windward[1:38] and leeward[39:76] of the building model. [28]

Data is generated for different durations and angles of attack. For this research a section of the long run measurements of the windward and leeward is used which have an angle of attack of 0° . Details of the wind tunnel test are summarized in Table 4. For further information see the report of La Gasse [28].

Wind tunnel and incident flow	Dimensions wind tunnel	13.5x3x2 m
	ρ_{air}	1.225 kg/m ³
	$v_{\text{ref,h}}$	14.5 m/s
Scaled model	Dimensions	0.48x0.12m
	Scale λ_g	1:250
	Taps	[1:38] windward; [39:76] leeward; [77;86]top;[87,88] reference
Test	Sampling duration	\approx 94 min
	Full-scale duration	\approx 176 hr
	Angle of attack	Frontal, 0°
	Sampling frequency	400 Hz

Table 4 - Wind tunnel and measurement data details

3.5.3 Average pressure distribution over the building width

As shown in Figure 39 there are multiple pressure taps over the width of the high-rise building at several heights. Every tap represent a the pressure for the area of the pressure tap (indicated with dashed lines in Figure 38). Since a simple beam model is analysed in FEM, the load can only be varied along the height-axis of the building. Therefore, the pressure measurements along the width are averaged as shown in Figure 39. According to La Gasse [28] this simplification is justified when only along wind response is considered, which is the case in this study.

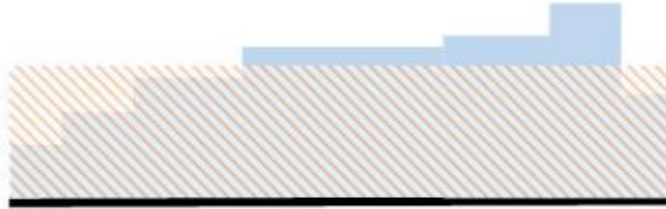


Figure 39 - Measured pressure distribution and averaged distribution [28]

3.5.4 Pressure distribution over the building height

As shown in Figure 38 there are pressure taps at six heights. To assess the influence of reduced wind load information on the identification of damping, a load model is needed which consists of wind loads at every node location along the height of the FEM model. Therefore new data points within the range of the discrete set of known data points need to be constructed. Linear interpolation is used for every timeframe of the wind tunnel data set. Figure 40 shows a plot of timeframe 160. The red dots represent the pressure values from the wind tunnel measurement and the blue line are the new constructed data. This was done at windward and leeward side of the building model for every timeframe.

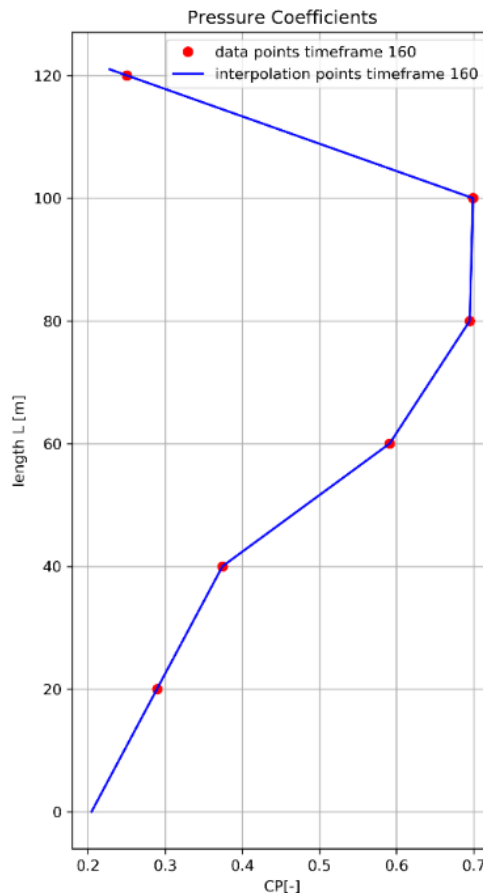


Figure 40 - Distribution of the pressure coefficients at timeframe 160. red points: data from wind tunnel measurement. blue: constructed new data by linear interpolation

3.5.5 *Full scale versus wind tunnel*

The pressure coefficients must be converted to full scale pressures that can be used for the FEM model. Guidelines have been developed for wind tunnel tests in which the minimum requirements for the development of flows representative of the wind over different types of terrain are given. (WTG,1995, ASCE, 1996). These requirements imply that the following equalities should be satisfied. The subscript WT means wind tunnel and FS means full scale.

Equation 3.5 is also known as the Jensen number similarity (Jensen,1958). It describes the similarity condition which ensures that the ratio between height and roughness length in the wind tunnel and in full scale are the same:

$$\left(\frac{H}{z_0} \right)_{WT} = \left(\frac{H}{z_0} \right)_{FS} \quad (3.5)$$

Equation 3.6 describes the similarity of the immersion ratio. It describes the similarity condition which account for the height and its gradient height of both models.

$$\left(\frac{H}{z_g} \right)_{WT} = \left(\frac{H}{z_g} \right)_{FS} \quad (3.6)$$

The third equality describes the similarity between the integral length scale.

$$\left(\frac{H}{L_{ux}} \right)_{WT} = \left(\frac{H}{L_{ux}} \right)_{FS} \quad (3.7)$$

The relation between the time scale t , wind velocity at building height $u_m(H)$ and building height H of the model and full scale is given by:

$$\left(\frac{tu_m(H)}{H} \right)_{FS} = \left(\frac{tu_m(H)}{H} \right)_{WT} \quad (3.8)$$

The time scale of the wind tunnel experiment corresponds to the full scale time scale, scaled by the geometric scale and the velocity scale:

$$t_{WT} = \frac{H_{WT}}{H_{FS}} \frac{u_m(H)_{WT}}{u_m(H)_{FS}} t_{FS} \quad (3.9)$$

See Appendix B for the calculation of the similarity conditions and the final applied time scale.

3.5.6 The full scale pressures

The pressure coefficients are converted to full scale pressures. By combining these pressure coefficients with the air density and the mean wind velocity at reference height, full-scale pressures can be given by:

$$p(x,t) = \frac{1}{2} \rho_{air} v_m^2(z) c_p(x,t) \quad (3.10)$$

Where:

- p = Distributed load
- ρ_{air} = Air density
- v_m = Mean wind velocity at reference height
- c_p = Pressure coefficient over time

The pressure coefficient is determined for every node in the FEM model and used as input file in Abaqus. See Figure 41 for the pressure coefficient at a height of 60 m. The amount of data is reduced to a timeseries of 120 seconds.

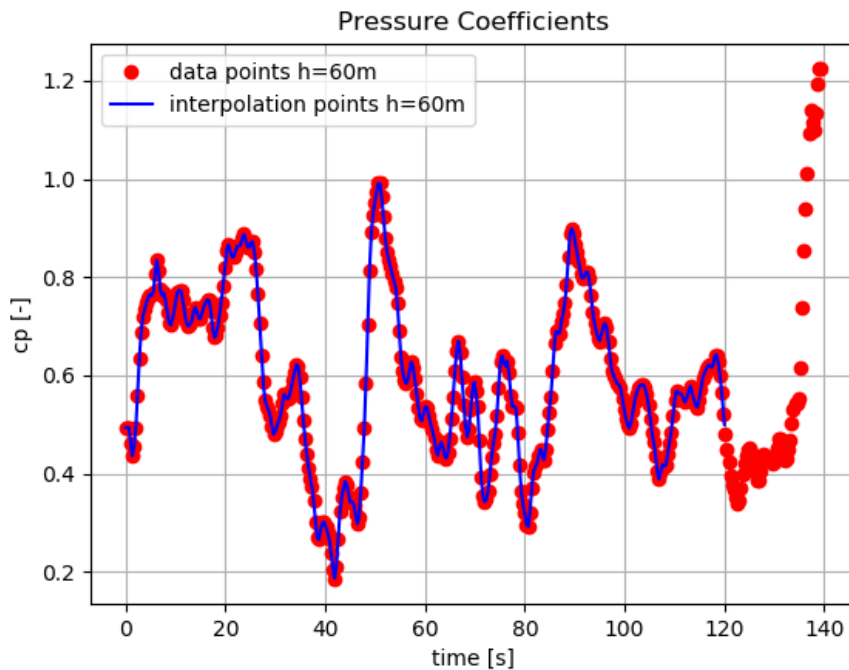


Figure 41 - Pressure coefficient obtained from wind tunnel data at a height of 60m. Wind data is extrapolated to fit the time serie in the Abaqus model.

4 Building Case and FEM modelling

4.1 Introduction – New Erasmus Medical Centre

The New Erasmus Medical Centre (NEMC) in Rotterdam is used as case study to investigate the EFA in a realistic situation. The NEMC is a high-rise building with a rectangular base and a height of 121 meters. The stability of the building is provided by a combination of a concrete core and a façade concrete tube. The lower part of the concrete core is made in-situ, while the upper part of the core, tube and floors are made out of prefabricated concrete. The wind induced loads are transferred from the façade tube to the foundation. But also by the concrete core transferred by the floors to the core to the foundation. Figure 42 shows a section of the building and the floor plan. Table 5 gives the dimensions and mass of the building.

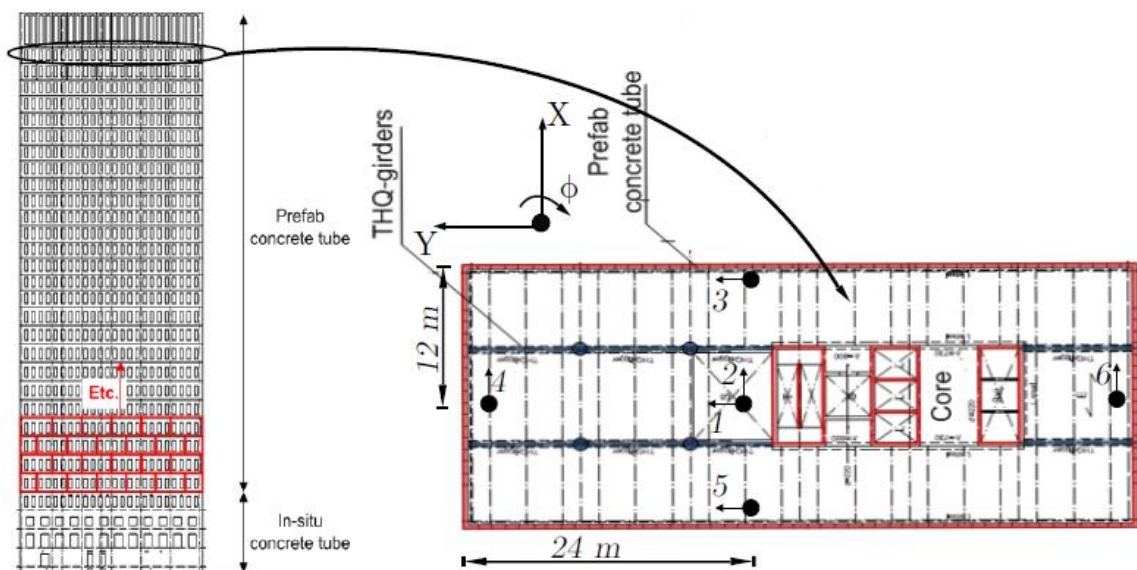


Figure 42 - NEMC layout, instrumentation set-up [3]

Parameters		value	unit
Building height		121	m
Building width		45	m
Building depth		21	m
Building mass		4.57E+07	kg
Building mass density		400	kg/m ³

Table 5 - parameters NEMC used in the FE model

4.2 Finite Element Modelling

Abaqus is designed as a flexible tool for finite element modelling (FEM). An important aspect of this flexibility is the manner in which Abaqus allows the user to step through the history to be analysed. This is accomplished by defining analysis procedures. In this section the FEM model used in this research, and how it is been modelled per module is explained. Knowledge is gained from the *Abaqus manual 6.14*.

For this research the New Erasmus Medical Centre (NEMC) in Rotterdam is used as case study to investigate the EFA in a realistic situation. Simplified modelling options are taken into consideration, for it is the goal to apply the EFA method on a realistic case with realistic values of damping and not to exactly numerically model the structural behaviour of the building. Geometrical, material and soil properties assumptions defined on structural design calculations made available to the author by TNO are used. The NEMC building is simplified and modelled as a continuous beam supported by a parallel system which consist of an idealized spring and dashpot representing the rotational behaviour of an elastic half-space, see Figure 43.

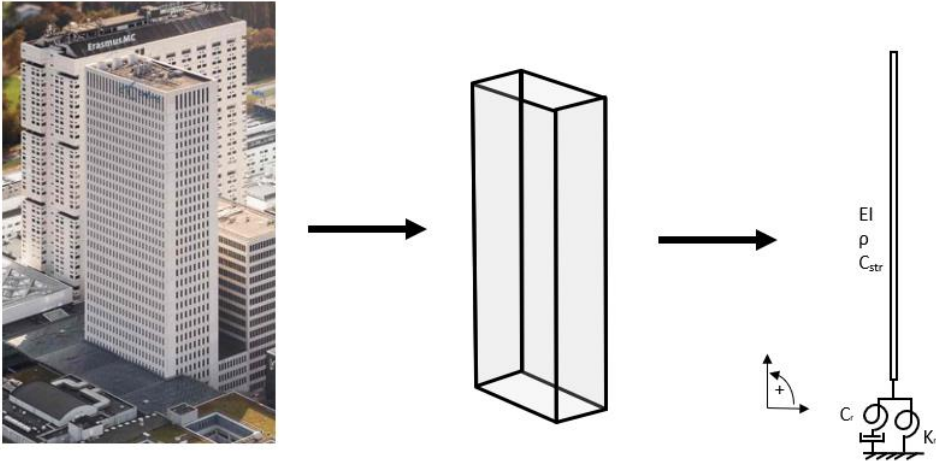


Figure 43 - Simplification of the case study. Using geometrical and material assumptions defined on structural design calculations. The model contains a continuous beam model supported by a parallel system which consists of an idealized spring and dashpot.

The geometry is defined with a rectangular profile $b \times d = 45 \times 21 \text{ m}$ with a length of 121 m. To this profile linear elastic material properties are assigned which are presented in Table 6:

Components	Parameter	Value	Unit
Concrete continuous model (B33 elements)	Modulus of Elasticity	6e+8	N/m ²
	Poisson's ratio	0.3	[-]
	Density	400	kg/m ³
	Damping (beta)	0.013*	[-]

Table 6 - Material properties of the model

*Only active in the cases 2 and 5.

In the 'Step'-module the analyses are defined. In total three analysis procedures were used which are:

- Frequency (Linear perturbation); For this research Lanczos solver is used to determine the eigenvalues. Abaqus offers two approaches for eigenvalue extraction procedures for symmetrized eigenproblems: Lanczos and Subspace Iteration methods. In general the Subspace Iteration method is used for eigenvalue analysis for FE systems with large

matrix systems and more complex systems. Lanczos method is adopted for relatively simpler structures to study the lower modes which is sufficient for this research.

- Static (General); This procedure is defined for the cases 1,2 and 3 to introduce the initial displacement at the top of the beam. The initial condition is introduced by defining a boundary condition at the top with a displacement of 0.5m for 2 seconds of the simulation. After the 2 seconds, this analysis is turned inactive and the dynamic, implicit procedure is started. For the cases 4,5 and 6 the static procedure is removed from the model because wind load is introduced to the model.
- Dynamic, Implicit (General); Dynamic implicit calculation based on Newmark-beta method to solve the differential equations of motion. A fixed time increment size is used for these simulations. Fixing the time increment size was needed for the energy flow analysis integration. A fixed time step can cause instability in which Abaqus will not automatically correct. Therefore, a time increment size of 0.01 is used. The total simulation time of 30 seconds for case 1, 2 and 3 is used. For case 4, 5 and 6 a simulation time of 120 seconds is used.

In the *'Interaction'*-module the dashpot and spring are attached to the continuous model at the bottom node of the model. For the 6th degree of freedom, describing the rotation about the z axis, a dashpot coefficient $6.60e+11$ Nms/rad and a spring stiffness $5.94e+12$ Nm/rad are used.

In the *'Load'*-module the loads applied to the model are defined. The wind loads for cases 4, 5 are applied by defining for every node an unique CSV-file with the associated timeseries dependent on the pressure coefficients determined in Chapter 3.

At last the *'Mesh'*-module is defined. The beam model is meshed homogeneously. The following mesh sizes were analysed: 1 m, 0.5 m, 0.25 m and 0.1m, see section 4.7. A mesh size of 0.25m is further used for the analysis.

4.3 Determination of the foundation properties

The resistance and the dissipation capacities of the ground should be quantified. These values can be computed via analytical expressions or with numerical software based on the soil characteristics. Gomez implemented the cone model by Wolf and compared the results with a numerical software package Dynapile to study the reliability. In this research the double cone model by Wolf was also used for the determination of the soil properties.

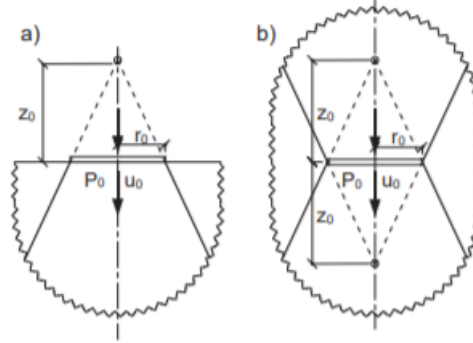


Figure 44 - a) Disk with corresponding cone model. b) Disk embedded in homogeneous full-space with double-cone model [29].

The double cone model by Wolf calculates the soil stiffness properties with:

$$k_x = \frac{2\rho_s V_s^2 \pi r_0}{z_{0,x}} \quad (4.1)$$

$$k_r = \frac{2 \cdot 3 \rho_s V_p^2 I_0}{z_{0,r}} \quad (4.2)$$

Where ρ_s , V_s and V_p are respectively the soil density and the shear and pressure wave velocity.

The equivalent radius r_0 is computed from the foundation area with:

$$r_0 = \sqrt{\frac{2b \cdot 2l}{\pi}} \quad (4.3)$$

Where $2b$ and $2l$ are respectively the width and length of the foundation. The moment of inertia I_0 is computed with:

$$I_0 = \frac{\pi r_0^4}{4} \quad (4.4)$$

The apex height $z_{0,x}$ and $z_{0,r}$ are computed with:

$$z_{0,x} = \frac{1}{32} \frac{7-8\nu}{1-\nu} \pi r_0 \quad (4.5)$$

$$z_{0,r} = \frac{9}{128} \frac{3-4\nu}{1-\nu} \frac{2(1-\nu)}{1-2\nu} \pi r_0 \quad (4.6)$$

Within the case studies only rocking soil stiffness and damping is considered. Research had shown that the contribution of rocking damping to the system is dominant compared with horizontal soil stiffness and damping [30]. In the Abaqus model the rotational stiffness and the rotational soil damper are defined as spring and dashpot that exhibit the same linear behaviour acting in parallel. The connectivity type 'connect points to ground' is used in Abaqus.

With the above procedure the following values are determined:

Rotational damper value	1.32e+11 Nms/rad
Rotational spring stiffness	5.94e+12 Nm/rad

4.4 Determination of beam model

In order to derive the equations needed for the energy flow analysis, a realistic beam model needs to be chosen to describe the dynamic behaviour of the system. The classical beam theory based on the Euler Bernouli beam model does not take into account the shear deformation or rotary inertia. Rotary inertia is the inertia associated with local rotation of the beam cross section during flexural deformation. Therefore, the impact of the shear stiffness of the building on the first eigenfrequency is analysed.

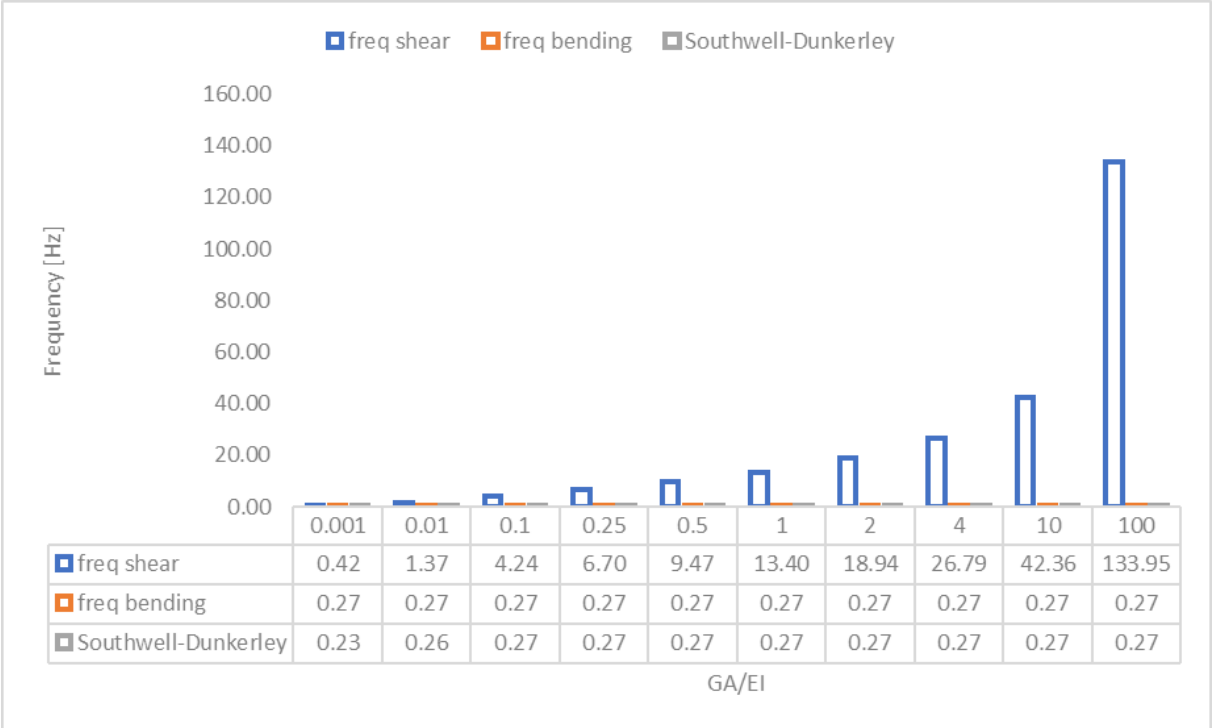


Figure 45 - Analysis of the impact of the shear stiffness of the building on the first eigen frequency

Figure 45 shows the shear and flexure eigenfrequency calculated separately. These eigenfrequencies are parallel coupled to determine the total eigen frequency by using the Southwell-Dunkerley equation:

$$\frac{1}{f^2} = \frac{1}{f_f^2} + \frac{1}{f_s^2} \tag{4.7}$$

With f_f being the flexure eigen frequency and f_s being the shear eigen frequency. From this figure it can be concluded that systems with a high shear/flexure stiffness ratio (describing slender beams) are dominated by the flexural behavior. not influenced by the shear behavior of the system. However, the eigenfrequency of systems with a low shear/bending stiffness ratio (for example low rise buildings) are influenced by the shear behavior. Considering the NEMC building a ratio of 0.01 is found. The first natural frequency is barely influenced by the contribution of the shear deflection (2%).

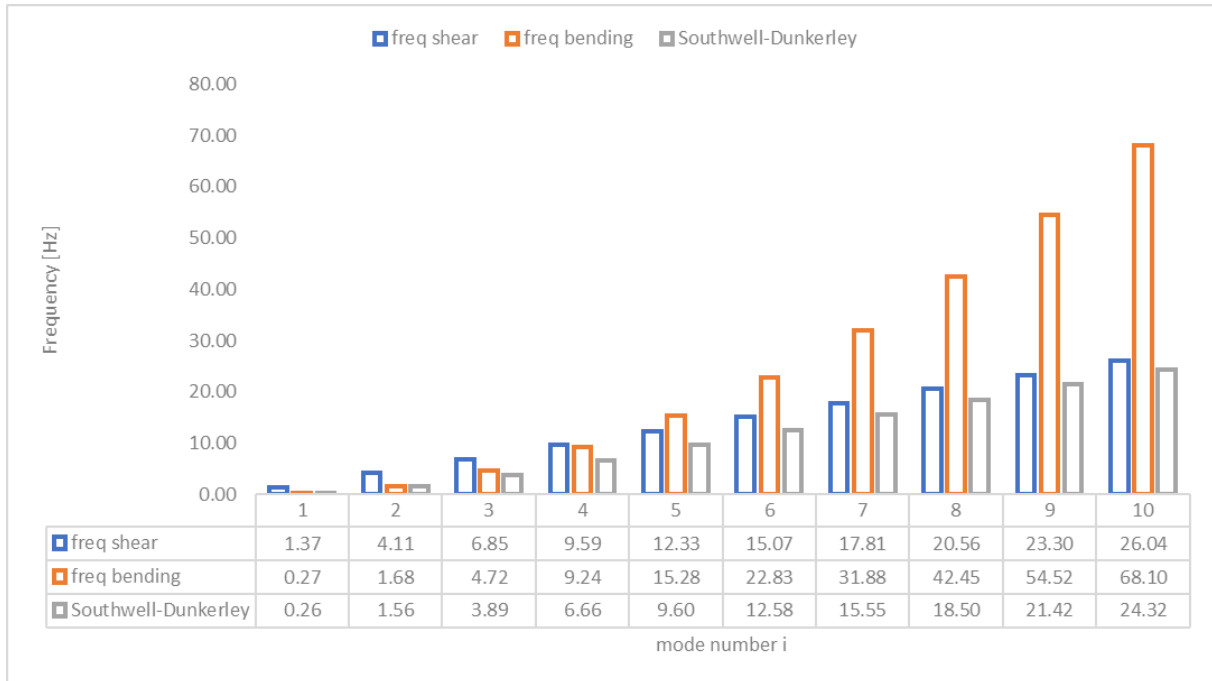


Figure 46 - Analysis of the impact of shear stiffness of the building on the higher modes

However shear deformation can be important in the higher modes of slender beams. Figure 46 shows the impact of the shear frequency on higher modes. From this figure we can conclude that the contribution due to shear is more noticeable for higher frequencies as the wavelength becomes shorter.

For this research the Euler Bernouli beam model is used which neglected shear deformations. From the results in Figure 45 it can be stated that the first natural frequency is barely influenced by the contribution of the shear deflection. The contribution due to shear is more noticeable for higher frequencies as shown in Figure 46.

4.5 Structural versus Soil damping

In this section the impact of the structural and soil damping applied to the model are investigated. Structural damping, which represent the damping in the main bearing structure is introduced by means of Rayleigh damping. First a realistic value for the structural damping needs to be determined. This is done by using the Jeary damping estimator:

$$\xi_{Jeary} = 0.01f_n + 10\sqrt{D/2} x / H + 0.0015 \quad (4.8)$$

Using the Jeary damping estimator results in a damping ratio of the structure of 0.50%. Rayleigh damping describes the damping matrix by a linear combination of the mass and stiffness matrices:

$$[C] = \alpha[M] + \beta[K] \quad (4.9)$$

Where α and β are the constants selected to achieve the desired damping ratio at two preselected frequencies. The damping ratio for the n-th mode of vibration is then given by:

$$\zeta_n = \frac{1}{2\omega_n} \alpha + \frac{\omega_n}{2} \beta \quad (4.10)$$

Substituting the damping ratio of 0.50% and the first two natural frequencies based on the clamped system, resulted in a β value of 0.013 [-]. The α value is equal to zero. Applying the structural damping on the clamped system resulted in Figure 47.

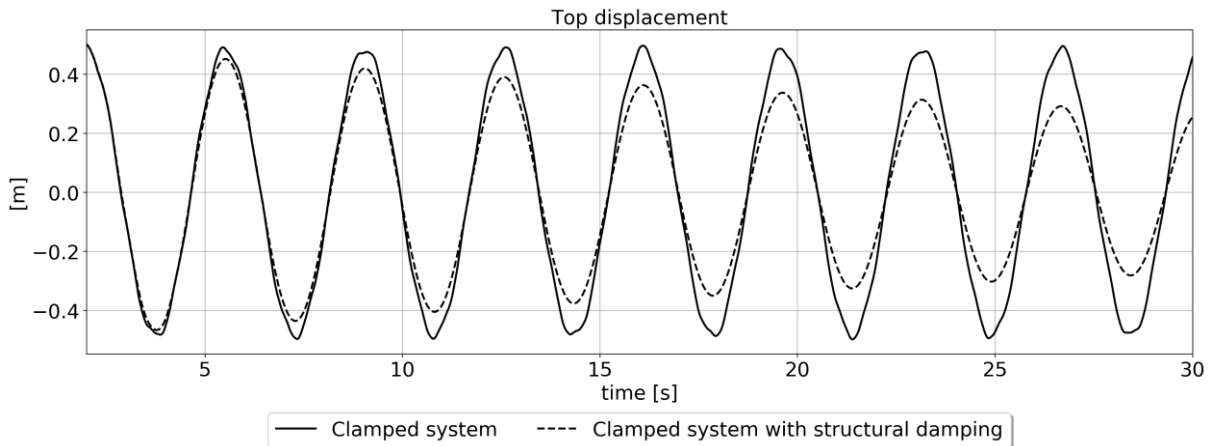


Figure 47 - Clamped system and the applied structural damping

As can be seen, the applied structural damping results in a decay of the amplitude. Applying the logarithmic decrement method on the computed signal gives a damping ratio of 0.43%, which is slightly lower than the implemented value of 0.50%.

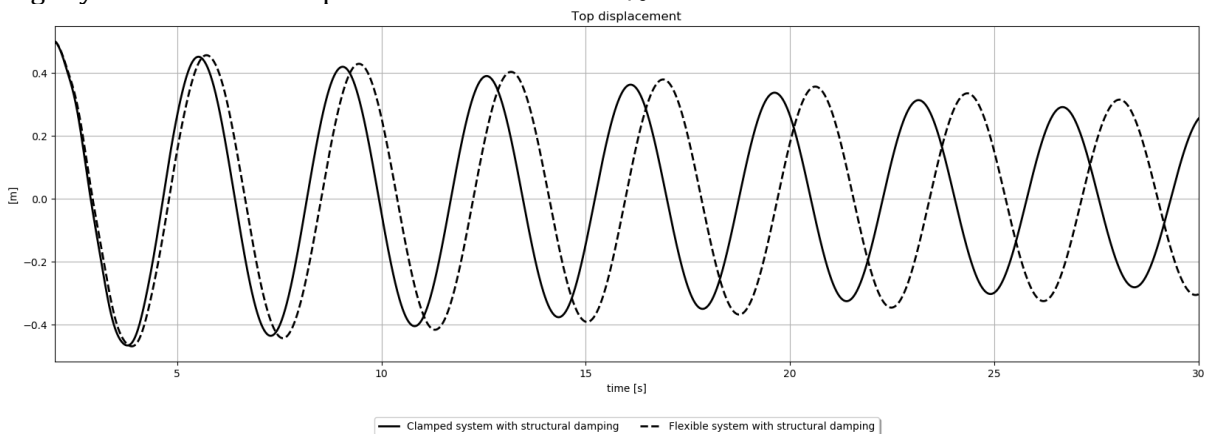


Figure 48 - Clamped system versus flexible system (rotational spring at the base), both systems are with structural damping

In Figure 48 a comparison is made of a clamped and flexible system both with structural damping. This figure depicts the influence of the rotational spring on the displacement at the top of the system. It can be noted that the frequency of the system is decreased which means that the period of the flexible system is increased. A first natural frequency of the clamped system found of 0.28 Hz while the first natural frequency of the flexible system is 0.27 Hz.

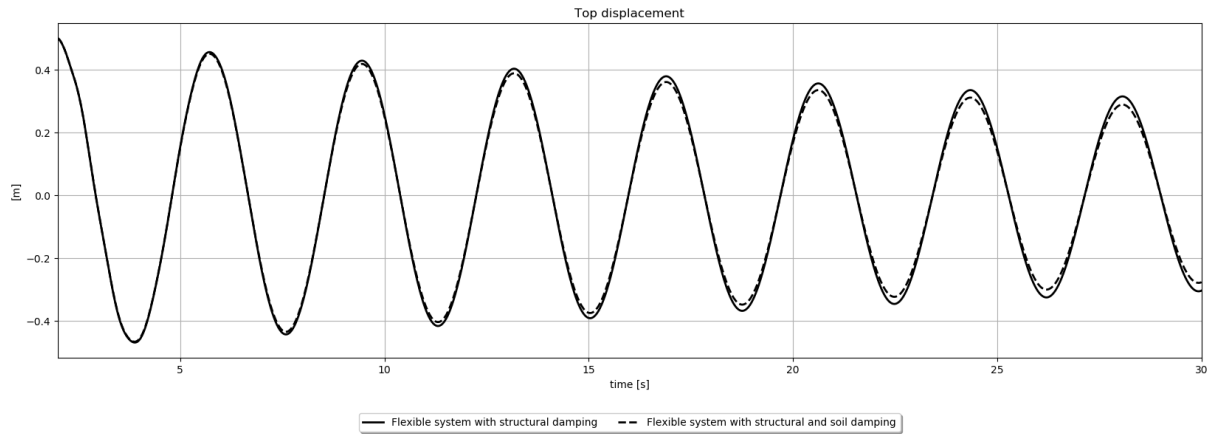


Figure 49 - Flexible system with structural damping versus Flexible system with structural and soil damping

Figure 49 depicted the results of the flexible system with only structural damping and the flexible system with soil and structural damping. The soil damper computed with the Wolf model in paragraph 4.3 is used. Figure 49 shows that the soil damper has a small contribution to the overall damping of the system when structural damping is active. Using the logarithmic decrement method to express the dashpot value of $1.32e+11$ Nms/rad into a damping ratio results in a contribution of 0.12% which is relatively small compared to the structural damping of 0.43%. Therefore, the soil damper value is increased into an value of $6.60e+11$ Nms/rad to equalize the contribution of the two damping mechanisms to the whole system.

In Figure 50 the increased damping value is applied to the system and compared to the flexible system with only structural damping. An clear contribution of the soil damper is now visible. The logarithmic decrement method is applied and resulted in a total damping ratio of 0.84% in which 0.43% is due to structural damping and 0.41% due to soil damping. With this analysis the input values of the dampers are determined and can now be identified in terms of energy dissipation by the EFA method.

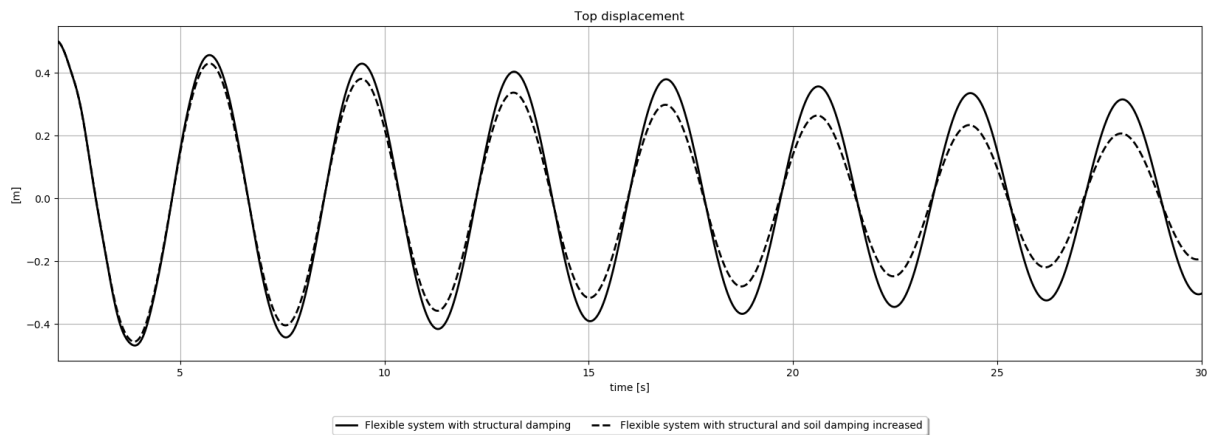


Figure 50 - Flexible system with structural damping versus flexible system with structural and increased soil damping

4.6 Mesh sensitivity study

The influences of the mesh of the finite element model to the identification of the damping value C_r is studied. A mesh study is done which is depicted in Figure 51. The damping error slightly decreases when applying a finer mesh. A mesh size of 0.25m is chosen to continue the analysis. This size gives a low damping error and has an amount of analysis time which is a workable simulation time.

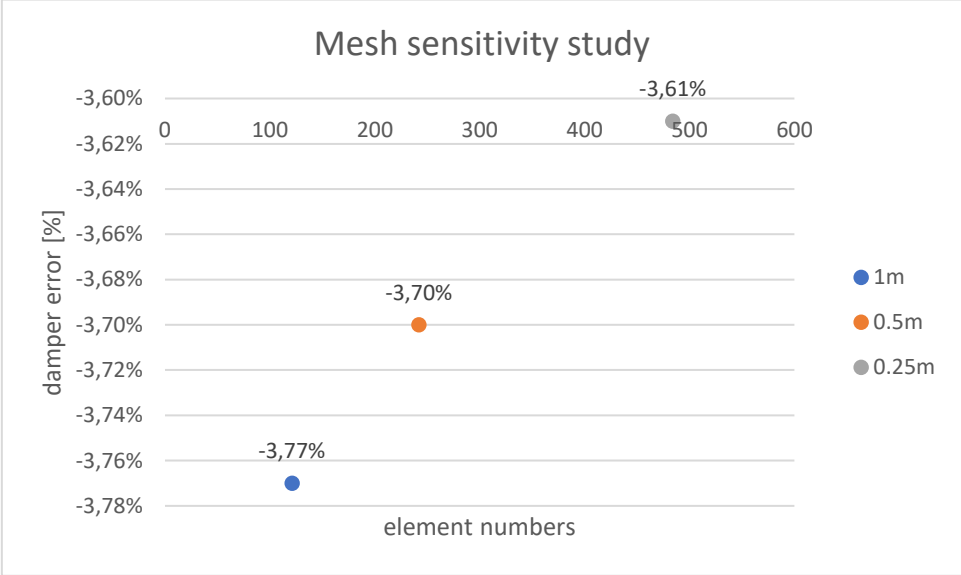


Figure 51 - Mesh study

Note that the damping errors are higher than the final damping error of this case according to the results. During the discretization study the beam elements of the FE model consisted of B31 elements. These are Timoshenko beam elements which allow for transverse shear deformation. As studied in section 4.4 the eigenfrequency is influenced by the shear deformation by 2%. This phenomena is also presented in the errors shown in Figure 51 in which the EFA model does not incorporated the shear behaviour of the beam.

An attempted is done to extent the energy balance by introducing the potential energy introduced by the shear behaviour of the model. Since, the curvature of every node in the FE model is used to calculated the potential energy of the beam, a separation within this curvature between shear and bending was not found.

In addition, during full scale measurement the shear component is present which means that identifying the damper value with the EFA method will give an error. This is quantified with an simulation where the FE model allows shear deformation but the energy analysis consist of only bending elements. A demping error of +2.19% is found.

4.7 Sensitivity analysis rotational soil stiffness versus building stiffness

For case 3 analytical expressions for the mode shape are used to predict the dynamic behaviour of the system when only a limited number of sensors are available. The analytical expressions of the mode shape supported by an rotational spring are derived in Appendix A. *Figure 52* shows the derived first three mode shapes of the system. The impact of the rotational soil stiffness on the mode shape of the building is investigated in this section.

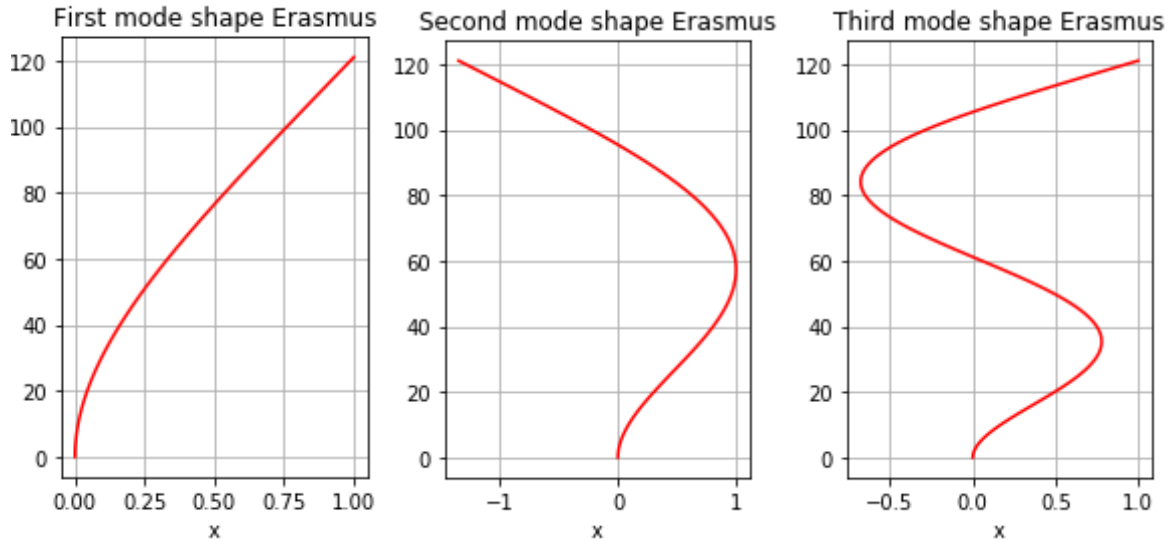


Figure 52 - first three mode shapes of a system influences by a rotational spring at the bottom

Fout! Verwijzingsbron niet gevonden. shows the first eigen modes of four different configurations in which the rotational stiffness is changed. The bending stiffness of the beam is remained constant for the four calculations. The blue line describes the fixed system which means that the bottom is fully constrained. The red dashed line represent the first eigen mode were the calculated rotational soil stiffness of $Kr = 5.94e+12 \text{ Nm/rad}$ is used from section 4.3. for the purple and yellow line, $Kr=5.94e+11 \text{ Nm/rad}$ and $Kr=5.94e+10 \text{ Nm/rad}$ are used respectively.

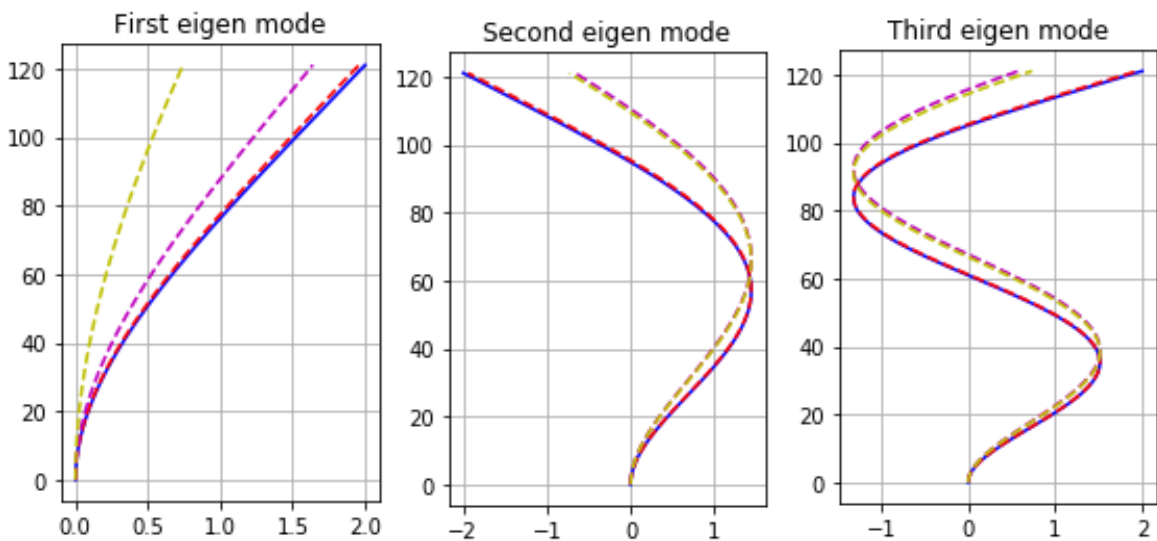


Figure 53 - Impact rotational soil stiffness on the eigen modes of the building

From Figure 53 it can be seen that a low value of rotational soil stiffness results in decreasing the top displacement of the mode shape of the building. Comparing the fixed system with the flexible system, it can be seen that the rotational soil stiffness hardly effect the mode shape of the building. However, Figure 53 only present the top displacement due to the mode shape of the building. The influence of the rotational soil stiffness which results in the rotation of the building is not taken into account yet. Expected is that a lower value of rotational soil stiffness will increase the top displacement. Superposition of the two system will finally describe the total system, this is illustrated in Figure 54.

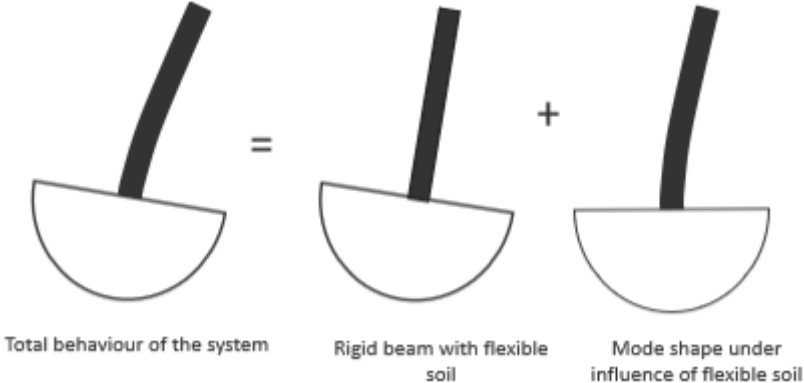


Figure 54 - Dynamic behaviour of a continuous system supported by a rotational spring

It is tempting to conclude that the fixed system mode shape can be used instead of the flexible system mode shape because of the small divergence. This conclusion is put up in a test. The fixed mode shape will result in an error of 16.25% on the identification of the soil damper.

5 Results and discussion

Now all parameters for the cases have been defined in Chapter 4, the assessment described in Chapter 2 can be applied. The result and discussion of every case are presented in this Chapter. Every section of a case starts with an overview of the energies extracted from Abaqus. Hereafter, the kinetic, potential and dissipated energy extracted from the FEM model are compared with the determined EFA energies. The comparison of the models is expressed in a relative error which is given by:

$$RE = \frac{efa(t) - fem(t)}{fem(t)} \cdot 100\% \quad (5.1)$$

where $efa(t)$ is the data obtained with the equations described in Chapter 2. And $fem(t)$ is the data directly extracted from the FEM model.

After analysing the energies needed for the energy balance, the identified damping value and its accuracy is given. Every last paragraph gives a summary of the main findings.

5.1 Case 1 - Only soil damping

The EFA technique is first applied to determine the energies and damping value with the output for all nodes and integration points of the FEM model. In this case only soil damping is considered, which is modelled with a dashpot damper at the bottom of the system.

5.1.1 Abaqus Energy output

Figure 55 shows the energies which are obtained directly from the FEM model in Abaqus. This plot shows how the kinetic, potential and dissipated energy of the model are related to each other, and how they behave over time. The kinetic and potential energy of the system decrease over time while the dissipated energy increases over time. A detailed plot of the energy dissipation displayed in Figure 55. The slight fluctuation in the energy dissipation is the result of the fluctuation in the velocity of the beam during an oscillation. It can be explained by the beam oscillation since the energy dissipation is dependent on the velocity.

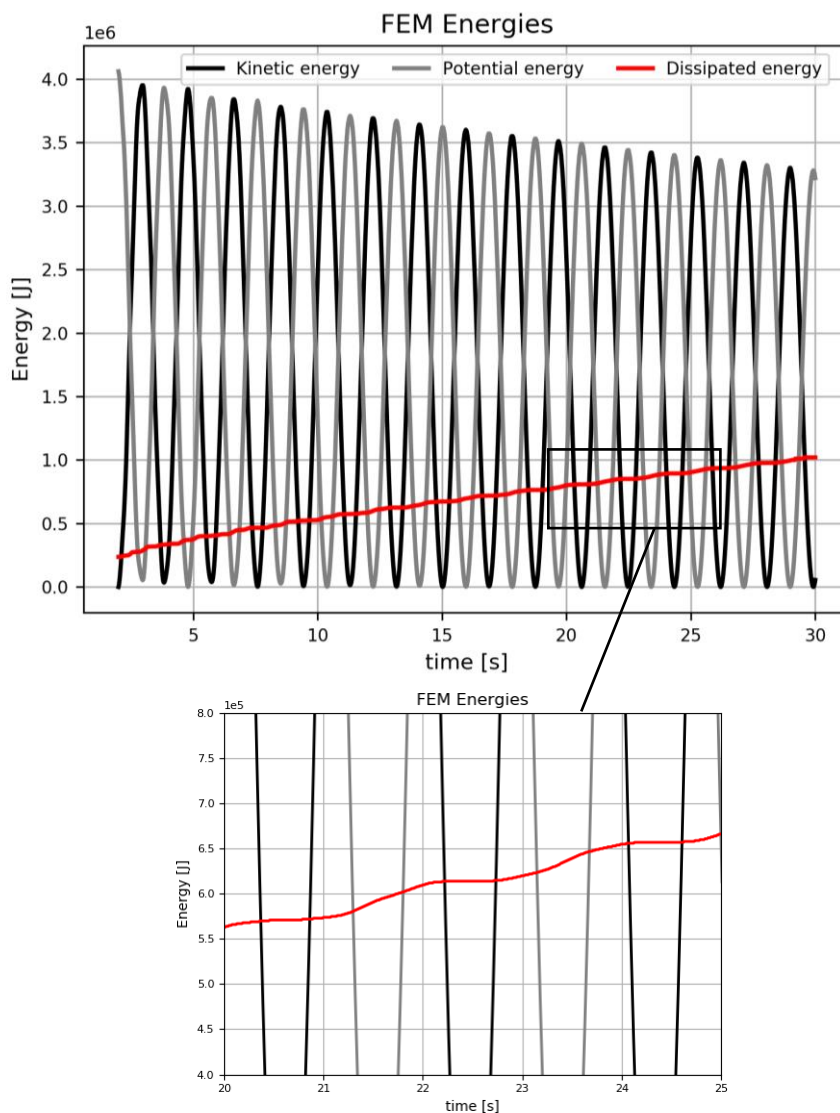


Figure 55 - Plot of the extracted energies from the FEM model. with a detailed plot showing the slight oscillation in the energy dissipation .

Figure 56-I shows the initial state of the system when applying the initial condition. The velocity dw/dt at this moment in time is equal to zero. This means that the system has zero kinetic energy, but the potential energy is maximum. Because the velocity is zero, there is no energy dissipated by the soil damper. After releasing the beam, the velocity, kinetic energy and energy dissipation increase until it passes the equilibrium position of the system, depicted in Figure 56-II. Here, the beam passes this position with the maximum velocity, which means the kinetic energy and energy dissipation are at their maximum, and the potential energy is zero. The velocity decreases while approaching the outer position displayed in Figure 56-III. Figure 56-IV and Figure 56-V complete a full oscillation of the beam.

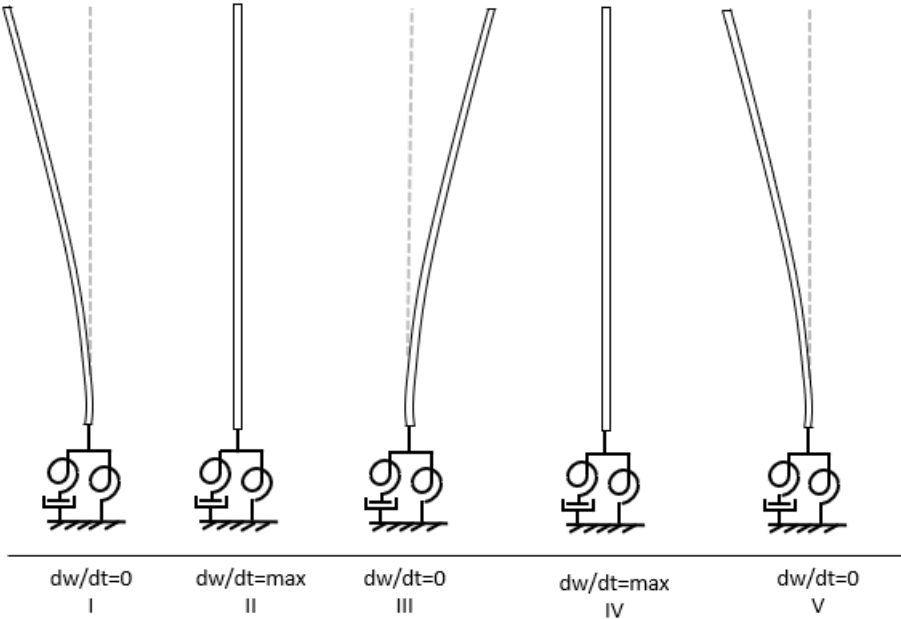


Figure 56 - Illustration of 1 period of the system explaining the fluctuation of the linear viscous damper

5.1.2 Kinetic energies

Figure 57 shows the kinetic energy determined with the EFA technique and the kinetic energy directly obtained from the Abaqus FEM model. The figure shows that the energies are in good agreement with each other.

The relative error between the kinetic energy determined with the EFA technique and the kinetic energy obtained from Abaqus are also plotted in Figure 57. This figure shows the error is small and fluctuates randomly between -0.45% and 0.45%. This indicates that there are no bias errors in the kinetic energy computation with the EFA technique.

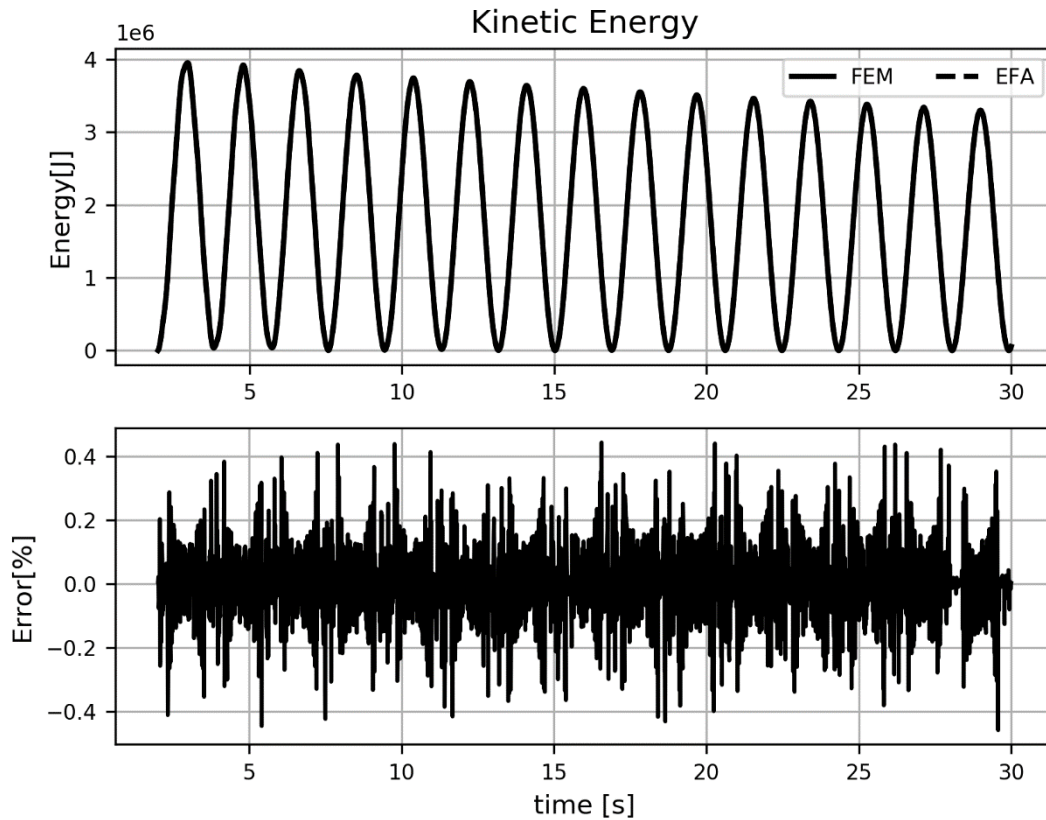


Figure 57 - The top graph shows the kinetic energies determined with the EFA technique and directly obtained from the FEM model. The bottom graph shows the relative error between these energies

5.1.3 Potential energies

Figure 58 shows the potential energies obtained from Abaqus, and determined with the EFA technique. The figure shows that the energies are in good agreement with each other. Figure 58 also shows the relative error between the FEM and EFA results. The error fluctuates between 0.45% and -0.67%. The mean error is -0.16%, which means that the FEM potential energy is larger than the potential energy determined with the EFA technique.

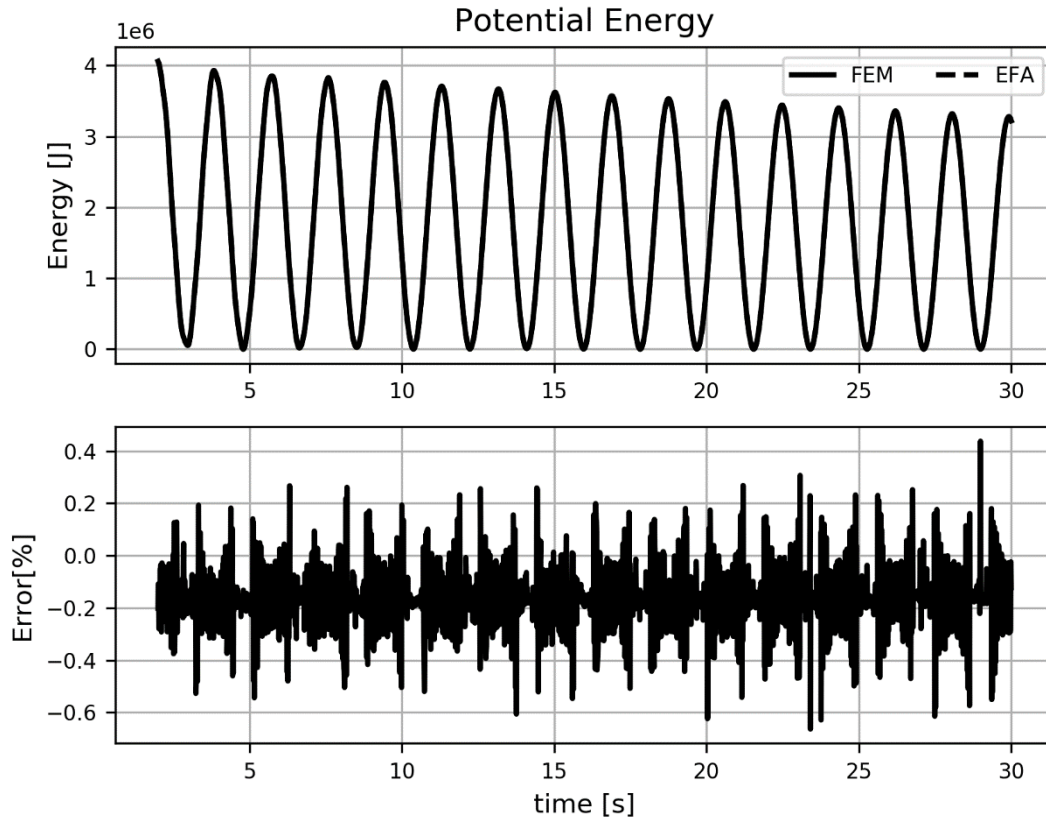


Figure 58 -The top graph shows the potential energies determined with the EFA technique and directly obtained from the FEM model. The bottom graph shows the relative error between these energies.

The underestimation of the potential energy derived with the EFA technique might be caused by the way the needed data is extracted from the FEM model which are used as input for the EFA technique. Abaqus uses integration points for generating the curvature output, see Figure 59. The linear and cubic elements have three and the quadratic elements have six additional variables. For this analysis 2-node linear elements were used. Using 2- node cubic elements may results in more accurate results and a smaller error on the determination of potential energy.

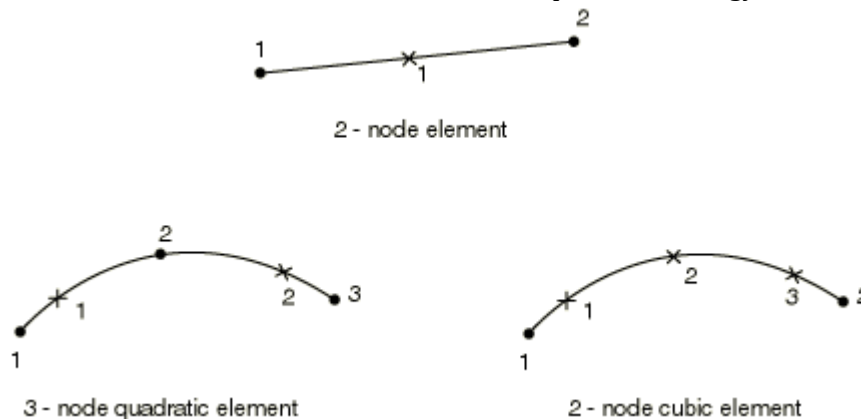


Figure 59 - Integration points for generating the output in Abaqus

Further, the FEM model derives an initial energy which combines the potential energy of the beam and spring. The ratio between these energies is shown in Figure 60. This figure shows the total potential energy, the beam potential energy and the spring potential energy derived with the EFA technique separately. The total potential energy of the model consists of 10% of potential spring energy and 90% of beam potential energy calculated over the full simulation time. The potential spring energy (blue line) in Figure 60 transforms from a distorted sine to a smooth sine signal. The distortion is caused by the higher modes excited at the start of the simulation. These higher modes are less present, later in the simulation, due to damping in the system.

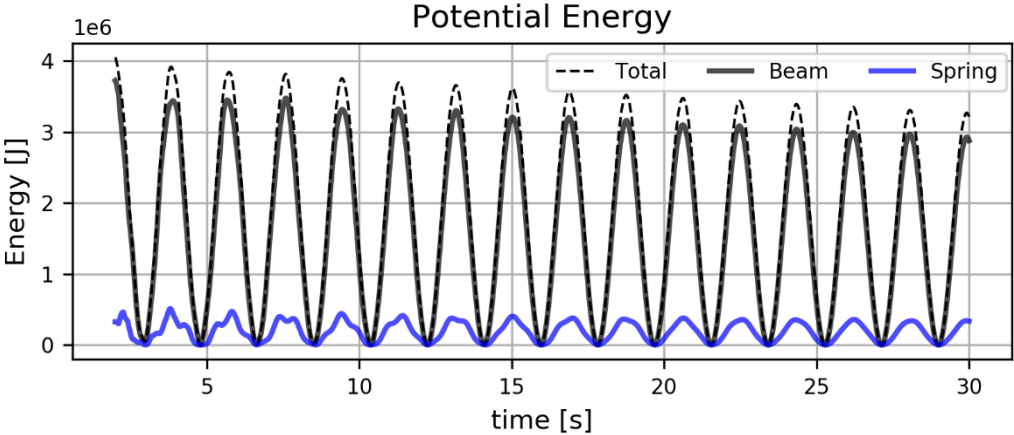


Figure 60 - Potential energies derived with the EFA technique.

5.1.4 Energy dissipation

Figure 61 shows the energy dissipation of the system directly obtained from FEM and determined with the EFA technique. The figure shows that the energy dissipation of both methods are in good agreement with each other. Figure 62 shows the relative difference between the dissipated energy obtained with FEM and the energy obtained with the EFA versus time. In the first 5 seconds higher damping error are found. After 5 seconds the error is converged to a more stable damping error and fluctuates between 0.95 % and -2.40%. A detailed plot between 20 and 25 seconds of the simulation is also shown in Figure 62. It can be seen that the mean of the error fluctuates over -0.47% when eliminating the first 5 seconds of the simulation.

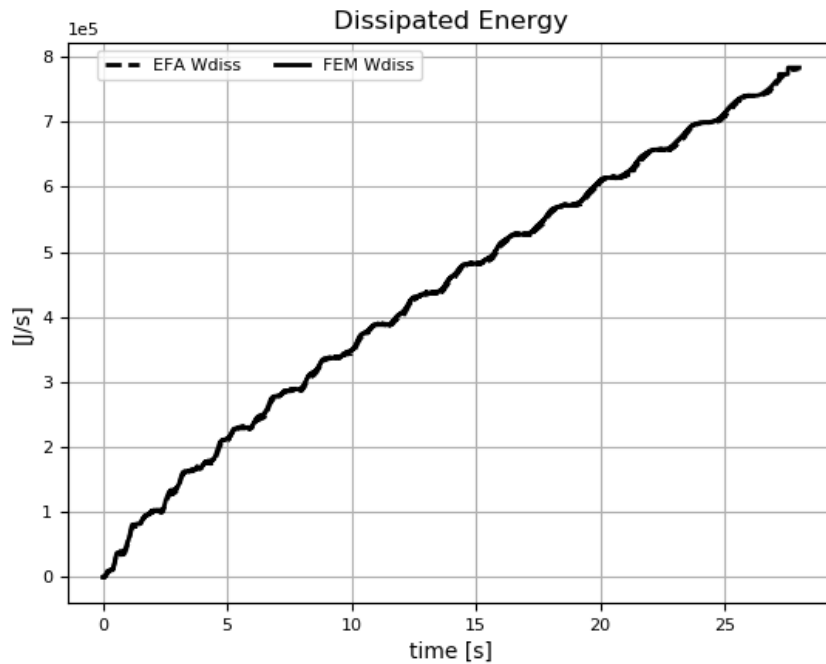


Figure 61 - Comparison of the extracted FEM dissipated energy and the derived EFA energy dissipation.

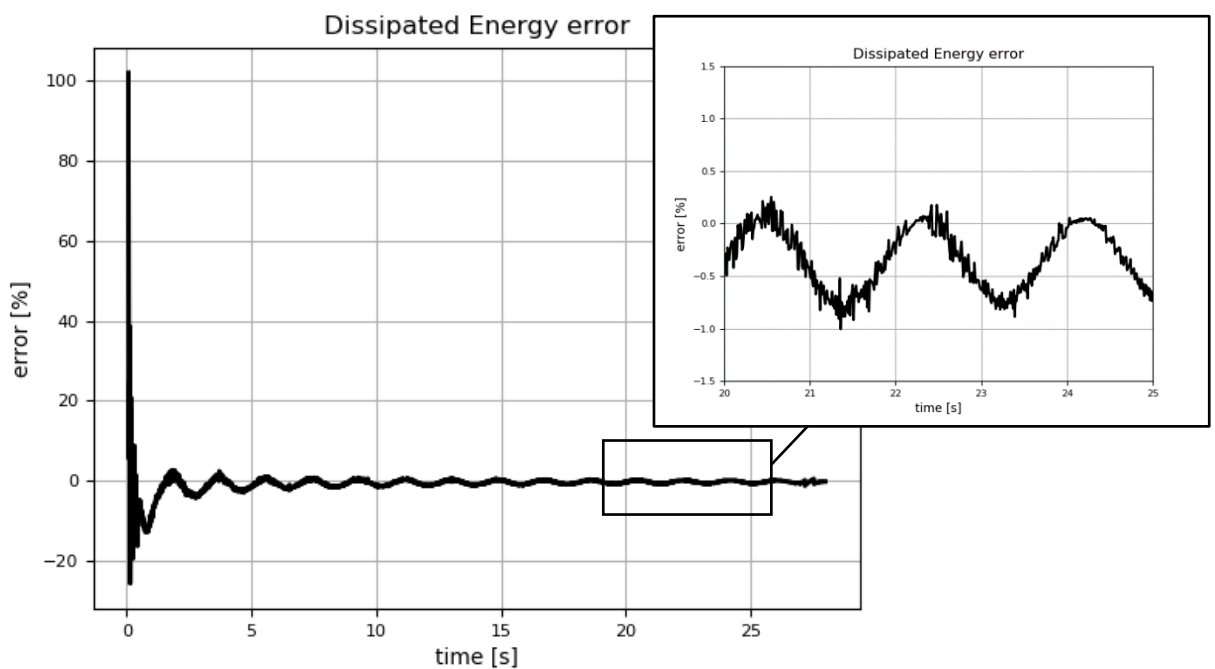


Figure 62 - Relative error between FEM and EFA energy dissipation

5.1.5 Damping value

Figure 63 shows the results of the damping values. The energy dissipation determined with FEM and the EFA technique are translated to a damping value with eq. 2.6. The dashpot damper value $Cr = 1.32e+11$ Nms/rad that was used as input for the FEM model is also provided as reference. Over time the Cr values obtained with FEM and the EFA technique converge to a stable value, which deviate only slightly from the original Cr input value. The detailed plot shows that the Cr EFA value deviates more than the Cr FEM value and fluctuates between $1.32e+11$ and $1.30e+11$ Nms/rad. The fact that the Cr FEM value is not equal to the original input value shows that numerical damping is slightly present.

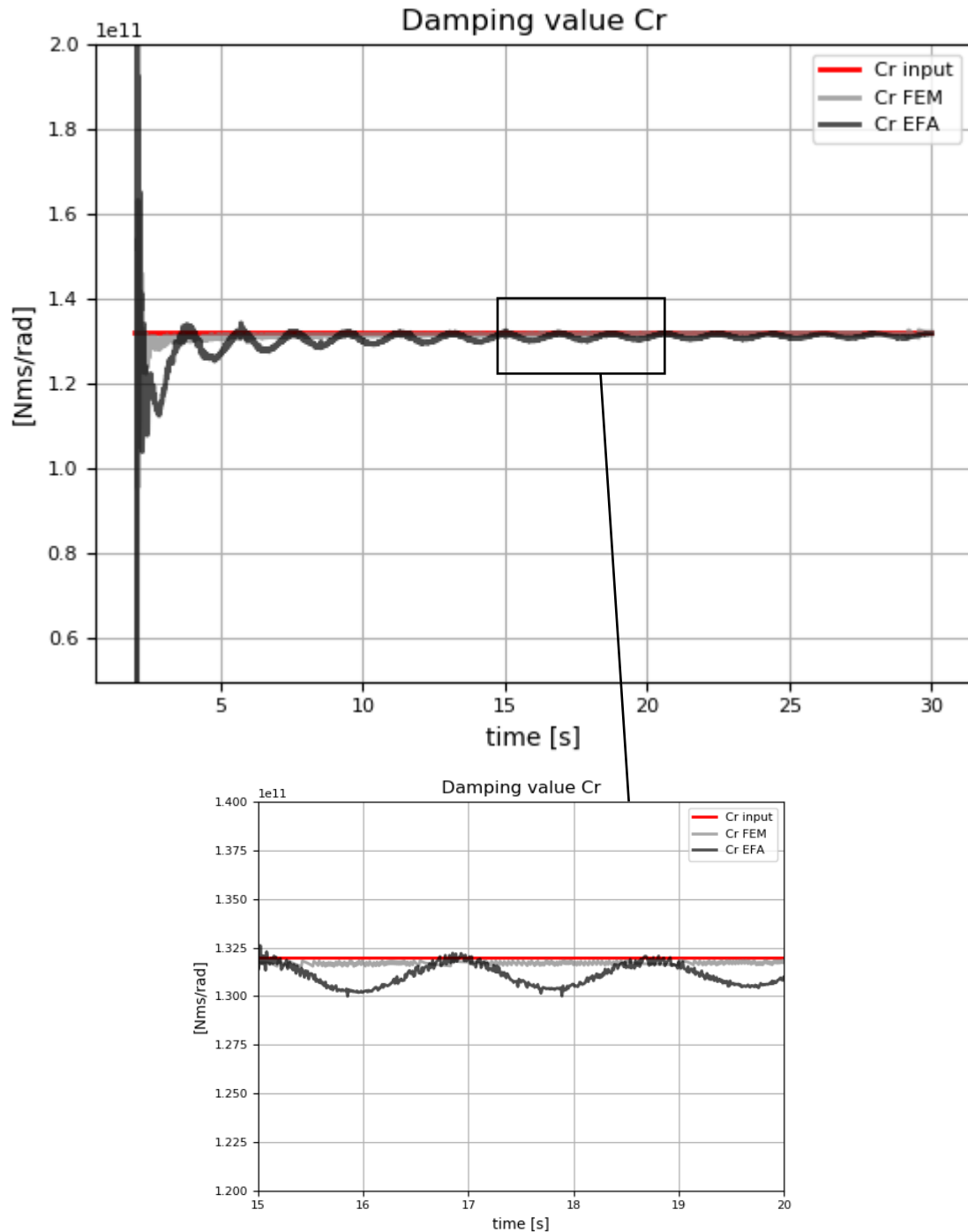


Figure 63 - Plot of the damping values.

As shown in Figure 63 the derived EFA damper value converges to the input value with a small bias deviation. This convergence is expressed in the relative error between the damper input value for the FEM model and the derived damping value by the EFA technique displayed in Figure 64. Between 25 and 30 seconds the mean error is -0.43%.

It can be noted that error converges to zero over time which means that the duration of a simulation has an impact on the determination of energy dissipation with the EFA technique. Therefore, different time instances are analysed. The lowest value of the oscillation at certain time positions are compared in Table 7. The slope between the last values in the table indicates that the dynamic analysis in FEM should be extended to 180 seconds to arrive at a converged value for the damper when the system is excited by the applied initial displacement.

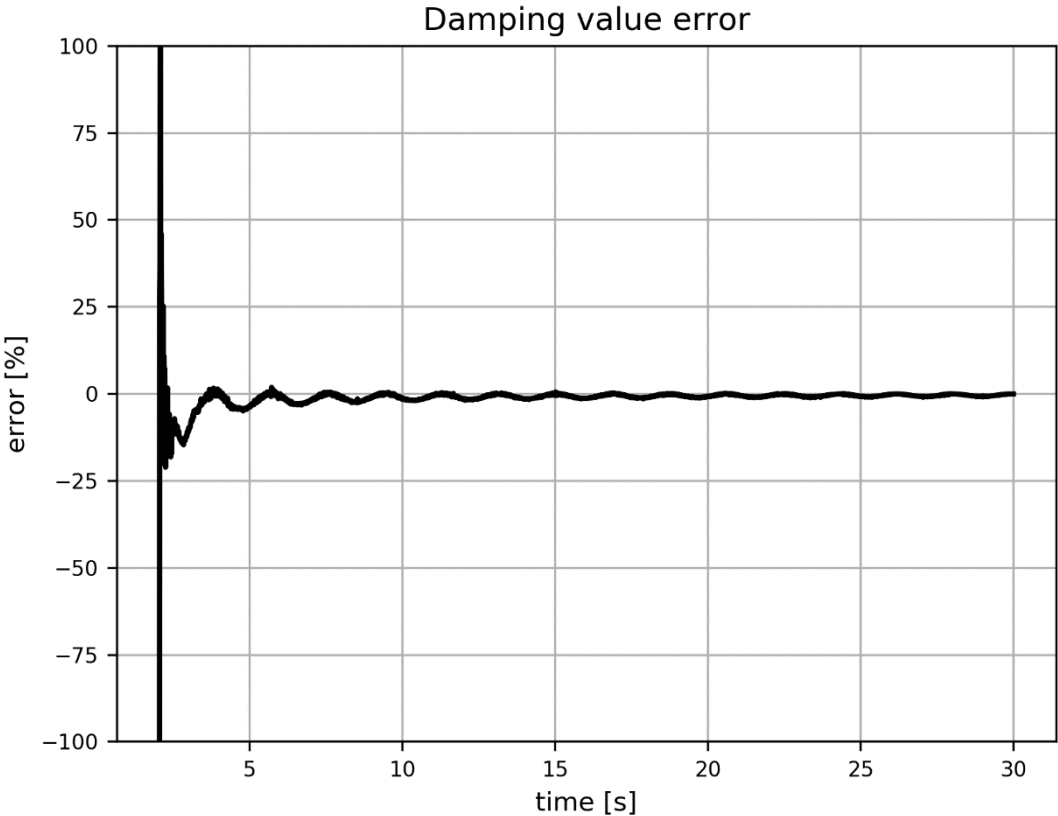


Figure 64 - Relative error between input damping value and damping value derived by the EFA technique.

time [s]	Damping value error [%]
5	-4.94
10	-2.01
15	-1.52
20	-1.19
25	-0.97
30	-0.94

Table 7- Damping value error over time

5.1.6 *Summary*

Damping was introduced to the system by means of a dashpot damper at the bottom. Of each node of the Abaqus FEM model the following data were obtained: displacements, velocity, and curvature. These data were used in the EFA technique to determine the kinetic, potential and dissipated energy of the system. To assess the accuracy of the EFA technique, these energies were compared with the energies obtained from Abaqus. The dissipated energy obtained from the FEM model and determined with the EFA technique were used to determine damper values of the dashpot at the bottom of the system. These were compared to the input value for the dashpot damper in the FEM model. This case resulted in the following findings:

Kinetic energy

- The kinetic energy determined with the EFA technique deviates between 0.45% and -0.45% from the kinetic energy directly obtained from the FEM model.

Potential energy

- The potential energy has a fluctuating error between 0.45% and -0.67% with a mean of -0.16% which means that the derivation of the potential energy by the EFA method gives a underestimation compared with the FEM potential energy.
- The underestimation of the potential energy derived with the EFA technique might be caused by the way the curvature is extracted from the FEM model which are used as input for the EFA technique.

Energy dissipation

- The energy dissipation determined with the EFA technique deviates around -0.47% eliminating the first 5 seconds of the simulation.

Damping value

- The identified damping value with the EFA technique has an error of 0.43%. This error might be caused by the earlier discussed integration points combined with the time span of the simulation.
- The error converges to zero over time which means that the duration of a simulation have impact on the determination of energy dissipation with the EFA technique.
- By analysing the relative error made on the identification of the damper value, the dynamic analysis of case 1 in FEM should be extended to 180 seconds to arrive at a converged value for the damper.

5.2 Case 2 - Soil and Structural damping

In this case a combination of a structural and soil damper is considered. An assessment is made of the accuracy with which the EFA technique quantifies the kinetic, potential and dissipated energy and the soil dashpot damper. Insight is gained in the accuracy with which two damping mechanisms can be separated.

5.2.1 Abaqus Energy output

Figure 65 shows the FEM energies which are a result of the dynamic analysis performed on the system that contains structural and soil damping. This plot gives insight in the energy balance and how the energies are related to each other. It can be seen that the kinetic and potential energy of the system decrease rapidly over time compared with the FEM results from case 1 presented in Figure 55. This is due to the increased soil damping and added structural damping, explained in Chapter 4. The dissipated energy increases over time and has an initial value that is caused in the first two seconds of the simulation while the initial displacement was applied. The cause of this initial value is due to equilibrium of the static position of the system during the initial displacement. In further analyses the initial value of the dissipated energy is set to zero.

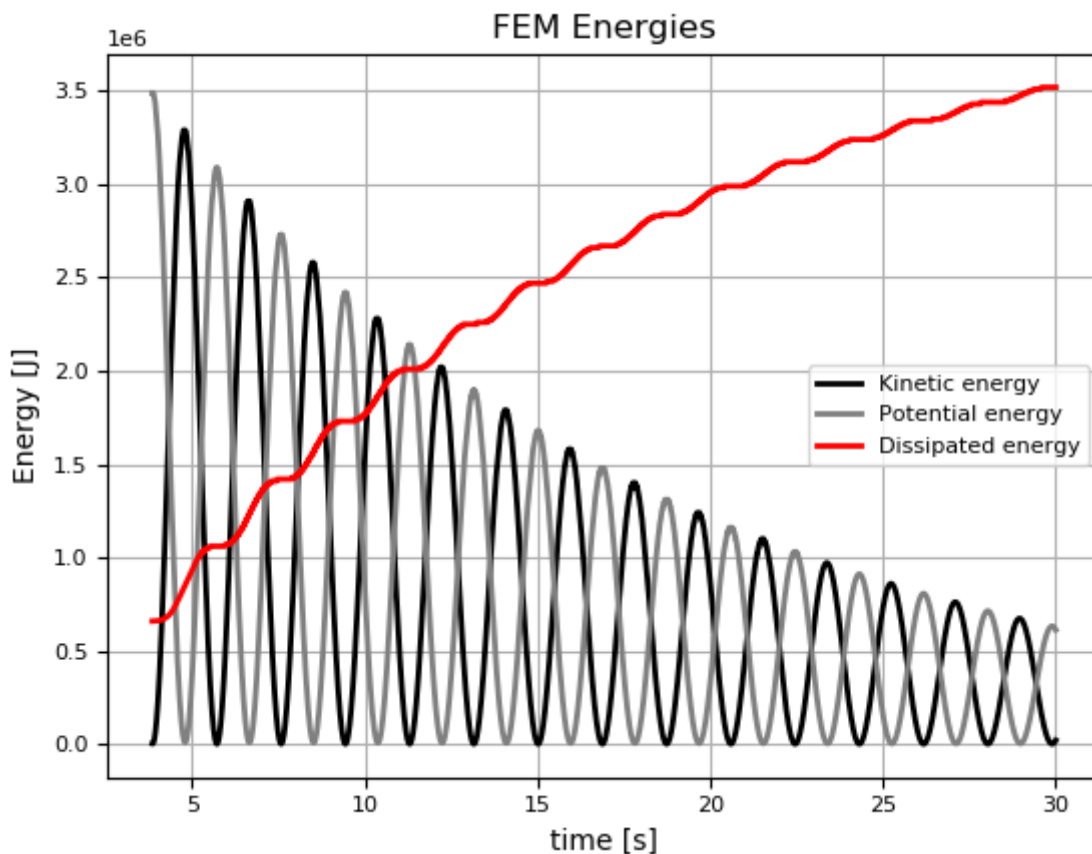


Figure 65 - Plot of the extracted energies from the FEM model.

5.2.2 Kinetic energies

Figure 66 shows the kinetic energy determined with the EFA technique and the kinetic energy directly obtained from the Abaqus FEM model. The figure shows that the energies are in good agreement with each other.

The relative error between the kinetic energy determined with the EFA technique and the kinetic energy obtained from Abaqus are plotted in Figure 66 as well. This figure shows the error is small and fluctuates randomly between -0.47% and 0.47% until 23 seconds. After 23 seconds the error fluctuates decreases and fluctuate between 0.14% and -0.09%. This indicates that there are no bias errors in the kinetic energy computation with the EFA technique.

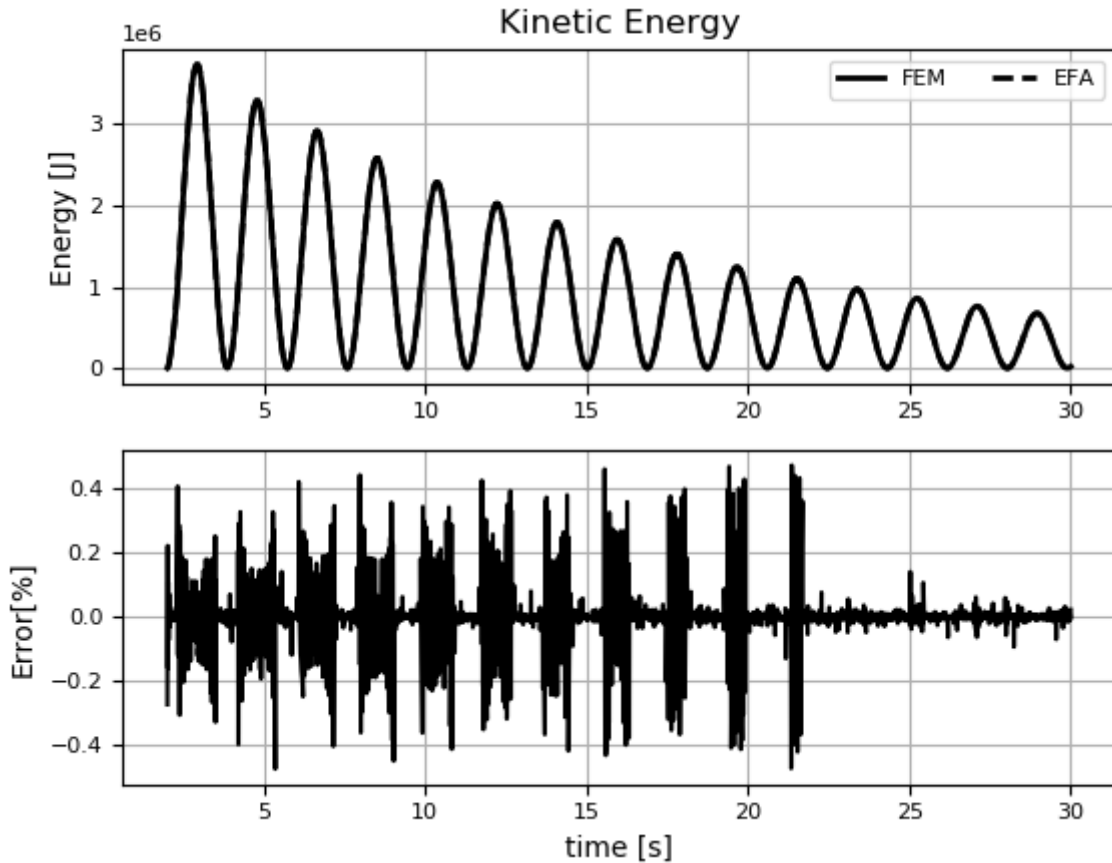


Figure 66 – The top graph shows the kinetic energies determined with the EFA technique and directly obtained from the FEM model. The bottom graph shows the relative error between these energies.

5.2.3 *Potential energies*

Figure 67 shows the potential energies obtained from Abaqus, and determined with the EFA technique. Figure 67 also shows the relative error between the FEM and EFA results. The error deviates between 0.30% and -0.62% until 23 seconds. After 23 seconds the error fluctuation decreases and is between 0.28% and -0.32%. The mean error is -0.16% and is the same as in case 1. The cause of the underestimation of the potential energy derived with the EFA technique might be the same as Case 1.

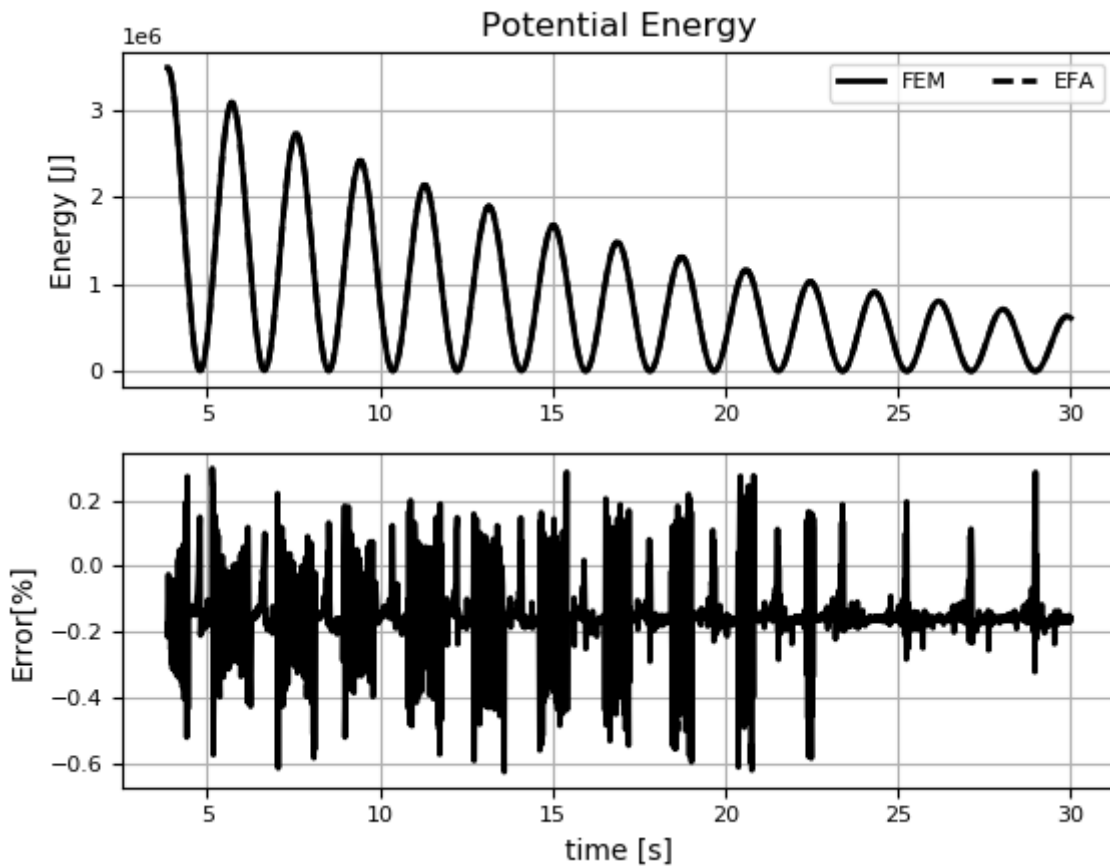


Figure 67 - The top graph shows the potential energies determined with the EFA technique and directly obtained from the FEM model. The bottom graph shows the relative error between these energies

Determining the structural and soil damping the potential energy is disassembled in spring potential energy and beam potential energy as shown in Figure 68. This figure shows the total potential energy, the beam potential energy and the spring potential energy derived with the EFA technique separately. Compared with case 1 the soil spring contribution to the total potential energy decrease rapidly over time resulting in a gradual development of the beam potential energy and total potential energy.

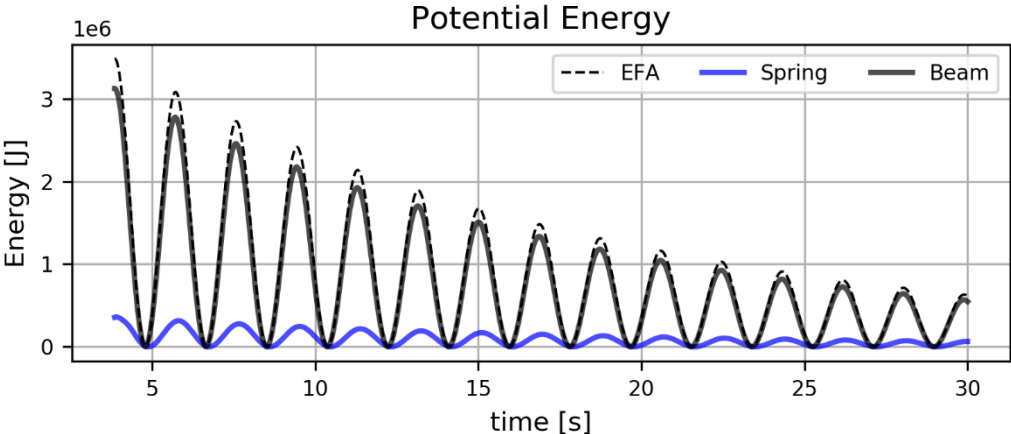


Figure 68 - Potential energy derived with the EFA technique.

5.2.4 Total energy dissipation

Figure 69 shows the total energy dissipation of the system extracted from the FEM model and derived with the energy balance according to eq. 2.2. The identified energy dissipation is larger compared with the FEM energy.

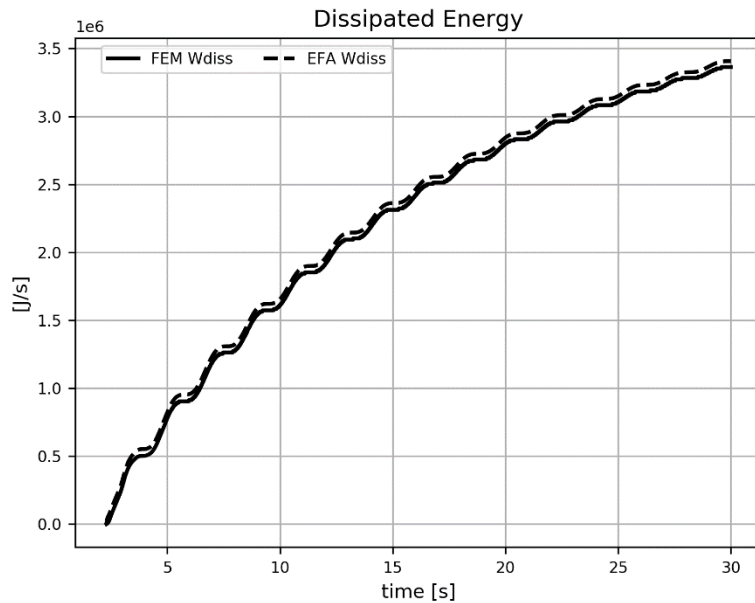


Figure 69 - Comparison of the extracted FEM dissipated energy and the derived EFA energy dissipation

The energy dissipation increases over time. Compared to the energy dissipation graph of Case 1 (Figure 61), the small fluctuations at the beginning of the simulation are not present. Case 1 has a damping ratio of 0.12% while Case 2 has a damping ratio of 0.84%. This means a higher damping ratio of 0.72% which causes a fast damping of the higher modes presented in the system. Furthermore, the slope of the line decreases over time, which is a result of the damping that causes an overall cumulative decreasing velocity of the system.

Figure 70 shows the dissipated error converges over time. The error converged to a more stable damping error and fluctuates to a value of 1%.

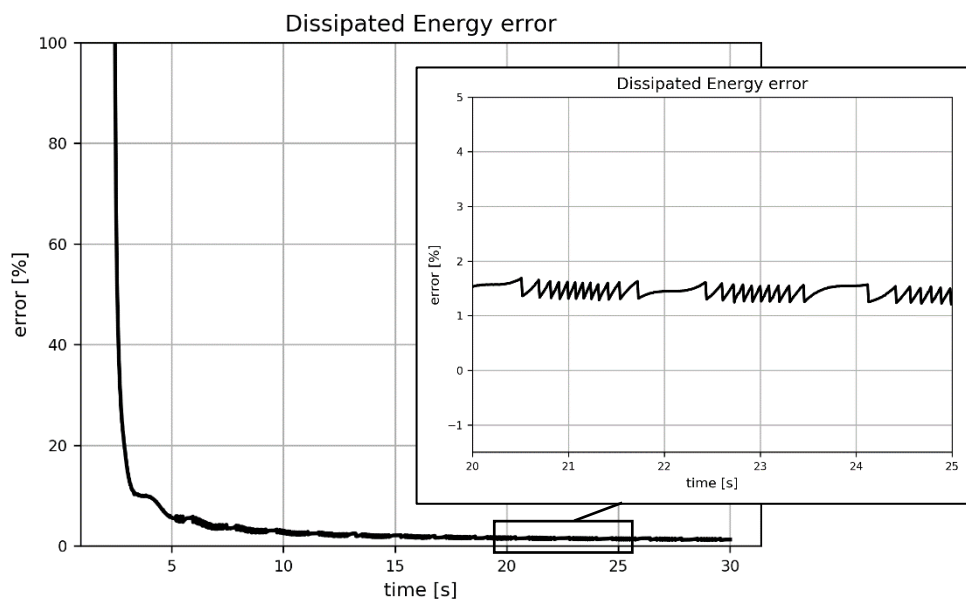


Figure 70 - Relative error between FEM and EFA energy dissipation

5.2.5 Soil energy dissipation

The soil damper is computed with the procedure described in 2.5.2.2. In order to identify the soil energy dissipation, equilibrium must be found between the bottom part of the building and its foundation. Figure 71 shows the energy flux (dashed line) derived with eq. 2.13. The curvature and rotational velocity of the bottom node are used from the FEM model to determine the energy flux at the bottom of the system. The energy flux by the spring (solid black line) is also plotted in Figure 71. The energy flux of the spring is the first derivative of the energy in this system described with eq. 2.12 and the rotational velocity of the spring is used from the FEM model. Figure 71 also shows the difference between these energies which is the energy dissipation when cumulative presented.

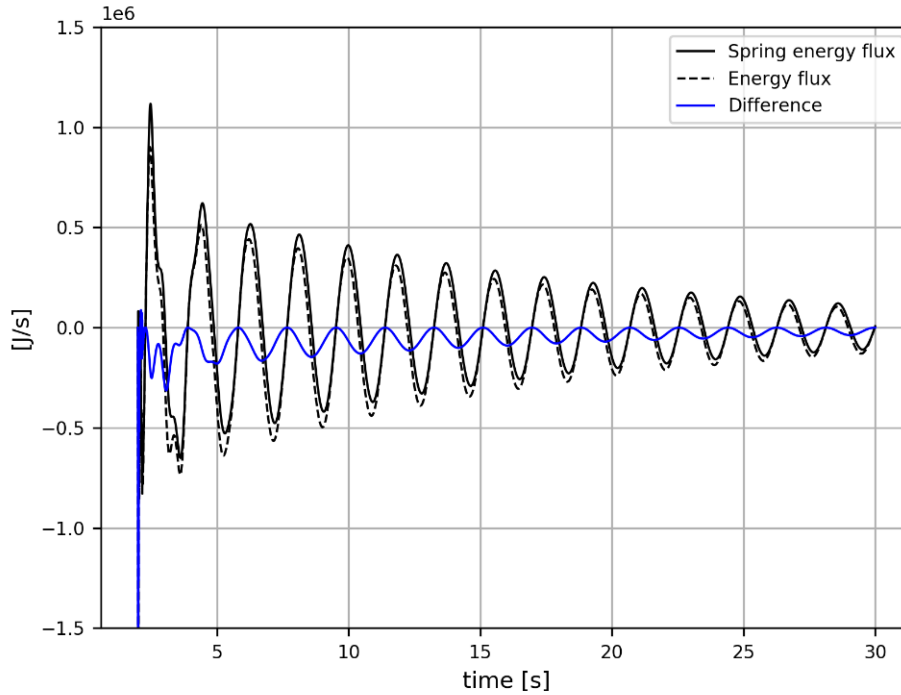


Figure 71 – Energy flux of the bottom part of the system (dashed line) and the spring energy flux (solid line). The difference between the bottom energy flux and spring energy is displayed in blue.

The FEM model only gives the total energy dissipation of the system when applying multiple damping mechanisms. It does not provide the dissipation in the soil and building separately. Therefore the identified energy dissipation of the soil is compared with:

$$w_{diss_soil} = C_{r_input} \dot{\varphi}(x, t)^2 \quad (5.2)$$

With C_{r_input} being the damper input value of the FEM model and $\dot{\varphi}(x, t)$ is the rotational velocity extracted from the bottom element of the FEM model. Figure 72 shows the comparison between the identified EFA soil energy dissipation and the energy dissipation determined with eq. 2.14.

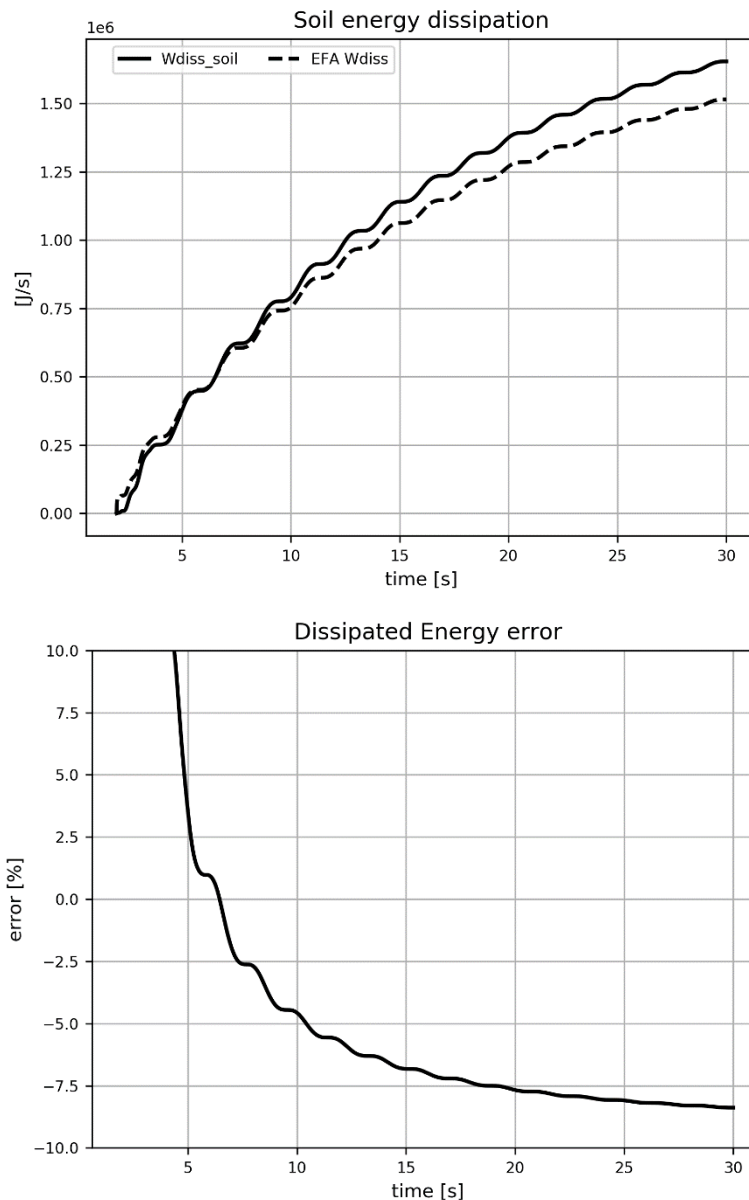


Figure 72 – The top graph the comparison of the identified soil energy dissipation with the EFA technique and the energy derived with eq. 4.37. The bottom graph shows the relative error between the above compared energies.

Figure 72 (top graph) shows that in the first 6 seconds of the simulation the EFA identified energy gives a higher value than the energy dissipation determined with eq. 2.14. This higher value is caused by the integration of the spring potential energy which has a large value at the beginning. This distortion is caused by a low sampling rate which results in aliasing effects. After the intersection of the two energies at 6 seconds, the identified soil dissipation is lower than the energy dissipation computed with eq. 2.14. There are two explanations for the cause of the founded error:

- A reason of the founded error might be that the determination of the EFA energy dissipation is based on the bottom curvature. The curvature is needed to determine the base moment to finally determine the energy flux. As explained before, Abaqus uses integration point for generating the curvature output, (see Figure 59 Case 1). These

integration points are located in the middle of the bottom element. Half of the bottom element length is therefore not taken into account when determining the base moment. This phenomena might be the reason why the EFA identified soil energy dissipation is underestimated.

- Another reason might be that the rotational velocity at the bottom of the model is affected by the structural damping in this lower element of the FEM model. This small interaction between the two damping mechanisms results in a larger FEM energy dissipation of the soil.

Since there is no damper operator yet which describes the dissipated energy of the structure, the impact of the structural damping in the lowest element can therefore not be described properly. To eliminate the contribution of the structural damping in the lower element, a possibility might be to switch off the structural damping in this particular element. Within this research this possibility is not investigated.

5.2.6 Soil damping value

The identified energy dissipation is translated to a damping value according to eq. 2.15 and displayed in Figure 73. The rotational velocity at the bottom is used which contains of a small influence of the structural damping as explained before. The input value and the identified damping value are plotted over time. The final values at the end of the simulation have a relative error of -8.38%.

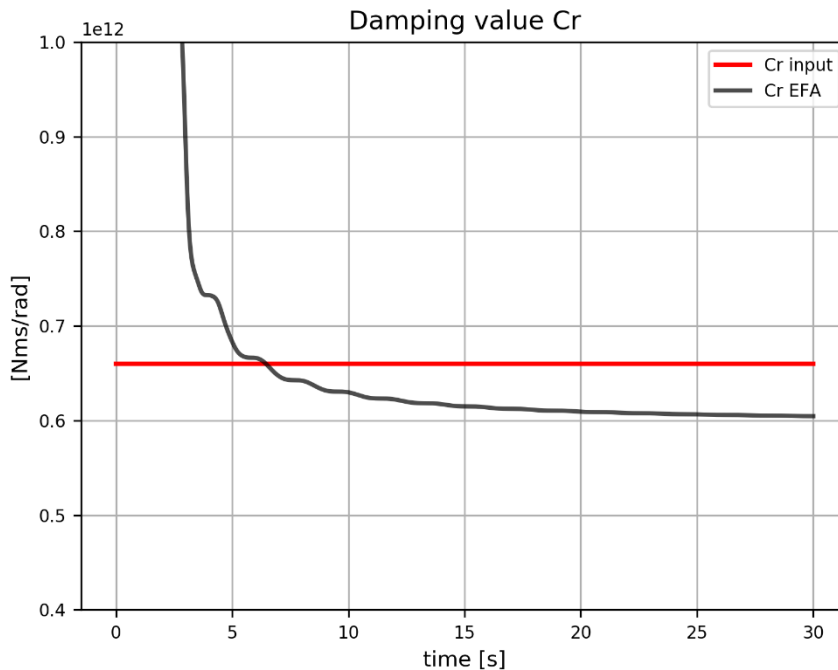


Figure 73 - Plot of the damping values

	Input	EFA
Cr	6.60 E+11 Nms/rad	6.05 E+11Nms/rad

Table 8 - comparison of the damping values

Another addition method of the identification of the soil damper is by using the frequency domain instead of time domain. See Appendix C. This method gives insight in the frequency distribution of the system.

5.2.7 Structural energy dissipation

The energy dissipation of the structure is determined by the procedure described in 2.5.2.1. To determine the energy dissipation of the structure, the energy flux $S(x,t)$ must be introduced as described with eq. 2.9.

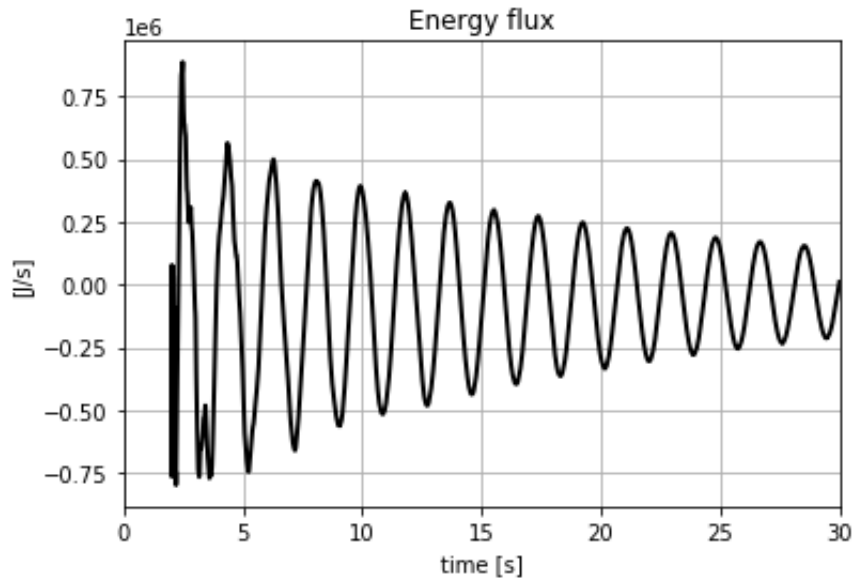


Figure 74 - Energy flux of the system

The energy flux at the given boundaries is plotted in Figure 74. The curvature over time from the FE model is multiplied by EI and used to compute the bending moment at the bottom of the structure. The rotational velocity at the bottom is also used from the FE model. During the first 5 seconds of the simulation the amplitude is fluctuating which might be a result of the higher modes present in the system. The energy flux decays over time because the rotational velocity and curvature decrease due to damping.

Figure 75 shows the energy dissipation of the structure. The energy dissipation of the soil dashpot according to eq. 5.2 is subtracted from the total FEM energy dissipation of the model in order to only display the structure damping.

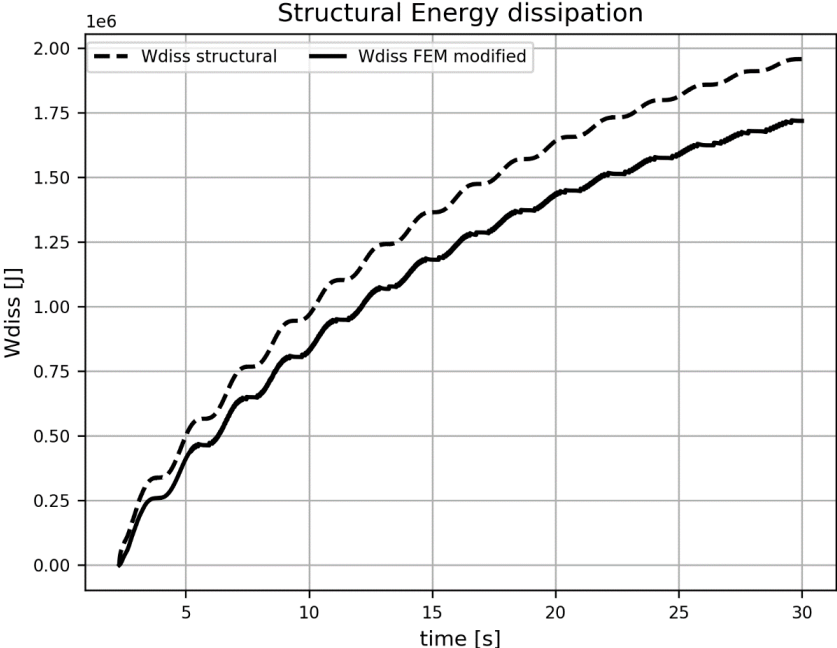


Figure 75 - Comparison of the extracted FEM dissipated energy and the derived EFA energy dissipation

Figure 76 shows how the dissipated energy error converges over time. After 5 seconds the error converged to a more stable damping error and fluctuates to a value of 13.61%.

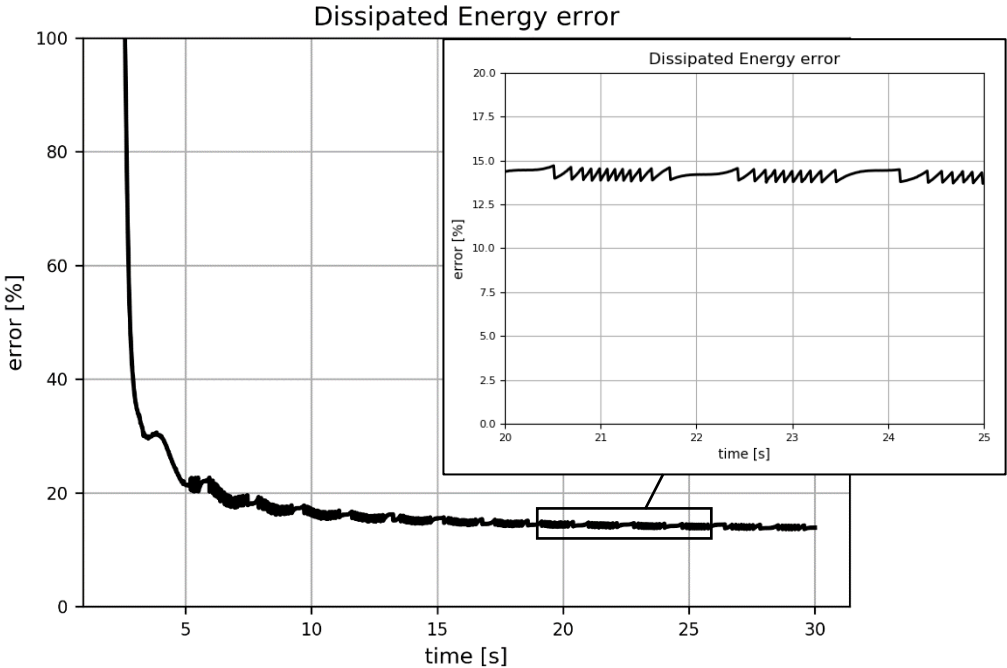


Figure 76 - Relative error between FEM and EFA energy dissipation

5.2.8 *Summary*

In this case a combination of a structural and soil damper is considered. An assessment of the error in which the energy method quantifies several damping mechanisms can be investigated. Insight will be gained in the separation of multiple damping mechanisms. Of each node of the Abaqus model the following data were obtained: displacement, velocity and curvature. From the bottom node rotational velocity is also used. This case resulted in the following findings:

Kinetic energy

- The kinetic energy has a fluctuating error between 0.47% and -0.47% until 23 seconds. After 23 seconds the error fluctuates decreases and fluctuate between 0.14% and -0.09%. the mean value is 0%.

Potential energy

- The potential energy has a fluctuating error between 0.30% and -0.62% until 23 seconds. After 23 seconds the error fluctuation decreases and is between 0.28% and -0.32%. the mean value is -0.15%. This means that the derivation of the potential energy by the EFA gives a underestimation compared with the FEM energy. This finding was also described at Case 1.
- The spring contribution to the total potential energy decrease rapidly over time resulting in a gradual development of the beam potential energy and total potential energy. A sufficient simulation time will result in the possibility to neglect the spring energy.

Total energy dissipation

- The assessment of the total energy dissipation gives an error of 1 % compared with the FEM energy dissipation. Concluded can be that the identification of the total amount of energy dissipation is reached with a high accuracy.

Soil energy dissipation

- The determination of the energy flux is important for the separation of structural and soil.
- The error on the identification of the soil energy dissipation converges over time to a value of -8.38%.
- The identified soil dissipation is underestimated compared with the energy dissipation computed with eq. 2.14. The cause of this phenomena might be that the rotational velocity at the bottom of the model is effected by the present structural damping in this lower element. This small interaction between the two damping mechanisms results in a larger energy dissipation of the soil.
- Since the collaboration of the damping mechanisms (e.g. soil and structure damping) affect each other, eq. 2.14 does not give an accurate comparison. However, since there is no damper operator yet which describes the dissipated energy of the structure, this small contribution cannot be described and added to eq. 2.14. Further research on this matter is needed.
- This small collaboration between damping mechanisms is also observable by identifying the damping value with the EFA technique. Compared with the input value the identified value has an error of -8.38%.

Structural energy dissipation

- A relative error on the identification of the structural energy dissipation of 13.61% is found. The identification of the structural energy dissipation gives an overestimation compared with the modified FEM energy.
- Since there is no damper operator yet which describes the dissipated energy of the structure, an accurate comparison is not possible yet. FEM generates only the total amount of energy dissipation of the system and does not separate the contribution of several damping mechanisms.

5.3 Case 3 - only soil damping - reduced node information

In this case the amount of information extracted from the FEM model is reduced by only using data at the top and bottom node of the system. From the top node, the displacement and velocity of the model are used. And from the bottom node, the rotational displacement and velocity are used. An assessment of the error with which the energy method quantifies a single damping mechanism when a reduced amount of information is available is investigated with this case. Analytical expression for the mode shapes are used to describe the dynamic behaviour of the system at other node positions, see Appendix A for the derivation. In Figure 77 the first bending mode shape is shown. The rotational spring at the bottom of the system not only influences the mode shape of the building, but also allows for a rotational at the base which results in a rigid body displacement with height. Both shapes are normalized and shown in Figure 77.

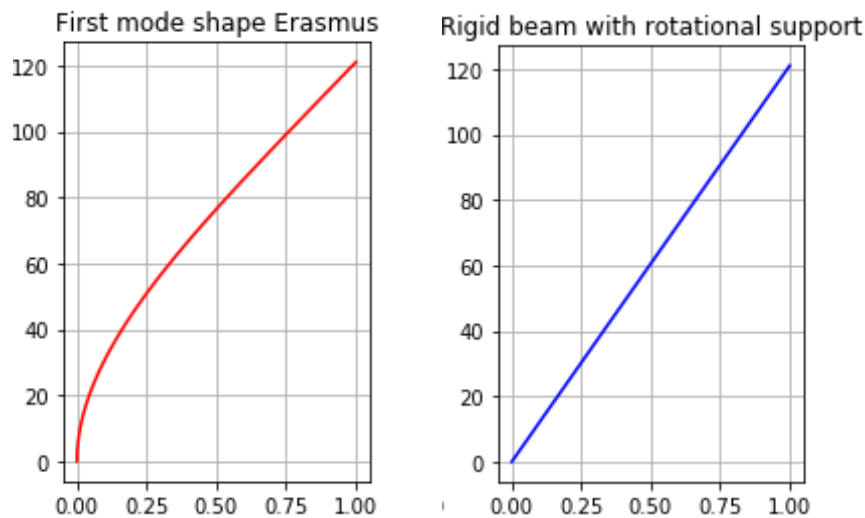


Figure 77 -(left) Normalized first mode shape derived analytically based on Euler-Bernoulli beam theory. (right) normalized shape which describes the rigid behaviour of the beam influence by the rotational spring at the bottom of the system

In Figure 78 the top displacement and velocity over time of the FEM model is plotted. Assumed is that the top displacement and velocity can be divided into the displacement or velocity due to the bending mode shape and the displacement or velocity due to the rigid beam behaviour influenced by the rotational spring. Hereby, the rotational displacement of the bottom part is multiplied with the length of the building to determine the horizontal displacement. This distinction has been pursued in determining the energies needed to solve the energy balance. For the determination of the potential energy of the beam the curvature of the beam is calculated by multiplying the top displacement (due to the bending mode shape as shown in Figure 77) over time by the normalized bending mode shape. This data set is differentiated twice with respect to length resulting in the curvature due to the bending mode shape. With the known curvature of the beam at every position in time the potential energy of the beam can be calculated. The same procedure is used when considering the top displacement due to the rigid beam behaviour under influence by the rotational spring.

For the calculation of the kinetic energy of the beam the velocity displayed in Figure 78 is used. The equations described in 2.5.1 Case 1 are applicable since the energy balance does not change. The analysis procedure of the FEM model is described in 2.3.2.

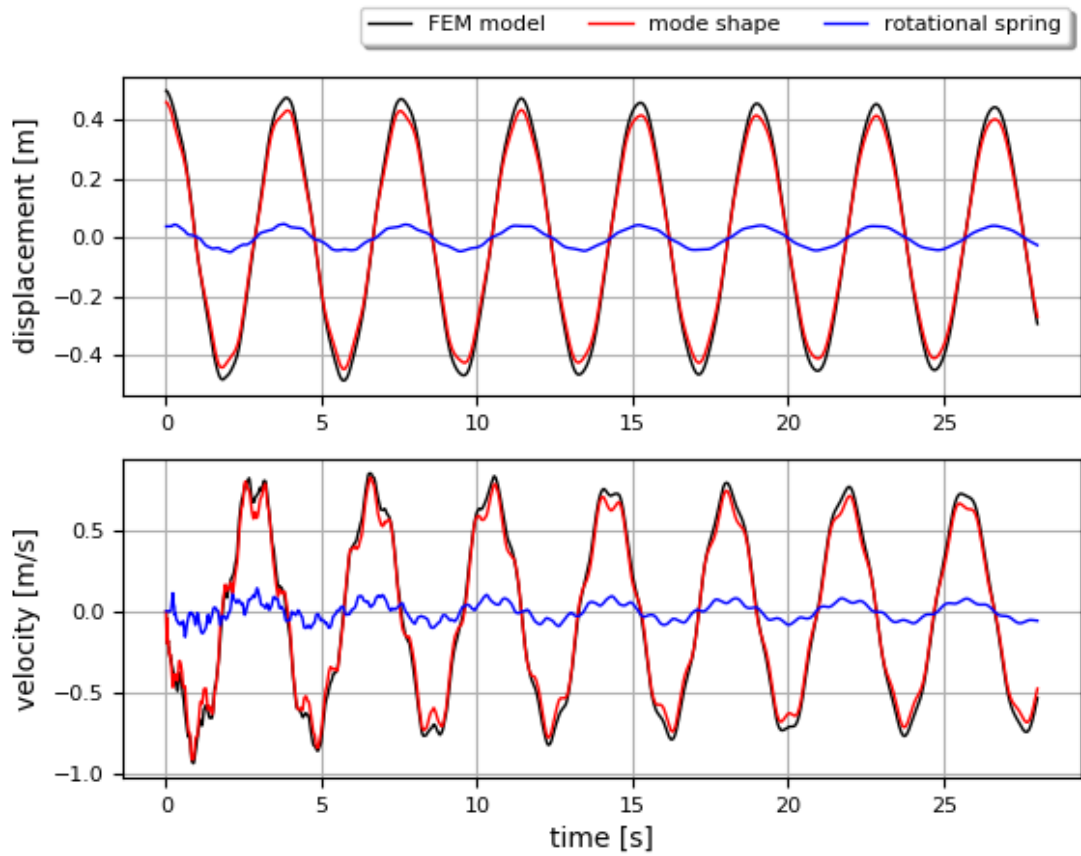


Figure 78 – This graph shows the top displacement (top) and velocity (bottom) over time of the FEM model (black line). Assumed is that the top displacement and velocity can be divided into the displacement or velocity due to the bending mode shape (red line) and the displacement or velocity due to the rigid behaviour of the beam influenced by the rotational spring (blue line).

5.3.1 Kinetic energies

Figure 79 shows the kinetic energy determined with the EFA technique and the kinetic energy directly obtained from the Abaqus FEM model. The figure shows that the energies matches well but larger differences are found compared to case 1.

The relative error between the kinetic energy determined with the EFA technique and the kinetic energy obtained from Abaqus are also plotted in Figure 79. The peak values in the bottom graph are caused by the near zero values of the FEM potential energy. The relative error is determined by calculating the difference between the two energies and divided with the FEM potential energy. Consequently, the small values for FEM potential energy results in large errors. By eliminating the large errors and only considering the minimum values of the relative errors, a mean relative error of -11,15% is found.

The reason for the underestimation of the kinetic energy derived with the EFA technique seems to be that only the first bending mode shape is considered when predicting the dynamic behaviour of the system. From this plot it can be seen that the period of the vibration varies, which indicates that multiple frequencies are presented.

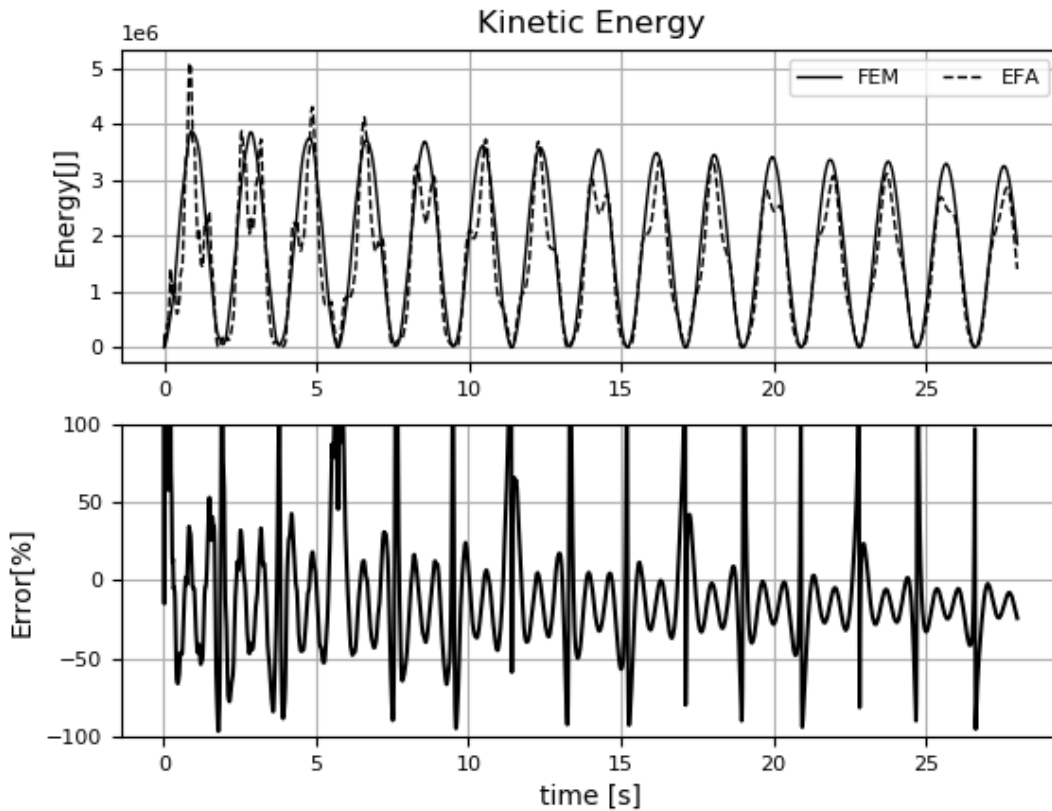


Figure 79 - The top graph shows the kinetic energies determined with the EFA technique and directly obtained from the FEM model. The bottom graph shows the relative error between these energies

5.3.2 Potential energies

Figure 80 shows the potential energies obtained from Abaqus, and determined with the EFA technique. The figure shows that the energies matches well but larger differences are found compared to case 1.

Figure 80 also shows the relative error between the FEM and EFA results. Whether the EFA underestimates or overestimates the potential energy is hard to conclude from this plot. It seems that the potential energy derived with the EFA is sometimes negative.

Part of the error is caused by the assumption that only the first bending mode shape is considered when predicting the dynamic behaviour of the system. From the top graph in Figure 80 it can be seen that the period of the vibration varies, which indicates that multiple frequencies are presented. The cause of the negative values determined with the EFA is unknown.

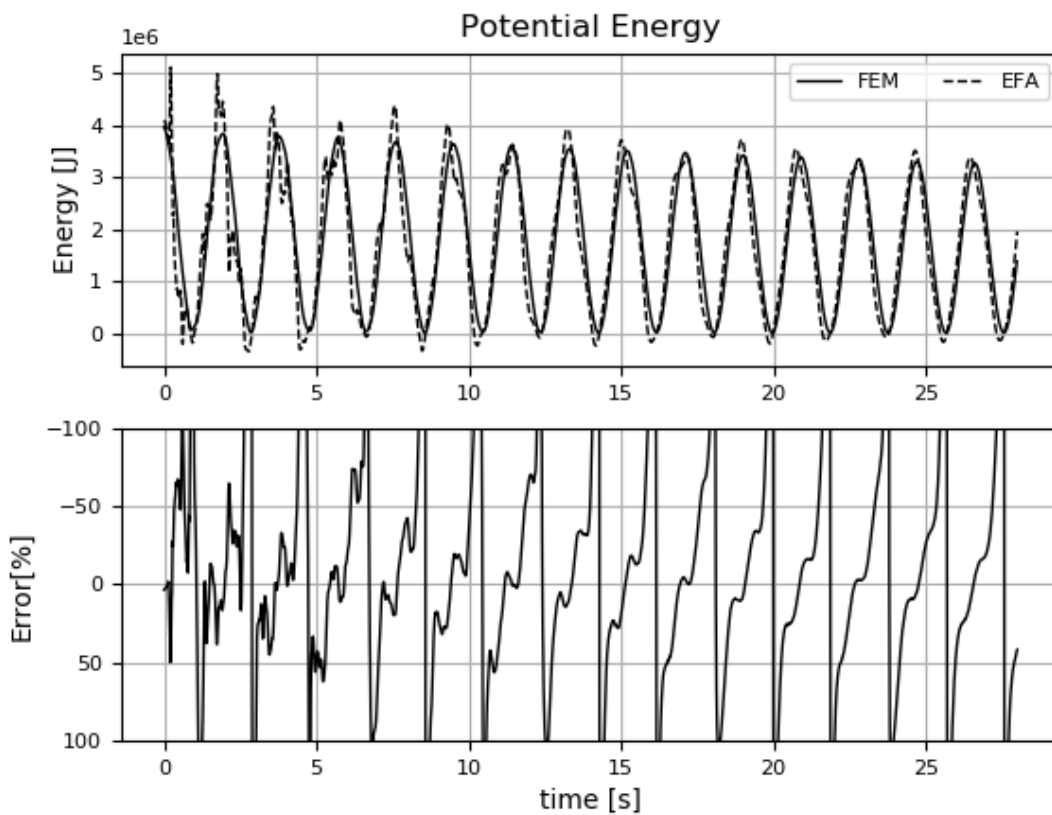


Figure 80 -The top graph shows the potential energies determined with the EFA technique and directly obtained from the FEM model. The bottom graph shows the relative error between these energies.

5.3.3 Energy dissipation

In the early stage of this research the determination of the accuracy of the identification of the soil damper value was done by integrating the energies needed for the EFA over the total simulation time of 28 seconds. With this approach the following damping value were found with a relative error of -1.47%.

	Input value	Identified value with the EFA
Cr	1.32 E+11 Nms/rad	1.34 E+11 Nms/rad

Expressing the energy dissipation over time gives more insight in the identification of the energy dissipation over time. *Figure 81* shows the energy dissipation of the system directly obtained from FEM and determined with the EFA technique. The figure shows that the energy dissipation over time derived with the EFA fluctuated over time. *Figure 82* shows the relative error between the dissipated energy obtained with FEM and the energy obtained with the EFA versus time. From the relative error it can be seen that the error reduces over time. Between 20 and 28 seconds the mean error value is 23.47%. The cause of the fluctuating differences might be caused by the lack of higher mode shapes when predicting the energies needed for the energy balance. To accommodate for the full dynamic behaviour of the system excited by an initial displacement, considering more modes might result in a higher accuracy of the identification of energy dissipation with the EFA method.

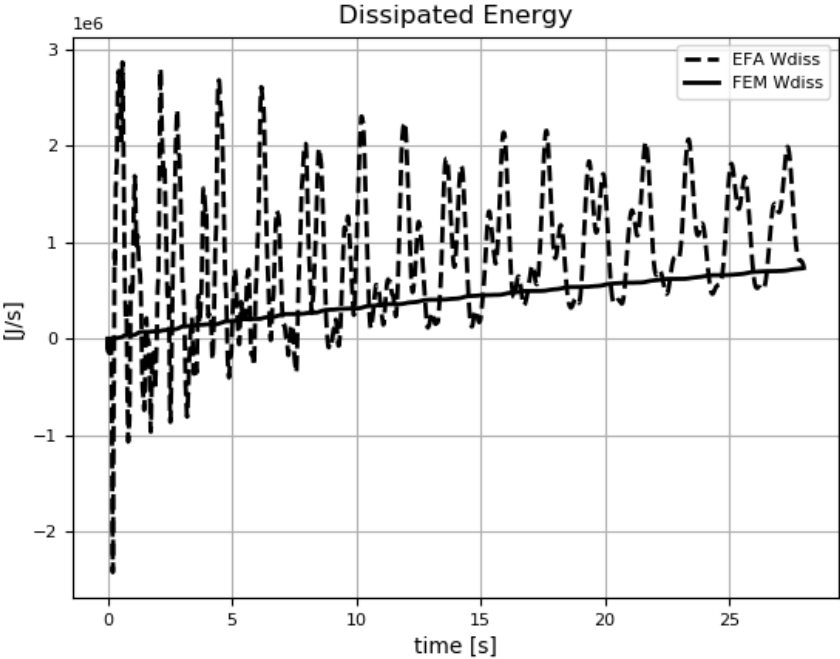


Figure 81 - Comparison of the extracted FEM dissipated energy and the derived EFA energy dissipation.

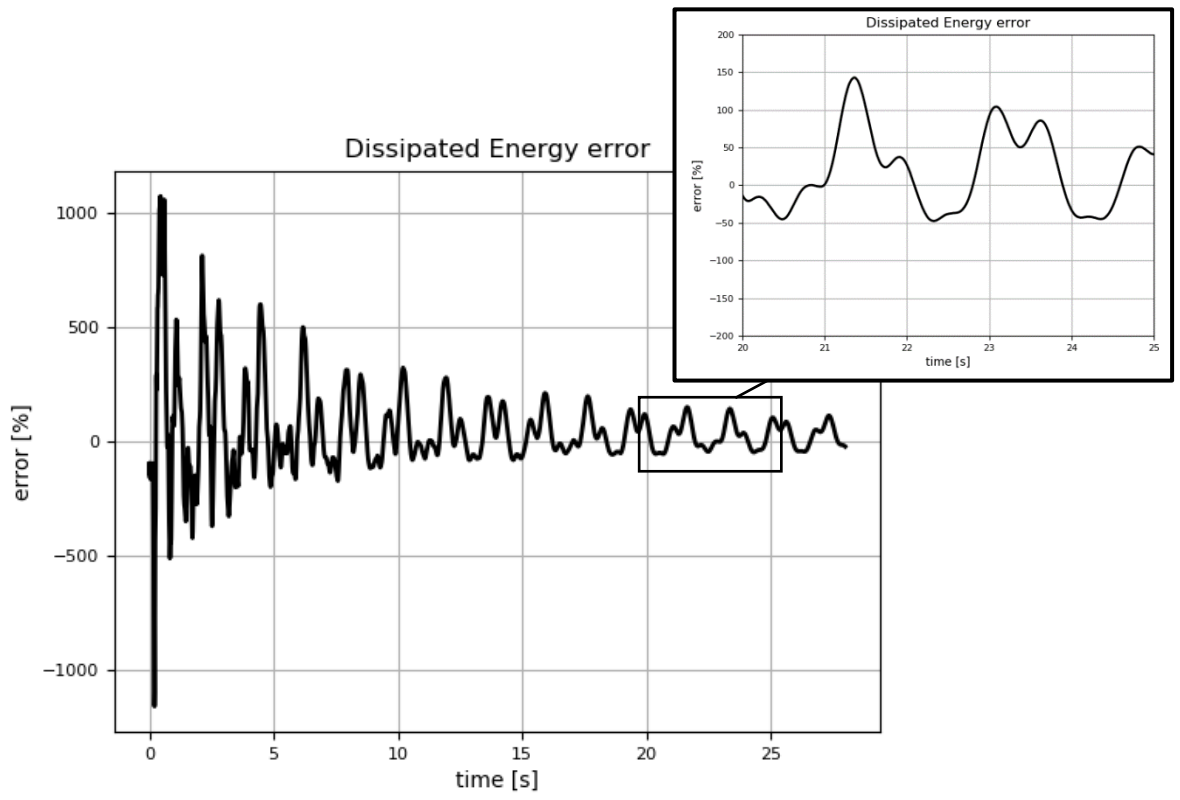


Figure 82 – Relative error between FEM and EFA energy dissipation

5.3.4 *Summary*

Damping was introduced to the system by means of a dashpot damper at the bottom. In this case the amount of information extracted from the FEM model is reduced. Of the top node of the Abaqus FEM model the horizontal displacement and velocity were obtained. From the bottom node the rotational displacement and velocity were obtained. These data sets, combined with analytical expressions for the first mode shape, were used in the EFA technique to determine the kinetic, potential and dissipated energy of the system. To assess the accuracy of the EFA technique, these energies were compared with the energies obtained from Abaqus. The dissipated energy obtained from the FEM model and determined with the EFA technique were used to determine damper values of the dashpot at the bottom of the system. These were compared to the input value for the dashpot damper in the FEM model. This case resulted in the following findings:

Kinetic energy

- The figure shows that the energies matches well but larger differences are found compared to case 1. A mean relative error of -11,15% is found between the EFA and FEM values.
- The underestimation of the kinetic energy derived with the EFA technique seems to be caused by the assumption that only the first bending mode shape is considered when predicting the dynamic behaviour of the system.

Potential energy

- Whether the EFA underestimates or overestimates the potential energy is hard to conclude from this case. It seems that the potential energy derived with the EFA is sometimes negative.
- A part of the errors are caused by the assumption that only the first bending mode shape is considered when predicting the dynamic behaviour of the system. The period of the vibration varies, which indicates that multiple frequencies are present. The cause of the negative values determined with the EFA is unknown.
-

Energy dissipation

- In the early stage of this research the accuracy of the identification of the soil damper value was done by integrating the energies needed for the EFA over the total simulation time. With this approach a relative error of -1.47% between the input value and identified soil damper is found.
- Expressing the energy dissipation over time gives more insight in the identification of the energy dissipation over time. The identified energy dissipation shows large fluctuations over time. From the relative error it can be seen that the error reduces over time. Between 20 and 28 seconds the mean error value is 23.47%.
- The cause of the fluctuating differences might be caused by the lack of higher mode shapes when predicting the energies needed for the energy balance. To accommodate for the full dynamic behaviour of the system excited by an initial displacement, considering more modes might result in a higher accuracy of the identification of energy dissipation with the EFA method.

5.4 Case 4 – Only soil damping with wind load

In this case wind tunnel data is introduced in the FEM model. An accurate assessment of the error in which the energy method quantifies a single damping mechanism when wind load is applied can be investigated with this case. The energy balance described in 2.5.2.2 to identify the soil damper is used for this case. The energy flux implicitly involves the influence of the wind load. The analysis procedure of the data from the FEM model is described in 2.3.3

5.4.1 Abaqus energy output

Figure 83 shows the energies which are obtained directly from the FEM model in Abaqus. This plot shows how the kinetic, potential and dissipated energy of the model are related to each other, and how they behave over time under influence of wind load. Influenced by the wind load, the energies fluctuates not uniform like Case 1. The external work due to the wind load applied to this system is plotted in Figure 83.

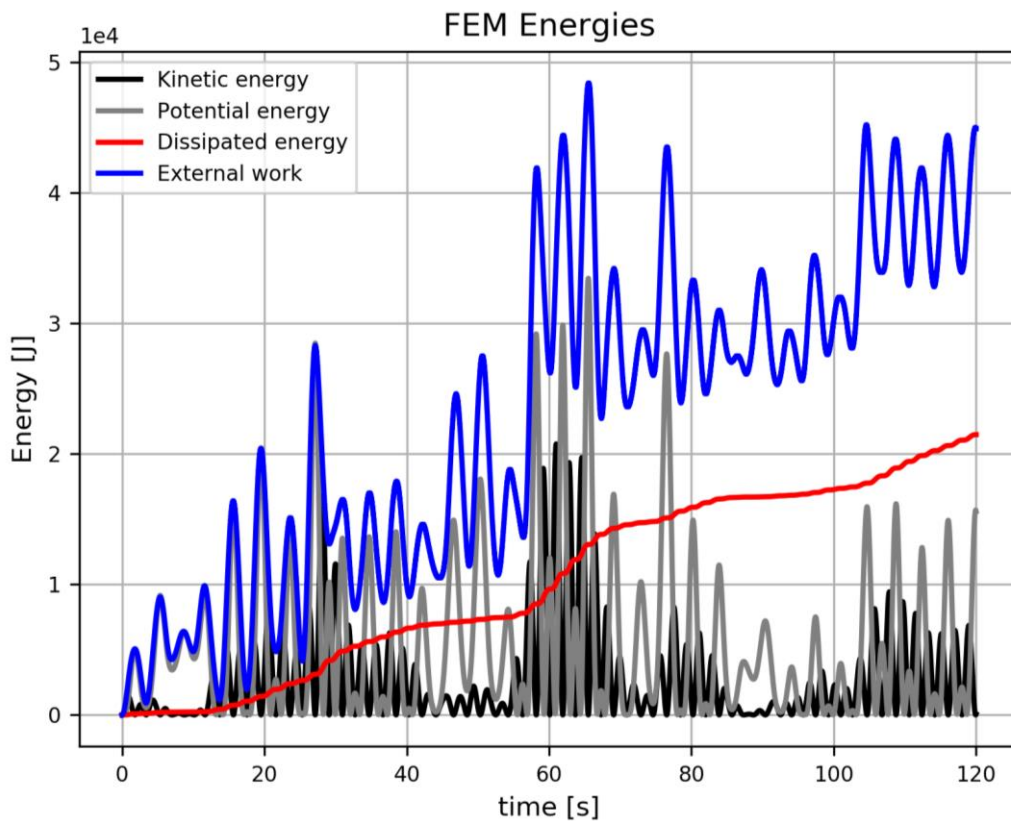


Figure 83 - Plot of the extracted energies from the FEM model.

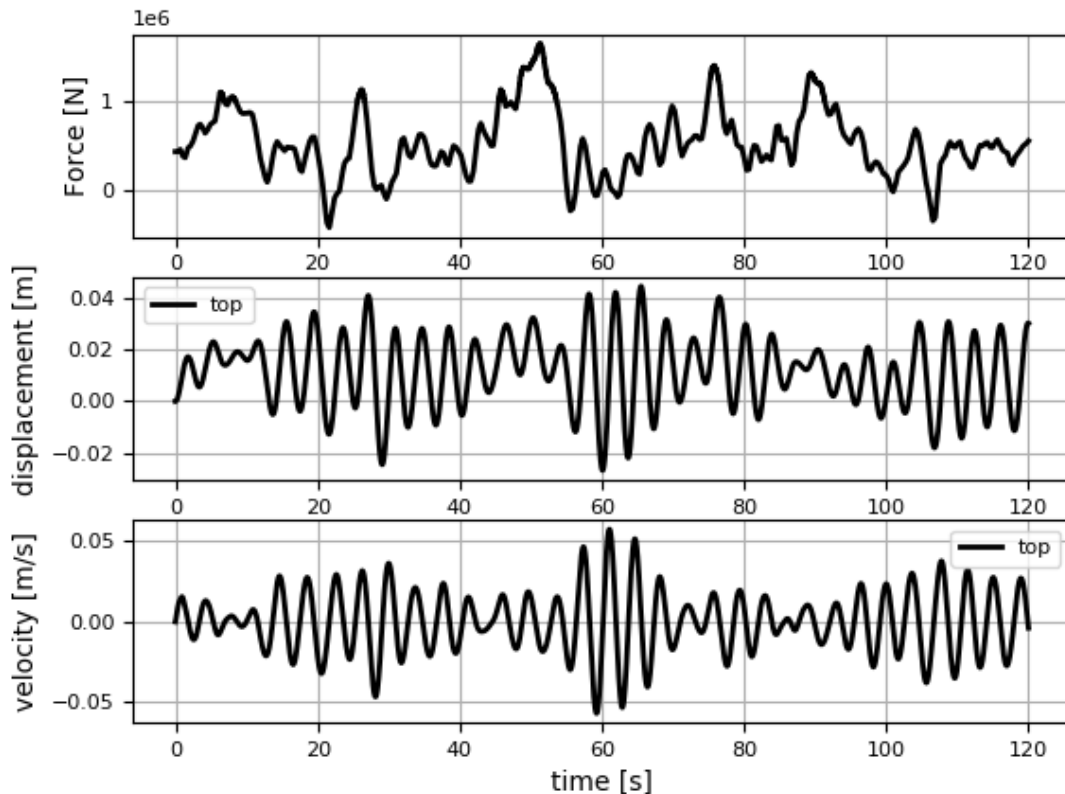


Figure 84 - The top graph shows the wind load on the whole system considering a full wind tunnel data analysis. The figure in the middle, represents the displacement over time at the top of the system. The bottom graph shows the velocity over time at the top of the system.

In Figure 84 the wind load is expressed in the force over time. This force depicted in Figure 84 is the summation of the wind time series applied on every node. Multiplying the wind load at each node with the velocity of that specific node results in the power added to the node. The total external power added to the system is shown in Figure 83. It can be seen that the maximum force at 52 seconds results in an increase in power and potential energy at 58 seconds. The time difference between applied load and the rapidly increase of the induced power is caused by the fact that the system needs time to response to the applied load before the velocity of the system and so the response can be adjusted accordingly. The displacement and velocity of the top of the system are also shown in Figure 84. Since the system wants to return to its equilibrium position, the velocity increases. The behaviour of the velocity is recognizable in the plotted kinetic energy of the system shown in Figure 83. While the displacement is recognizable in the potential energy. The energy dissipation in the time interval 60 to 75 seconds increases linear because of the increased velocity of the system.

Furthermore, the displacement and velocity in Figure 84 shows an interesting phenomenon which is called beating. This phenomenon occurs when the natural frequency and the frequency of the force are close.

At last, the force plotted in Figure 84 shows some notable negative values. A mistake has been made while combining the suction and compression coefficients. This resulted in lower pressure coefficients.

5.4.2 Kinetic energies

Figure 85 shows the kinetic energy determined with the EFA technique and the kinetic energy directly obtained from the Abaqus FEM model. The figure shows that the energies are in good agreement with each other.

The relative error between the kinetic energy determined with the EFA technique and the kinetic energy obtained from Abaqus are plotted in Figure 85. This figure shows the error is small and fluctuates randomly between -0.13% and 0.18%. This indicates that there are no bias errors in the kinetic energy computation with the EFA technique.

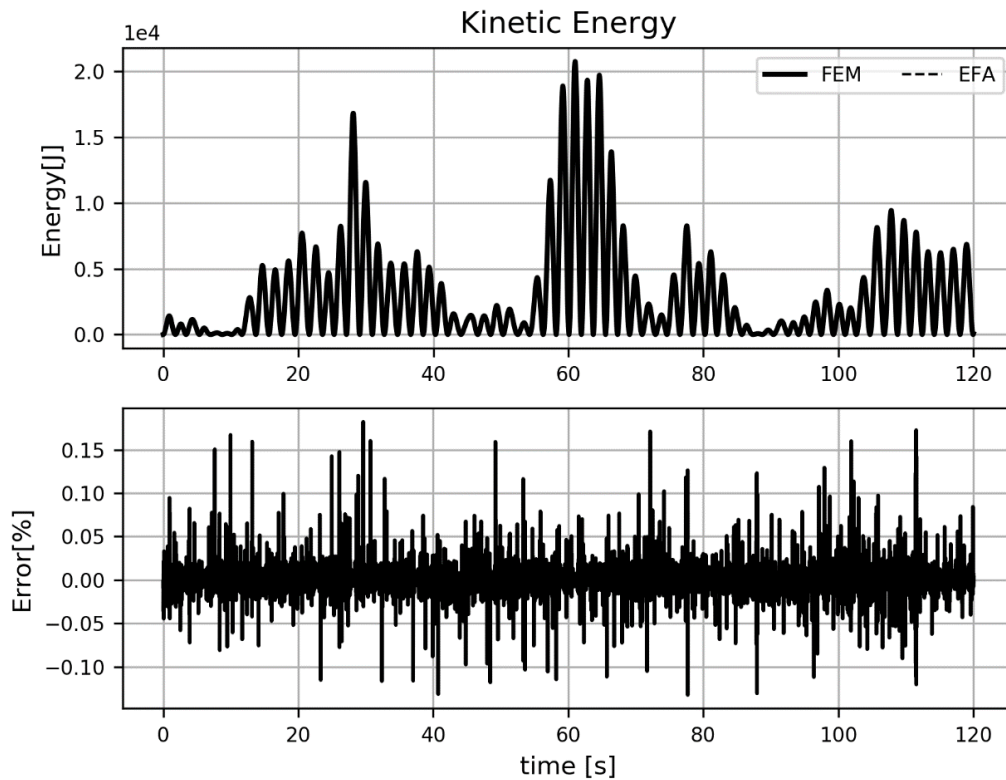


Figure 85 - The top graph shows the kinetic energies determined with the EFA technique and directly obtained from the FEM model. The bottom graph shows the relative error between these energies.

5.4.3 Potential energies

Figure 86 shows the potential energies obtained from Abaqus, and determined with the EFA technique. Figure 86 also shows the relative error between the FEM and EFA results. In this comparison large errors are found. The error deviates between -10% and 100%. The peak values in the bottom graph are caused by the near zero values of the FEM potential energy. The relative error is determined by calculating the difference between the two energies and divided with the FEM potential energy. Consequently, the small values for FEM potential energy results in large errors. By eliminating the large errors and only considering the minimum values of the relative errors, it can be seen that the EFA technique underestimates the determination of the potential energy. The cause of the underestimation of the potential energy derived with the EFA technique might be the same as Case 1. From this plot it can be seen that the period of the vibration varies, which indicates that multiple frequencies are presented.

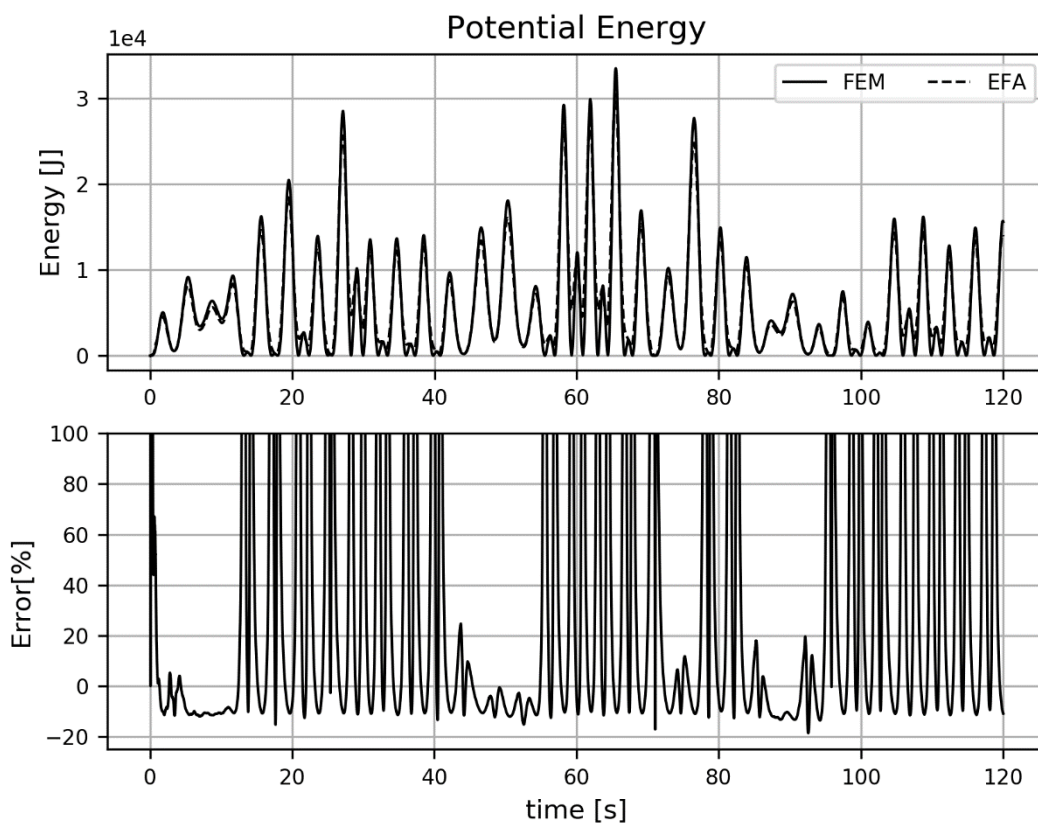


Figure 86 - The top graph shows the potential energies determined with the EFA technique and directly obtained from the FEM model. The bottom graph shows the relative error between these energies.

Further, the FEM model derives a potential energy which combines the potential energy of the beam and spring. The ratio between these energies is shown in Figure 87. This figure shows the total potential energy, the beam potential energy and the spring potential energy derived with the EFA technique separately. As a reference the potential energy obtained from the FEM model is plotted. The timespan between 45 and 75 seconds is plotted in detail. It is clear that the beam potential energy and the obtained FEM potential energy are in good agreement which each other and act in the same frequencies. However, at the amplitude small differences are noticeable. It appears that the potential energy of the spring has a different frequency than the potential energy of the beam. This suggest that local frequencies are presented at the bottom of the system, which are not strongly present when considering the whole system. By analysing the spring, beam and FEM potential energies in frequency spectrum, confirms the presence and the difference between frequencies in which these energies act, see Figure 88.

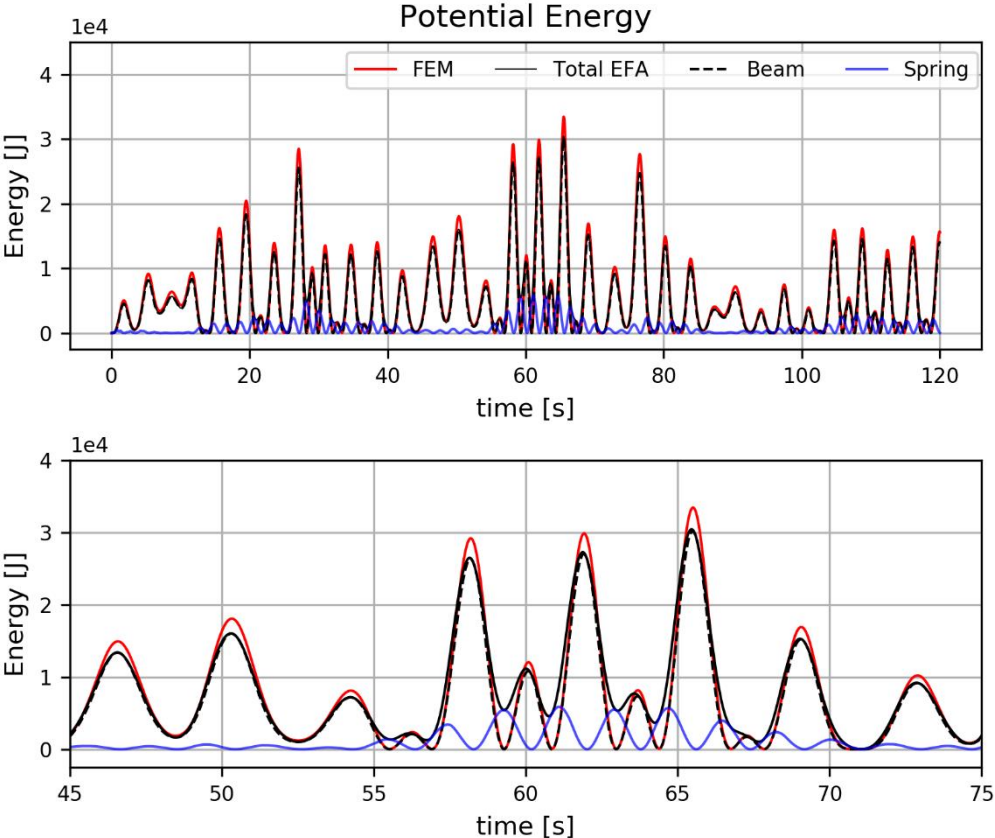


Figure 87- Potential energies derived with the EFA technique. The potential energy obtained from the FEM model is plotted as reference.

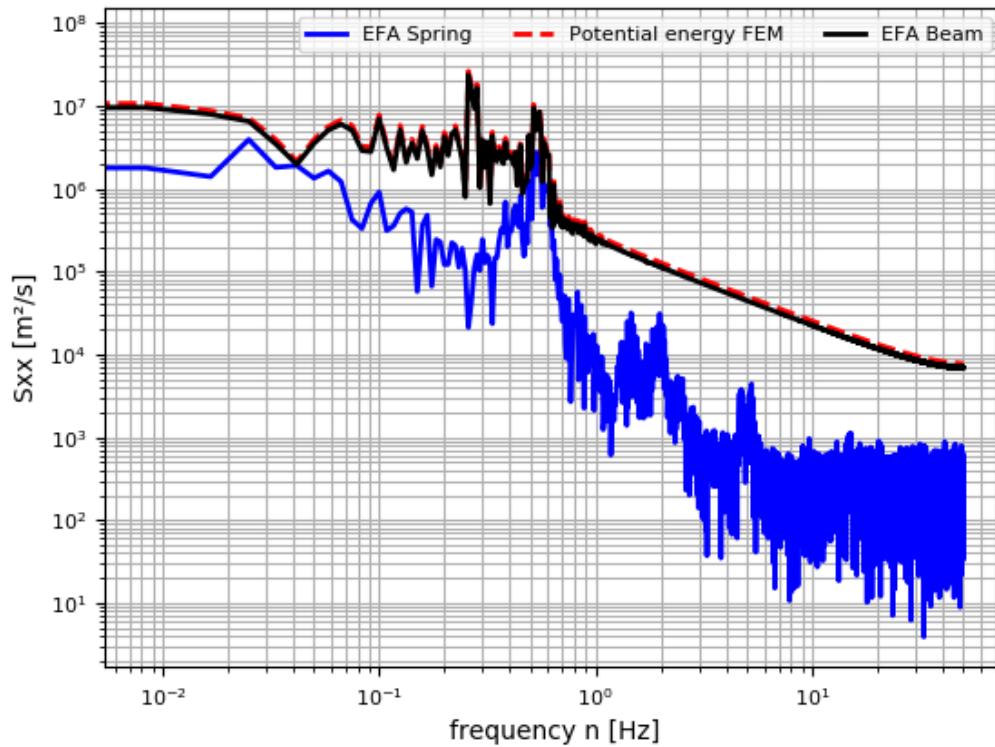


Figure 88 - Comparison of the potential energies in frequency spectrum. The potential energy of the spring (blue line). The potential energy of the beam (black line). The potential energy extracted from the FEM model (dashed red line).

Figure 88 shows the potential energies obtained from Abaqus in frequency spectrum. The potential energy of the beam derived with the EFA technique follows the FEM potential energy. The first frequency is found at 0.27 Hz and the second frequency 0.55 Hz. The spring potential energy seems to be active in the second frequency and shows the existence of some higher frequencies.

5.4.4 Energy dissipation

Figure 89 shows the energy dissipation of the system directly obtained from FEM and determined with the EFA technique. The figure shows that the energy dissipation of both methods are in good agreement with each other. Figure 90 shows the relative difference between the dissipated energy obtained with FEM and the energy obtained with the EFA versus time. In the first 40 seconds higher damping error are found. After 40 seconds the error is converged to a more stable damping error deviates around -0.60%. This error might be the caused by the earlier discussed integration points in case 1.

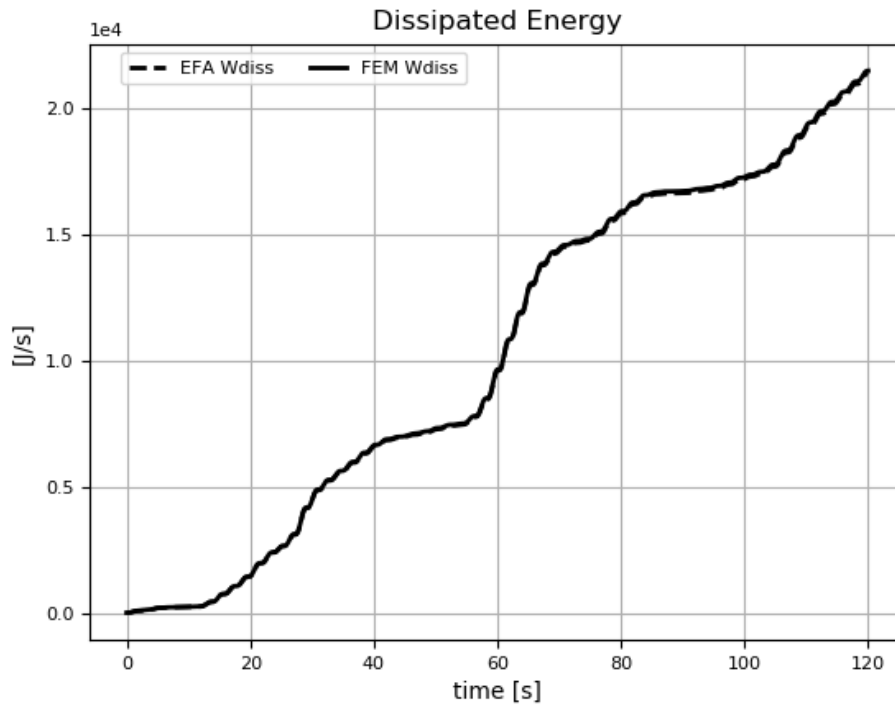


Figure 89 - Comparison of the extracted FEM dissipated energy and the derived EFA energy dissipation

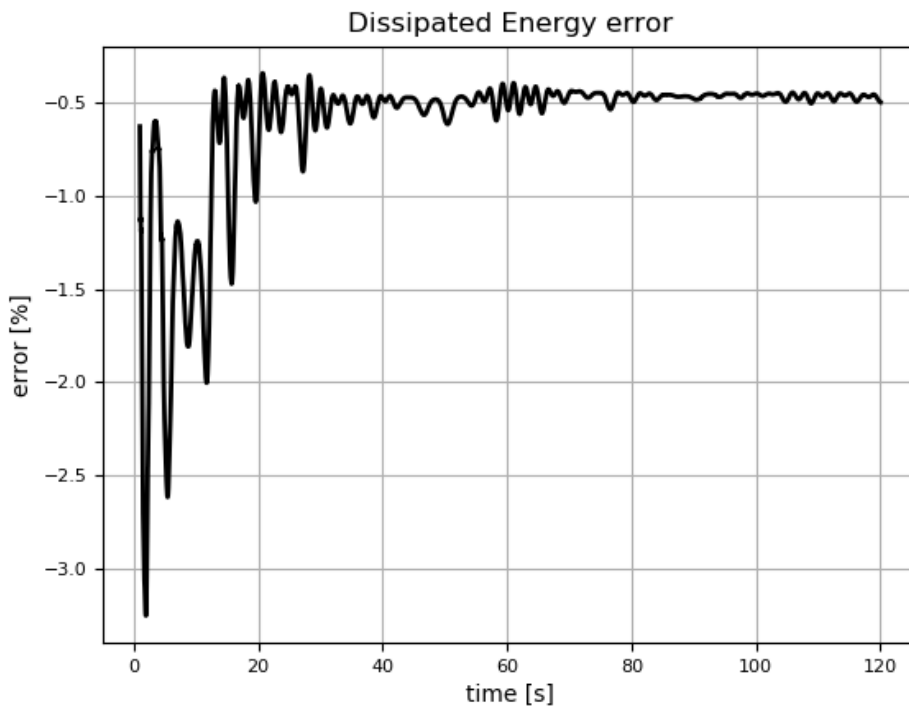


Figure 90 -Relative error between FEM and EFA energy dissipation

5.4.5 *Damping value*

Figure 91 shows the results of the damping values. The energy dissipation determined with the EFA technique are translated to a damping value with eq. 2.15. The dashpot damper value $C_r = 6.60e+11$ Nms/rad that was used as input for the FEM model is also provided as reference. Over time the C_r values obtained with the EFA technique converge to a more stable value, which deviate to an error of -0.60% as shown in Figure 92. This indicates that the EFA technique slightly underestimate the determination of the damping value. It appears that the simulation time contribute to the accuracy in which the identification with the EFA technique takes place.

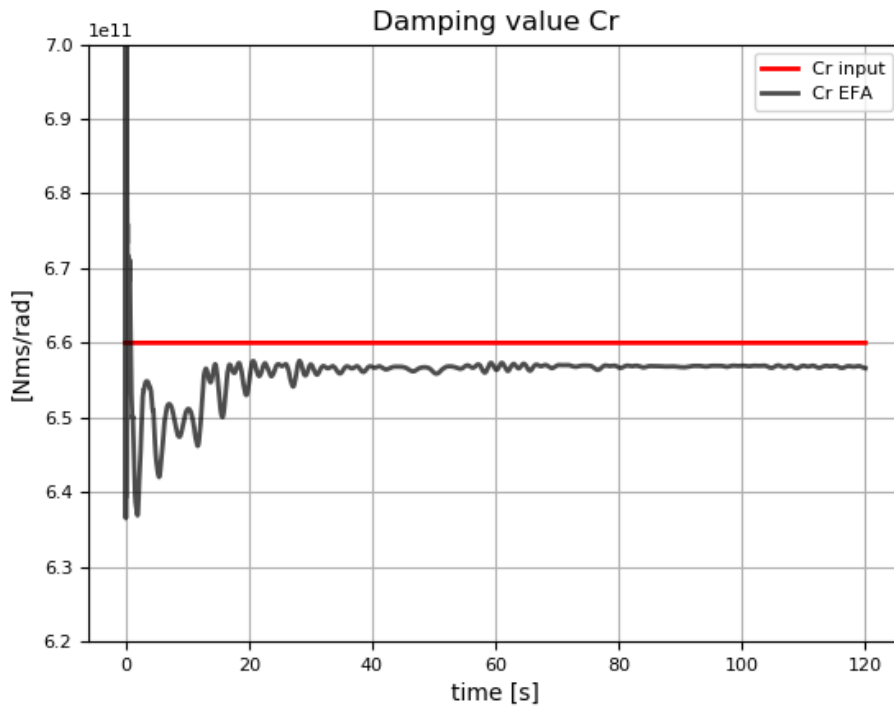


Figure 91- Plot of the damping values.

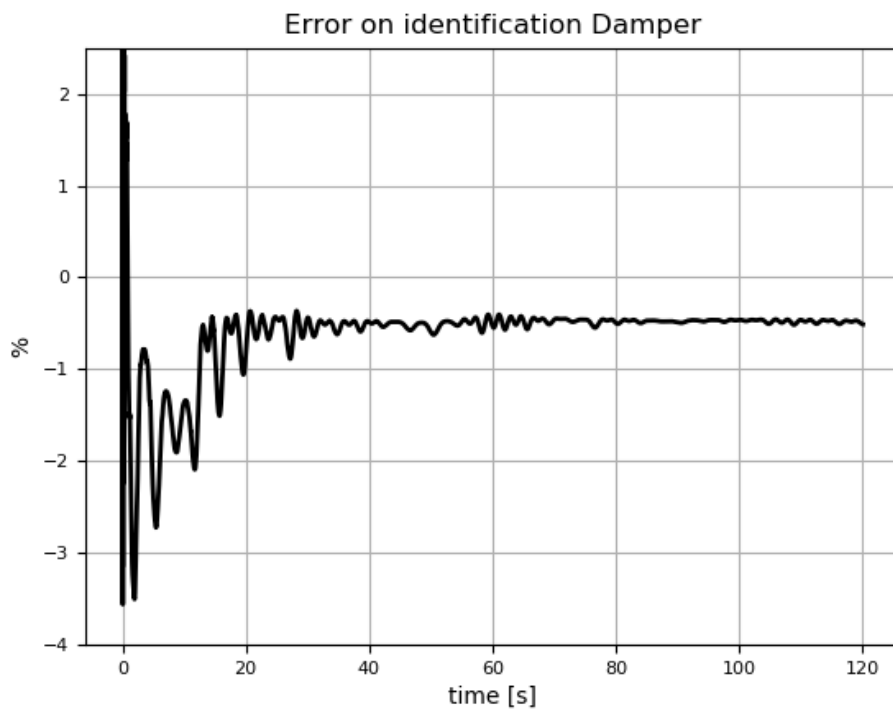


Figure 92 - Relative error between the damping input value and the damping value identified with the EFA technique.

5.4.6 Summary

Within Case 4 wind tunnel data is introduced to the FEM model. Damping was introduced to the system by means of a dashpot damper at the bottom of the system representing the rotational damping in the foundation. For the understanding of the energies influenced by wind load, first the kinetic and potential energy are explained. Hereafter the energy dissipation is identified by finding equilibrium in the bottom part of the system representing the foundation. The energy flux, which implicitly involves the influence of the wind load, and the spring energy flux where needed for this analysis. The following data were obtained from the Abaqus FEM model in order to identify the energy dissipation:

- Base energy flux:
 - o Curvature at the bottom
 - o Rotational velocity at the bottom
 - o EI
- Spring energy flux:
 - o Rotational displacement at the bottom
 - o Rotational velocity at the bottom
 - o Kr

To assess the accuracy of the EFA technique, the identified energy dissipation were compared with the energy dissipation directly obtained from Abaqus. The dissipated energy determined with the EFA technique were used to determine damper values of the dashpot at the bottom of the system. This determined damping value is compared to the input value for the dashpot damper in the FEM model. This case resulted in the following findings:

Kinetic energy

- The kinetic energy determined with the EFA technique deviates between -0.13% and 0.18 % from the kinetic energy directly obtained from the FEM model.

Potential energy

- Comparing the potential energy derived with the EFA technique with the potential energy directly obtained with the FEM model, resulted at first in small differences. Expressing these differences in relative errors resulted in large errors which deviate between -10% and 100%.
- To get a better understanding of the potential energy of the system in case 4, the spring and beam potential energy where investigated separately. It appears that the potential energy of the spring has a different frequency than the potential energy of the beam. This suggest that local frequencies are presented at the bottom of the system, which are not strongly present when considering the whole system. Analysing the spring, beam and FEM potential energies in frequency spectrum confirms the presence and the difference between frequencies in which these energies act.

Energy dissipation

- The energy dissipation determined with the EFA technique converges over time to an error value of -0.60%.
- This error might be caused by the earlier discussed integration points in case 1.
- The error converges to zero over time which means that the duration of the simulation have impact on the determination of energy dissipation with the EFA technique.

Damping value

- The identified damping value with the EFA technique also converges over time to an error of -0.60%. This error might be caused by the earlier discussed integration points combined with the time span of the simulation.

5.5 Case 5 - Structural and soil damping with wind load

In this case a combination of a structural and soil damper is considered. An accurate assessment of the error in which the energy method quantifies several damping mechanisms can be investigated. Insight will be gained in the separation of multiple damping mechanisms and the influence of wind load. The strategy of 2.3.3 is used to accomplish this goal and the equations of 2.5.2.2. are used for identification of soil damping. The energy flux implicitly involves the influence of the wind load. However, the identification of the energy dissipation of the structure is different since external power due to wind must be taken into account.

5.5.1 Abaqus energy output

Figure 93 shows the energies which are obtained directly from the FEM model in Abaqus. This plot shows how the kinetic, potential and dissipated energy of the model are related to each other, and how they behave over time under influence of wind load. Compared to Case 4 the energy dissipation is noticeable larger in case 5. In case 5 the system is also provided with structural damping. The soil damping is increased in order to separate these damping mechanisms.

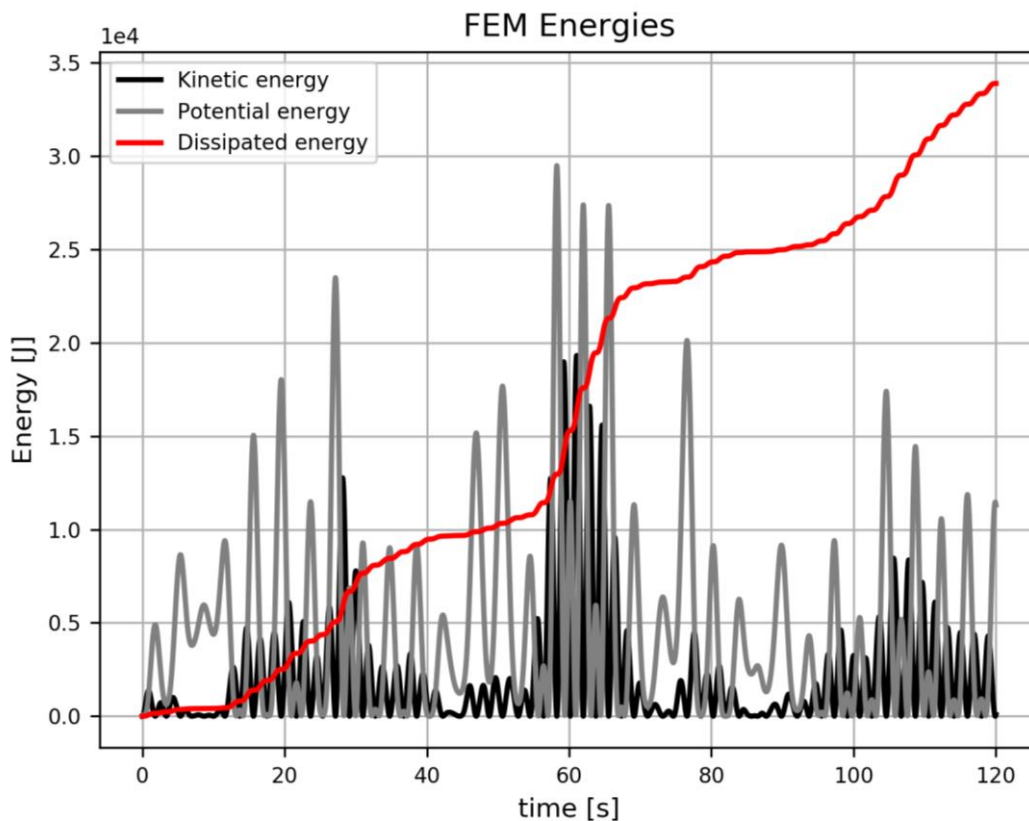


Figure 93 - Plot of the extracted energies from the FEM model.

5.5.2 Kinetic energies

Figure 94 shows the kinetic energy determined with the EFA technique and the kinetic energy directly obtained from the Abaqus FEM model. The figure shows that the energies are in good agreement with each other.

The relative error between the kinetic energy determined with the EFA technique and the kinetic energy obtained from Abaqus are also plotted in Figure 94. This figure shows the error is small and fluctuates randomly between -0.12% and 0.19%. This indicates that there are no bias errors in the kinetic energy computation with the EFA technique.

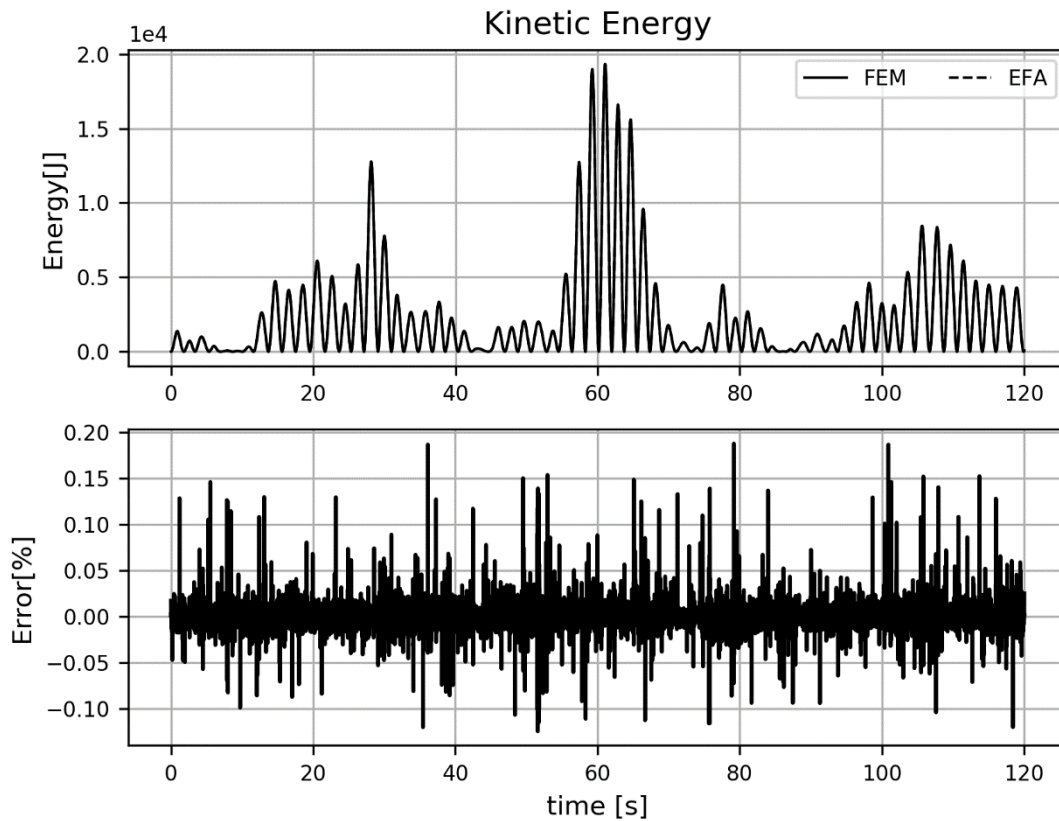


Figure 94 - The top graph shows the kinetic energies determined with the EFA technique and directly obtained from the FEM model. The bottom graph shows the relative error between these energies.

5.5.3 Potential energies

Figure 95 shows the potential energies obtained from Abaqus, and determined with the EFA technique. Figure 95 also shows the relative error between the FEM and EFA results. In this comparison large errors are found. The errors on the potential energy are almost similar to the errors found in Case 4 having some small deviations. The error in Figure 95 deviates between -10% and 100%. The peak values in the bottom graph are caused by the near zero values of the FEM potential energy. The relative error is determined by calculating the difference between the two energies and divided with the FEM potential energy. Consequently, the small values for FEM potential energy results in large errors. By eliminating the large errors and only considering the minimum values of the relative errors, it can be seen that the EFA technique underestimates the determination of the potential energy. From this plot it can be seen that the period of the vibration varies, which indicated that multiple frequencies are presented as also explained in figure .

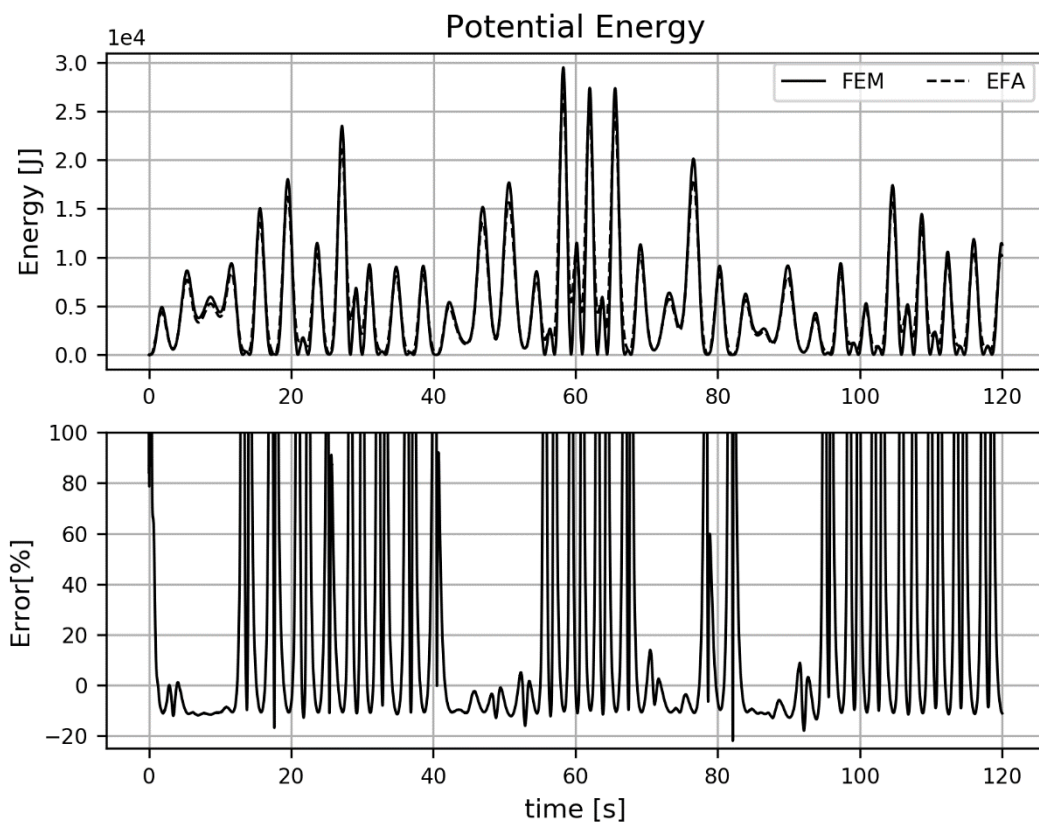


Figure 95 - The top graph shows the potential energies determined with the EFA technique and directly obtained from the FEM model. The bottom graph shows the relative error between these energies.

5.5.4 Total energy dissipation

Figure 96 shows the total energy dissipation of the system extracted from the FEM model and derived with the energy balance according to eq. 2.16.

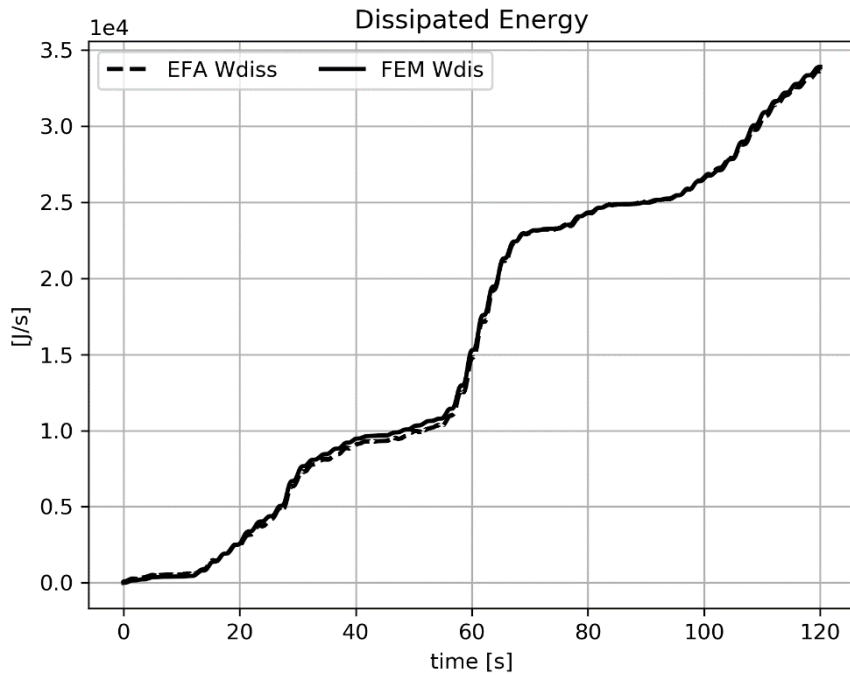


Figure 96 - Comparison of the extracted FEM dissipated energy and the derived EFA energy dissipation

Figure 97 shows the relative error of the total dissipated energy over time. The error converged to a more stable damping error of -0.83%. Note that the error converges to a stable value over time which means that the duration of the simulation have impact on the determination of energy dissipation with the EFA technique. From Figure 97 it appears that the total energy dissipation of the system can be identified with a high accuracy with the EFA technique.

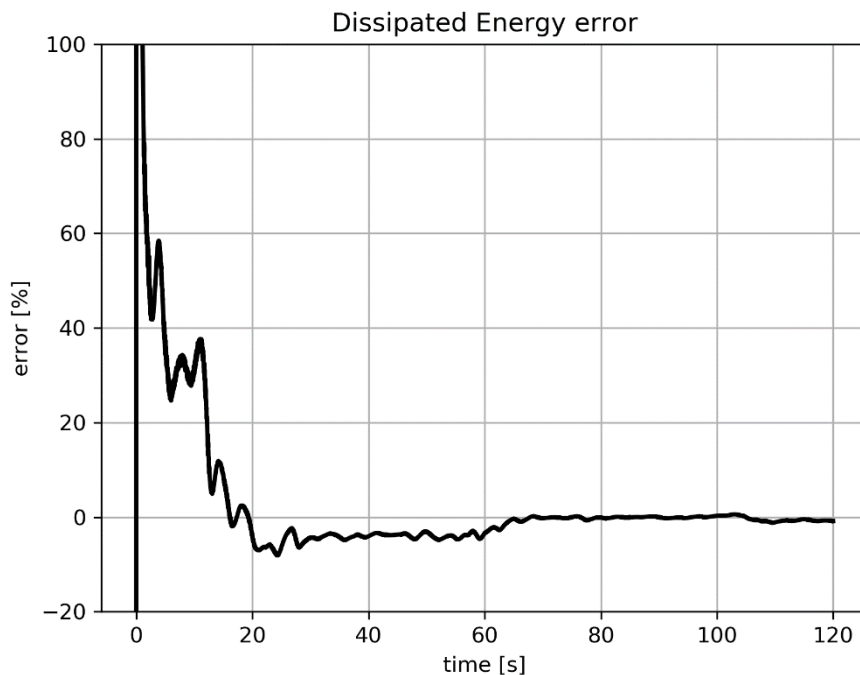


Figure 97 - Relative error between FEM and EFA energy dissipation

5.5.5 *Soil energy dissipation*

The soil damper is computed with the procedure described in 2.5.2.2. In order to identify the soil energy dissipation, equilibrium must be found between the bottom part of the building and its foundation. Figure 98 shows the energy flux (dashed line) derived with eq. 2.13. The curvature and rotational velocity of the bottom element are used from the FEM model to determine the energy flux at the bottom of the system. The energy flux by the spring (solid black line) is also plotted in Figure 98. The energy flux of the spring is the first derivative of the energy in this system described with eq. 2.12 and the rotational velocity of the spring is used from the FEM model. Figure 98 also shows the difference between these energies which is the energy dissipation when cumulative presented. It appears that larger differences are found at large amplitudes of the energy flux. The energy flux comprises the base moment and rotational velocity. Since the base moment is maximum at large displacement at the top it can be concluded that the energy dissipation is amplitude dependent.

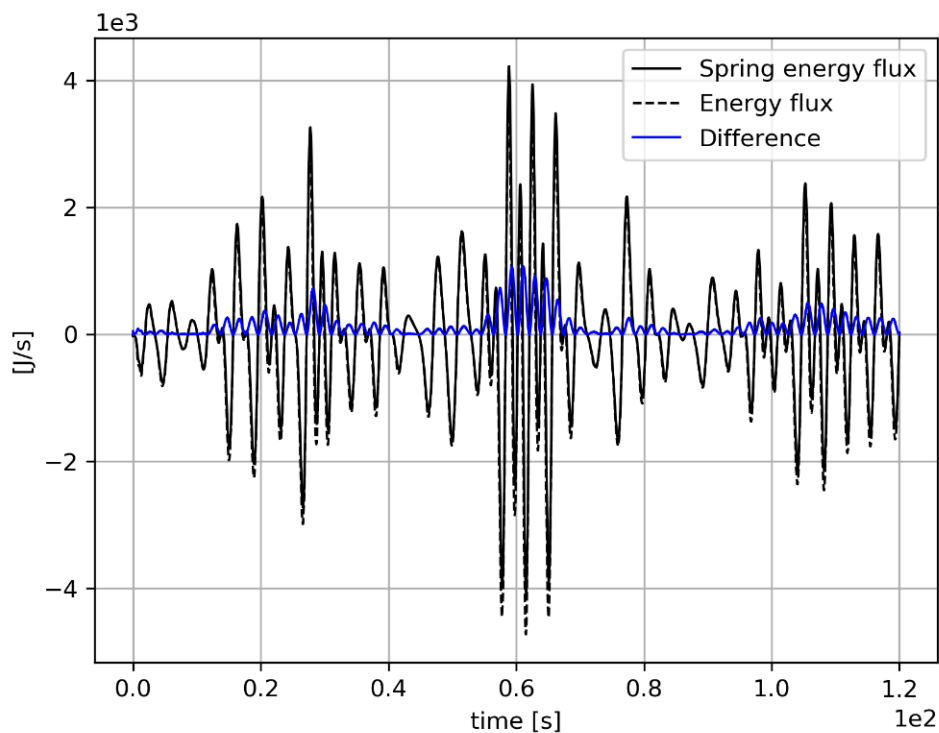


Figure 98 - Energy flux of the bottom part of the system (dashed line) and the spring energy flux (solid line). The difference between the bottom energy flux and spring energy is displayed in blue.

Furthermore, Figure 98 shows an interesting phenomenon which is called beating. This phenomenon occurs when the natural frequency and the frequency of the force are close. The energy flux 'beat' with a long period, which is inverse proportional to the difference between eigenfrequency (system) and frequency(wind). The beating can emerge only in the systems without (which is unrealistic) or with a small damping, which suppresses it in the course of time.

The FEM model only gives the total energy dissipation of the system when applying multiple damping mechanisms. It does not provide the dissipation in the soil and building separately. Therefore, the same procedure as in case 2 is used to identify the energy dissipation of the soil. Figure 99 shows the comparison between the identified EFA soil energy dissipation and the energy dissipation determined with eq. 5.2.

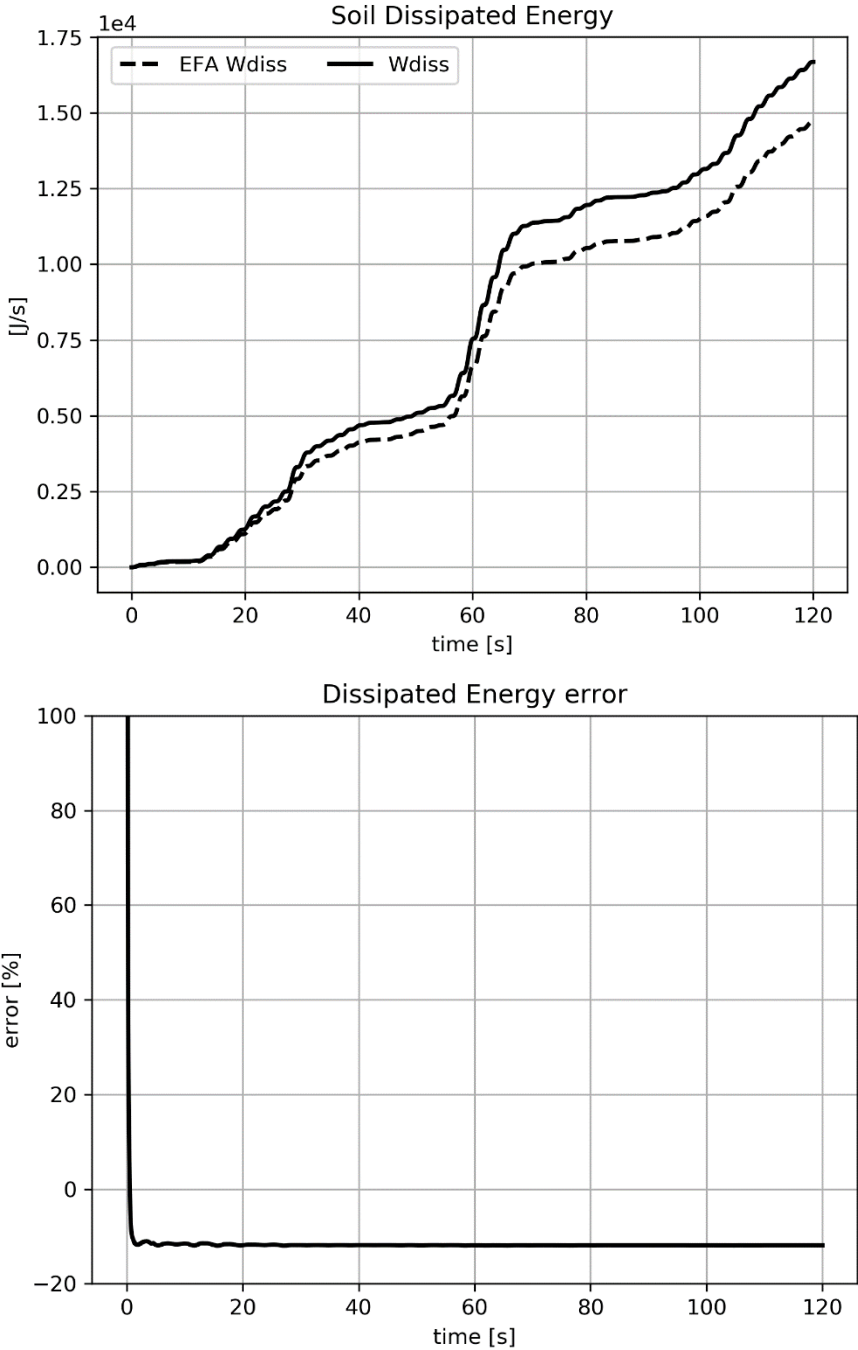


Figure 99 – The top graph the comparison of the identified soil energy dissipation with the EFA technique and the energy derived with eq. 4.32. The bottom graph shows the relative error between the above compared energies.

Figure 99 shows that the dissipated energy error converges to an error of -11.81%. This error is slightly larger than the value found in case 2 (-8.38%). This is caused by the effect of the stochastic wind load since this is the only difference between the two cases. The behaviour of the relative error over time is stable with the exception of the first 5 seconds.

A reason of the founded error might be that the determination of the EFA energy dissipation is based on the bottom curvature. The curvature is needed to determine the base moment to finally determine the energy flux. As explained before, Abaqus uses integration point for generating the curvature output, (see Figure 59 Case 1). These integration points are located in the middle of the bottom element. Half of the bottom element length is therefore not taken into account when determining the base moment. This phenomena might be the reason why the EFA identified soil energy dissipation is underestimated.

Another reason of the founded error might be that the rotational velocity at the bottom of the model is affected by the structural damping in this lower element of the FEM model. This small interaction between the two damping mechanisms results in a larger energy dissipation of the soil.

5.5.6 Soil damping value

The identified energy dissipation is translated to a damping value according to eq. 2.15 and displayed in Figure 100. The rotational velocity at the bottom is used which contains of a small influence of the structural damping as explained before. The input value and the identified damping value are plotted over time.

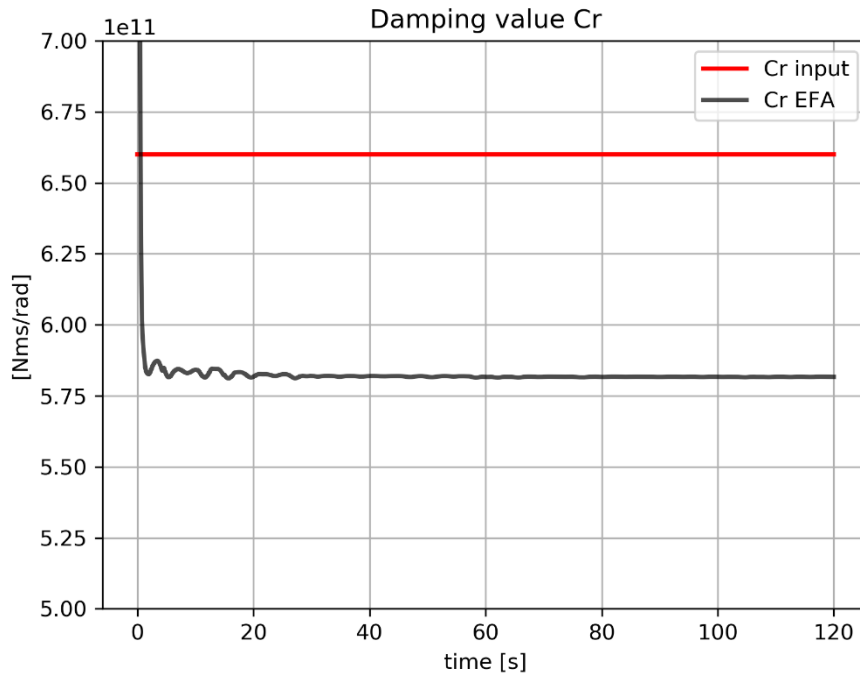


Figure 100 - Plot of the damping values

	Input	EFA
Cr	6.60 E+11 Nms/rad	5.82 E+11Nms/rad

Table 9 - comparison of the damping values

The final values at the end of the simulation have a relative error of -11.87%. The input value and the identified value at 120 seconds are shown in Table 9.

5.5.7 Structural energy dissipation

Figure 101 shows the energy dissipation of the structure. The energy dissipation of the soil dashpot according to eq. 5.2 is subtracted from the total FEM energy dissipation of the model in order to only display the structure damping.

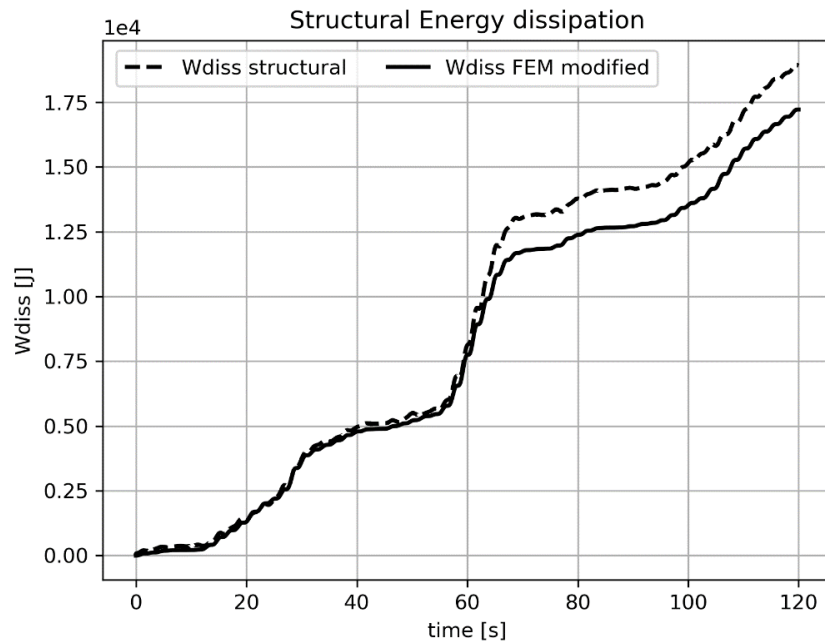


Figure 101 - Comparison of the extracted FEM dissipated energy and the derived EFA energy dissipation

Figure 102 shows how the dissipated energy error converges over time to a error of 9.86%. From the comparison of the relative error found at the structural dissipated energy, it can be inferred that the energy flux at the bottom is overestimated resulting in higher structural energy dissipation than the FEM modified values. On the contrary, the energy flux when determining the soil energy dissipation is underestimated resulting in lower values of identified soil energy dissipation. It appears that an accurate determination of the energy flux plays a paramount role on the identification of the separation of energy dissipations.

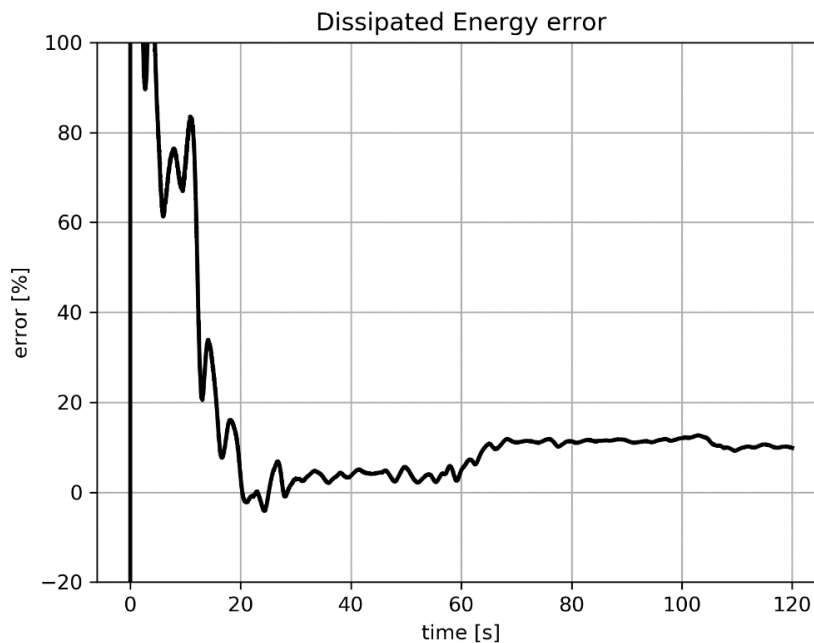


Figure 102 - Relative error between FEM and EFA energy dissipation

5.5.8 *Summary*

Within Case 5 wind tunnel data is introduced to the FEM model. Damping was introduced by a combination of a structural and soil damper. An assessment of the error in which the energy method quantifies several damping mechanisms is investigated. Insight is gained in the separation of multiple damping mechanisms and the influence of wind load. For the understanding of the energies influenced by wind load, first the kinetic and potential energy are explained. Hereafter the total energy dissipation, soil energy dissipation and structure energy dissipation are identified. The following data is used from Abaqus to obtain the energy dissipation terms:

Total energy:

- External power:
 - o Velocity of every node
 - o The wind force is obtained according to chapter 5.
- Potential energy spring:
 - o K_r
 - o Rotational velocity at the bottom
- Potential energy beam:
 - o EI
 - o Curvature of every node
- Kinetic energy:
 - o ρA
 - o Velocity of every node

Soil energy dissipation:

- Base energy flux:
 - o Curvature at the bottom
 - o Rotational velocity at the bottom
 - o EI
- Spring energy flux:
 - o Rotational displacement at the bottom
 - o Rotational velocity at the bottom
 - o K_r

Structure energy dissipation:

- External power
- Kinetic energy
- Potential energy
- Base energy flux

To assess the accuracy of the EFA technique, the identified energy dissipation were compared with the energy dissipation directly obtained from Abaqus. The dissipated energy determined with the EFA technique were used to determine damper values of the dashpot at the bottom of the system. This determined damping value is compared to the input value for the dashpot damper in the FEM model. This case resulted in the following findings:

Kinetic energy

- The kinetic energy has a fluctuating error between -0.12% and 0.19%. The mean value is 0%. This indicates that there are no bias errors in the kinetic energy computation with the EFA technique.

Potential energy

- The potential energy has a fluctuating error between -10% and 100%. This finding was also described at Case 4. The reason of this error is explained in case 4.

Total energy dissipation

- The assessment of the total energy dissipation gives an error of -0.83% compared with the FEM energy dissipation. The error converges to a stable value over time which means that the duration of the simulation have impact on the determination of energy dissipation with the EFA technique. Concluded can be that the identification of the total amount of energy dissipation is reached with a high accuracy.

Soil energy dissipation

- The determination of the energy flux is important for the separation of structural and soil damping.
- The error on the identification of the soil energy dissipation converges over time to a value of -11.81%. The identified soil dissipation is underestimated compared with the energy dissipation computed with eq. 4.7.
- A reason of the founded error comes from the way the required data for the EFA is extracted from the FEM model. The integration points for generating the curvature output are located in the middle of the bottom element. Half of the bottom element length is therefore not taken into account when determining the base moment.
- Another cause of the founded error might be that the rotational velocity at the bottom of the model is effected by the present structural damping in this lower element. This small interaction between the two damping mechanisms results in a larger energy dissipation of the soil.
- Since the collaboration of the damping mechanisms (e.g. soil and structure damping) affect each other, eq. 4.7 does not give an accurate comparison. However, since there is no damper operator yet which describes the dissipated energy of the structure, this small contribution cannot be described and added to eq. 4.7. Further research on this matter is needed.
- This small collaboration between damping mechanisms is also observable by identifying the damping value with the EFA technique. Compared with the input value the identified value has an error of -8.38%.

Damping value

- The identified damping value with the EFA technique converges over time to an error of -11.87%. This error might be caused by the earlier discussed integration points combined with the collaboration of multiple damping mechanisms.

Structural energy dissipation

- With the comparison made in 7.5.7 a relative error on the identification of the structural energy dissipation of 9.86% is found. The identification of the structural energy dissipation gives an overestimation compared with the modified FEM energy.
- It appears that an accurate determination of the energy flux plays a paramount role on the identification of the separation of energy dissipation.

5.6 Case 6 – Reduced wind information with only soil damping

The amount of information processed to determine the wind load along the beam will be reduced by using the top wind load time series only, see Figure 103. This wind load over time is introduced to the FEM model by using it on all the nodes.

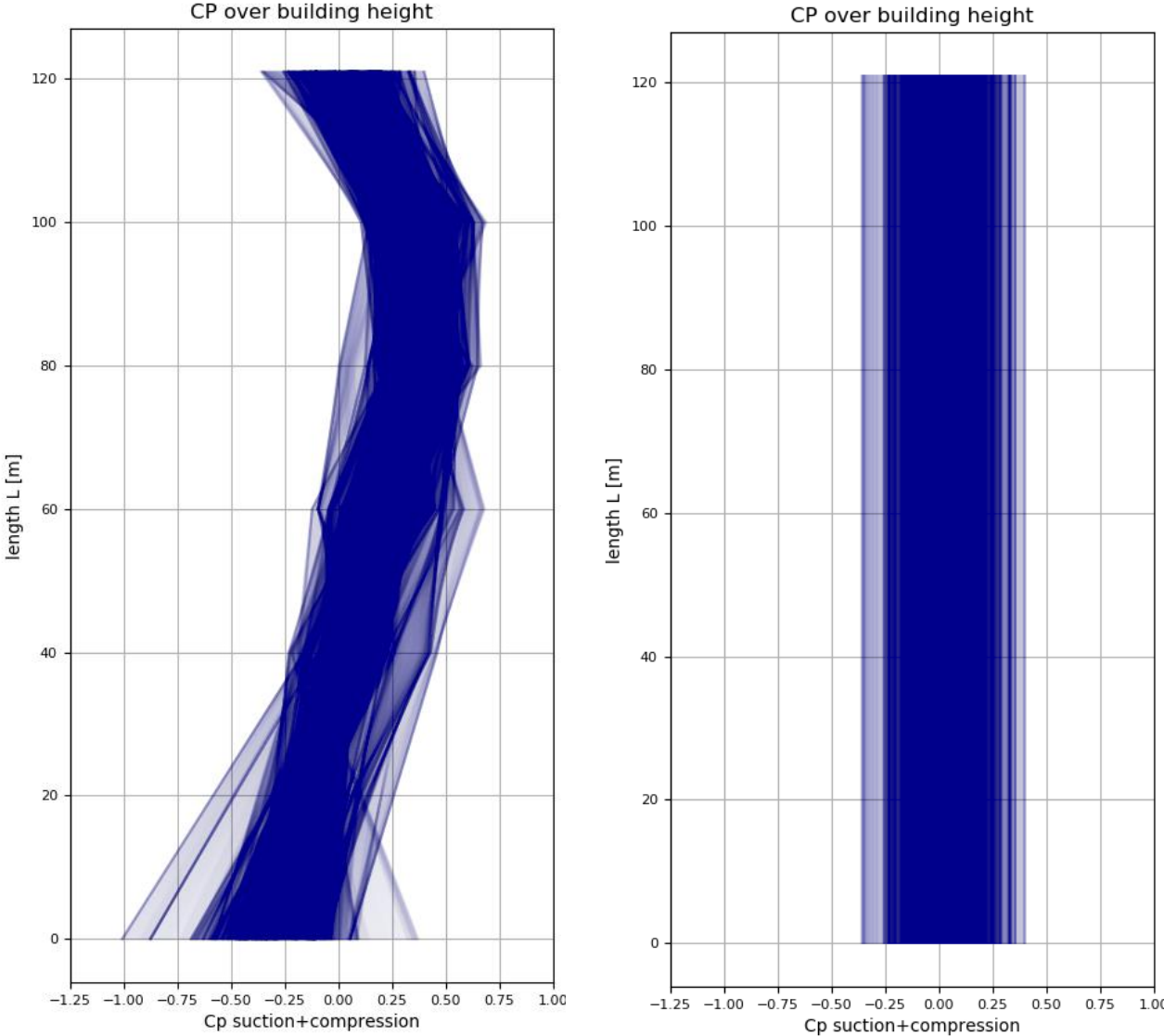


Figure 103 - The left plot shows the pressure coefficient over length obtained by postprocessing the wind tunnel data. The right plot shows the pressure coefficients over length by reducing the amount of wind tunnel data information. Here only the top pressure coefficients are used on all the nodes.

5.6.1 *Soil energy dissipation*

The soil damper is computed with the procedure described in 2.5.2.2. In order to identify the soil energy dissipation, equilibrium must be found between the bottom part of the building and its foundation. Figure 104 shows the energy flux (dashed line) derived with eq. 2.13. The curvature and rotational velocity of the bottom element are used from the FEM model to determine the energy flux at the bottom of the system. The energy flux by the spring (solid black line) is also plotted in Figure 104. The energy flux of the spring is the first derivative of the energy in this system described with eq. 2.12 and the rotational velocity of the spring is used from the FEM model. Figure 104 also shows the difference between these energies which is the energy dissipation when cumulative presented. It appears that larger differences are found at large amplitudes of the energy flux. The energy flux comprises the base moment and rotational velocity. Since the base moment is maximum at large displacement at the top it can be concluded that the energy dissipation is amplitude dependent.

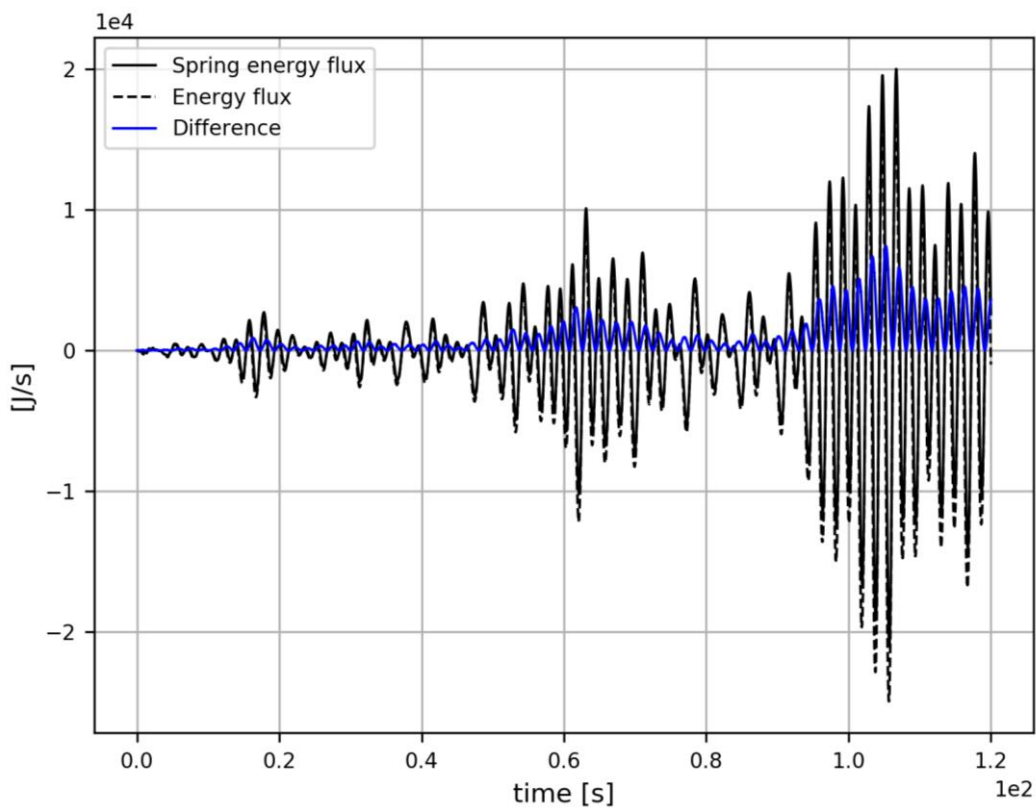


Figure 104 - Energy flux of the bottom part of the system (dashed line) and the spring energy flux (solid line). The difference between the bottom energy flux and spring energy is displayed in blue.

Furthermore, Figure 104 shows a less stable beating profile compared with Figure 98 of case 5. How the beating propagate over a longer simulation is not investigated and might be interesting to see how the natural frequency and the frequency of the force are related to each other over time.

Figure 105 shows the energy dissipation of the system directly obtained from FEM and determined with the EFA technique. The figure shows that the energy dissipation of both methods are in good agreement with each other. Figure 105 also shows the relative difference between the dissipated energy obtained with FEM and the energy obtained with the EFA versus time. In the first 20 seconds higher damping error are found. After 20 seconds the error is converged to a damping error of -0.16% . This error might be caused by the earlier discussed integration points in case 1.

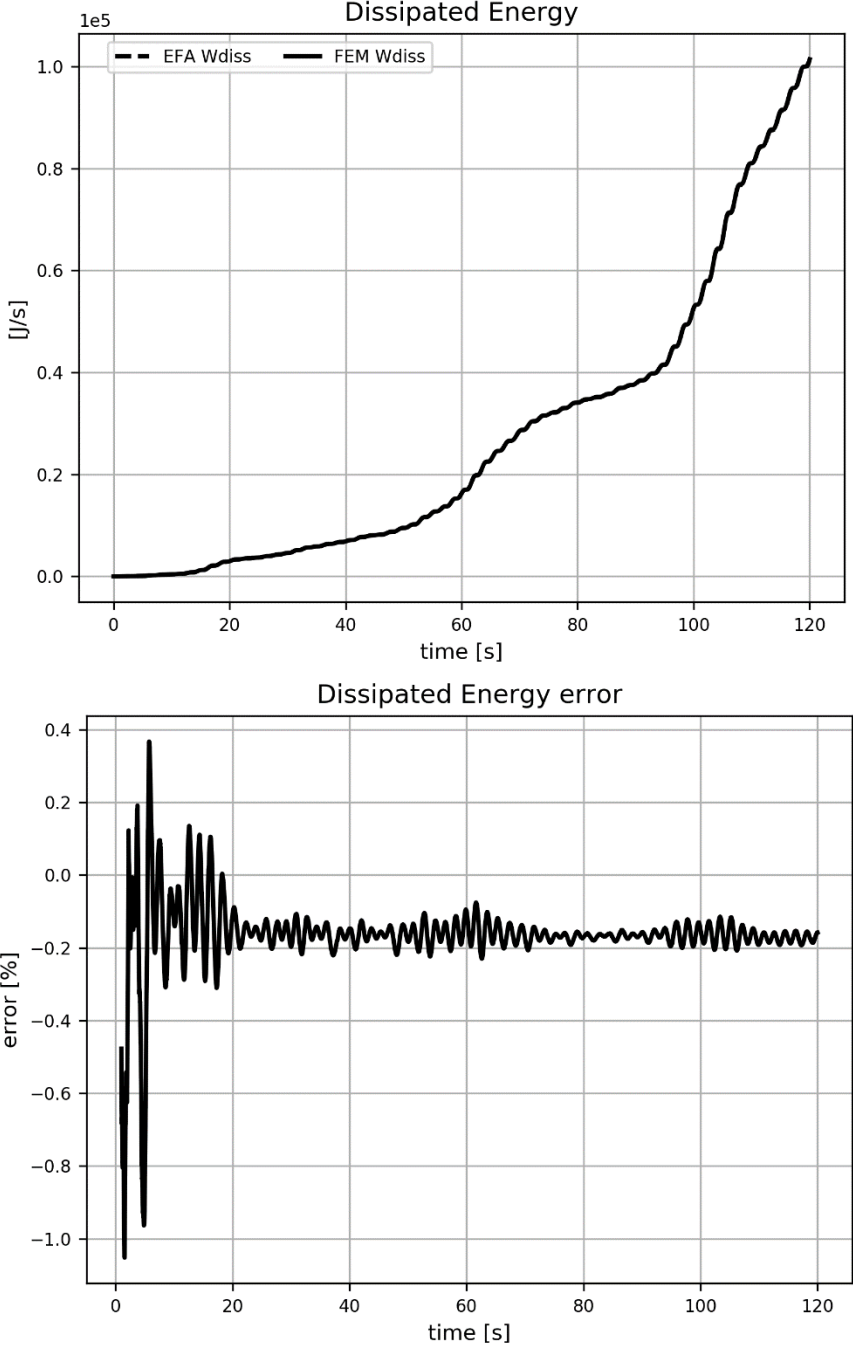


Figure 105 – The top graph the comparison of the identified soil energy dissipation with the EFA technique and the energy dissipation directly obtained of Abaqus. The bottom graph shows the relative error between the above compared energies.

It appears that a reduction on the wind data has no significant impact on the identification of the soil damping. In fact, compared with Case 4 (error of -0.60%), the error on the identified dissipated energy is slightly reduced. Although the comparison between case 4 and 6 shows a decreased relative error, the cause of reducing wind data has no significant impact. By using only the top pressure coefficients on all the nodes, the amount of external work induced to the system has a gentle propagation over time compared to a full wind data use. This is displayed in Figure 106.

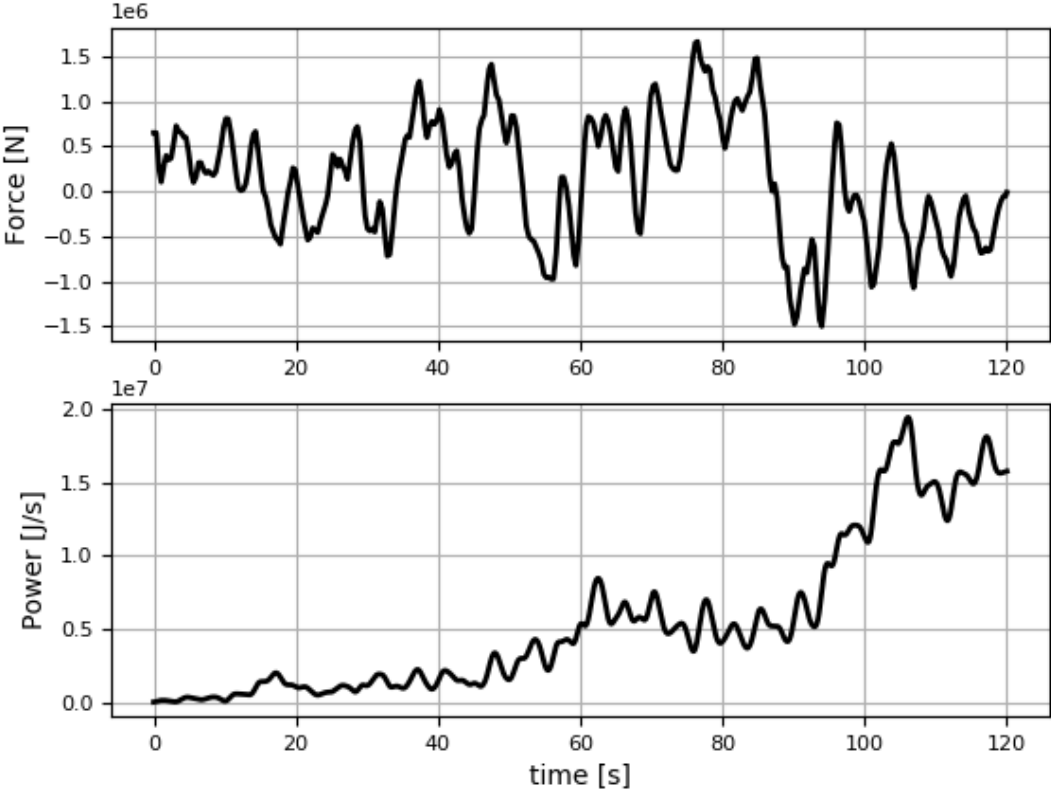


Figure 106 - The top graph shows the wind load on the whole system considering a reduced amount of wind load information. The bottom graph shows the cumulative external power added to the system.

In Figure 106 the wind load is expressed in the force over time. This force is the summation of all the wind time series applied on every node. Since this case considered a reduced amount of wind information, the pressure coefficients found at the top are also used for all the nodes. Multiplying the wind load at each node with the velocity at that specific node results in the external power added to the node. The cumulative summation of the external power of all nodes is shown in the bottom graph of Figure 106.

It can be seen that, compared with the wind force displayed in case 4, the fluctuations of the cumulative external power are decreased. Probably this has to do with the fact that the pressure coefficients distribution over height is equal since the time series are the same.

5.6.2 *Soil damping value*

The identified energy dissipation is translated to a damping value according to eq. 2.15 and displayed in Figure 107. The rotational velocity at the bottom is used. The input value of the FEM model and the identified damping value are plotted over time.

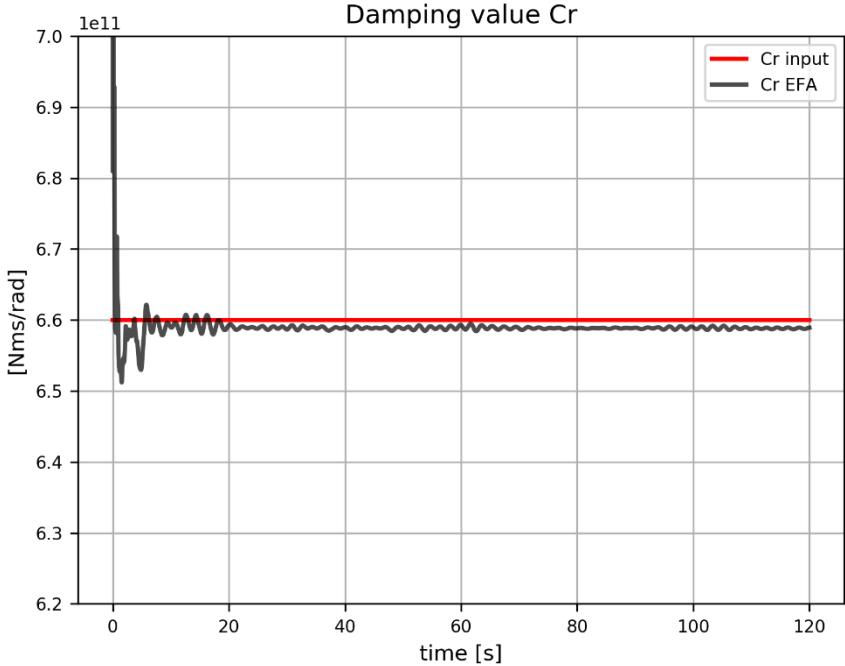


Figure 107 - Plot of the damping values

From Figure 107 it can be concluded that the damper value can be identified quite accurately with a relative error of -0.16%.

5.6.3 Summary

Within Case 6 reduced wind tunnel data is introduced to the FEM model. Damping was introduced to the system by means of a dashpot damper at the bottom of the system representing the rotational damping in the foundation. For the understanding of the energies influenced by reduced wind load, the energy fluxes at the bottom of the building were analysed. These parameters are of paramount importance for the identification of the soil damping. In 7.4.3. Summary case 4 is shown which data was needed from the Abaqus FEM model in order to identify the energy dissipation.

For this final case the assessment of the accuracy of the EFA technique, the identified energy dissipation were compared with the energy dissipation directly obtained from Abaqus. The dissipated energy determined with the EFA technique were used to determine damper values of the dashpot at the bottom of the system. This determined damping value is compared to the input value for the dashpot damper in the FEM model. This case resulted in the following findings:

Energy dissipation

- The energy dissipation determined with the EFA technique converges over time to an error value of -0.16%.
- This error might be caused by the earlier discussed integration points in case 1.

Damping value

- The identified damping value with the EFA technique also converges over time to an error of -0.16%.

It appears that a reduction on the wind data has no significant impact on the identification of the soil damping. In fact, compared with Case 4 (error of -0.60%), the error on the identified dissipated energy is slightly reduced. Although the comparison between case 4 and 6 shows a decreased relative error, the cause of reducing wind data has no significant impact. By using only the top pressure coefficients on all the nodes, the amount of external work induced to the system has a gentle propagation over time compared to a full wind data use.

5.7 Overview results

Table 10 presents an overview of all cases and the comparison of the input values and the identified damping values with the EFA method. The relative errors are also presented.

Case	Input FEM [Nms/rad]	Identified EFA [Nms/rad]	Relative error [%]
1.	1.32e+11	1.31e+11	-0.43
2.	6.60+11	6.05e+11	-8.38
3.	1.32e+11	1.30e+11	-1.47
4.	6.60e+11	6.57e+11	-0.51
5.	6.60e+11	5.82e+11	-11.81
6.	6.60e+11	6.58e+11	-0.16

Table 10 - Overview of the comparison of the input values and the identified damping values with the EFA.

6 Conclusions

This research has investigated the accuracy of the Energy Flow Analysis (EFA) for the prediction of damping in high-rise buildings. A study was made of the influence of a lack of data on the dynamic behaviour of the building and the wind load on the EFA damping identification. The goal was to determine the influence of this lack of data on the accuracy with which the EFA method predicts damping. This chapter gives the conclusions of the research described in this report. The objective of this research was divided into three objectives:

1. Assessment of the accuracy of the energy flow analysis as damping identification method.
2. Assessment of the influence of lack of information due to limited sensor positions on the identification of damping.
3. Assessment of the influence of lack of information on the wind load on the identification of damping.

The main findings and conclusions of each objective are described below.

6.1 Assessment of the accuracy of the EFA method

This research has provided insight in the accuracy of the identification of soil damping and total damping by using the EFA method. For the assessment an Euler Bernoulli beam model is used. It gave insight in the parameters that influence the damping identification. In the cases 1,2,4 and 5 the accuracy is investigated by using all available FEM model output that was needed for the EFA method. To assess the accuracy of the EFA energies, the energies were compared with the energies obtained from Abaqus. This resulted in the following general conclusions:

- The determination of the kinetic energy with the EFA technique has a high accuracy since no bias error is found for all cases.
- The equations derived for the EFA technique underestimate the potential energy. The underestimation of the potential energy derived with the EFA technique might be caused by the way the curvature is extracted from the FEM model which are used as input for the EFA technique.
- It appears that the error found on the identification of the damping values converges over time which means that the duration of a simulation have impact on the determination of the damping values with the EFA technique.
- The determination of the energy flux is important for the separation of structural and soil.
- A better understanding of the structural damping is needed to increase the reliability of the identification process.

CASE 1 – Conclusions and findings

With Case 1 insight is provided in the identification of energy dissipation by the EFA when only rotational soil damping is introduced. Furthermore, this case was used to determine appropriate settings for the setup of the model and to check the EFA routines. Within this FEM model a single soil damping mechanism was introduced and was excited by an initial displacement at the top. Data from all model nodes were obtained to determine the energy dissipation.

For this analysis the Energy flow analysis and its equations are based on the Euler Bernoulli beam theory. The Euler Bernoulli beam theory does not include shear. The amount of shear strain in a high-rise building depends on the ratio between bending and shear stiffness. For the New Erasmus MC building the total deformation are influenced by 2% of shear deformation.

The mesh discretization study shows that the mesh size has an impact on the identification of the damping. A sensitivity analysis was performed, which shows that a smaller element size results in a more accurate identification of the soil damper.

Case 1 shows a underestimation of the rotational soil damper value of -0.43% compared to the input value applied on the FEM model.

CASE 2 – Conclusions and findings

An assessment of the error in which the energy method quantifies two damping mechanisms are investigated with case 2. Insight is gained in the separation of two damping mechanisms.

The assessment of the EFA method in case 2 shows that the total energy dissipation can be identified with a relative error of 1% compared with the FEM energy dissipation. The EFA is therefore also suitable for the identification of the overall damping, which is obtained with other damping identification techniques such as the Half Power Bandwidth Method and the Random Decrement technique.

Case 2 shows that the EFA allows for the separation of damping mechanisms by applying multiple energy balances within the same system. The soil energy dissipation is identified with a relative error of -8.38% and the structural energy dissipation is identified with a relative error of 13.61%. A possible reason for these errors is related to way the required data for the EFA is extracted from the FEM model. For the separation of energy dissipation the curvature is needed to determine the base moment that is part of the energy flux at the bottom. The energy flux describes the amount of energy that flows from the building towards the foundation. The integration points for generating the curvature output from the FEM model are located in the middle of the bottom element. Half of the bottom element length is therefore not taken into account when determining the base moment. This phenomena causes an overestimation of the structure energy dissipation and underestimates the soil energy dissipation. For future monitoring campaigns an accurate determination of the energy flux towards the foundation is important.

Another reason for the error might be that the rotational velocity at the bottom of the model is affected by the present structural damping in this lower element. This small interaction between the two damping mechanisms results in a larger energy dissipation of the soil.

This last interaction and the fact that when the soil energy dissipation is underestimated by the EFA, the structural damping is overestimated, can be better understood when a proper damping operator is determined. Since there is no damper operator yet which describes the dissipated energy of the structure, an accurate comparison is not possible yet. FEM generates only the total amount of energy dissipation of the system and does not separate the contribution of several damping mechanisms.

CASE 4 – Conclusions and findings

In Case 4 wind tunnel data was introduced to the FEM model. Damping was introduced to the system by means of a dashpot damper at the bottom of the system representing the rotational damping in the foundation. With this case the impact of wind load on the energies can be analysed. The soil energy dissipation is identified by finding equilibrium in the bottom part of the system representing the foundation. The energy flux, which implicitly involves the influence of the wind load, and the spring energy flux where needed for this analysis.

Compared with the cases which were excited by the initial displacement, higher relative errors were found in this case when determining the potential energy with the EFA technique. To get a better understanding of the potential energy of the system in case 4, the spring and beam potential

energy where investigated separately. It appears that the potential energy of the spring has a different frequency than the potential energy of the beam. This suggest that local frequencies are presented at the bottom of the system, which are not strongly present when considering the whole system. Analysing the spring, beam and FEM potential energies in frequency spectrum confirms the presence and the difference between frequencies in which these energies act. It appears that the additional frequencies of the spring, are harmonic frequencies of the first eigen frequency of the system.

Case 4 has shown that with a realistic wind load the soil energy dissipation can be identified with a relative error of -0.60% by using the EFA method. This error might be caused by the earlier explained problem with the integration points.

CASE 5 – Conclusions and findings

In case 5 wind tunnel data was introduced to the FEM model. An assessment of the error in which the energy method quantifies several damping mechanisms is investigated influenced by a realistic stochastic wind load distributed over the system.

The assessment of the EFA method in case 5 had shown that the total energy dissipation can be identified with a relative error of -0.83% compared with the FEM energy dissipation. Compared with case 2, the accuracy of identifying the total amount of energy dissipation with the EFA method is slightly higher. The difference is that case 2 was excited by an initial displacement and case 5 by a stochastic load.

Case 5 had shown that with the EFA it is also possible to separate damping mechanisms in a system which is excited by a realistic wind load. An accurate determination of the energy flux plays a paramount role in the separation of the energy dissipation of the building and the foundation.

The soil energy dissipation is identified with a relative error of -11.81% and the structural energy dissipation is identified with a relative error of 9.86%. The reasons for the magnitude of these errors are the same reasons given in case 2. It is noticeable that the errors found in this case are slightly lower than the ones found in case 2. The way of exciting the structure is different. With the wind load a stochastic but smaller amplitude of the displacement is found at the top of the building. The initial displacement had a deliberated higher amplitude.

6.2 Assessment of the influence of lack of information due to limited sensor positions

This research has provided insight in the impact of reducing the amount of information due to limited sensor positions on the identification damping. Of the top node of the Abaqus FEM model the horizontal displacement and velocity were obtained. From the bottom node the rotational displacement and velocity were obtained. These data sets, combined with analytical expressions for the first mode shape, were used in the EFA technique to determine the kinetic, potential and dissipated energy of the system. This case resulted in the following findings:

- In the early stage of this research the accuracy of the identification of the soil damper value was done by integrating the energies needed for the EFA over the total simulation time of 28 seconds. With this approach a relative error of -1.47% between the input value and identified soil damper is found.
- Due to progressive insight, the determination of the energy dissipation changed and the accuracy of the determination of the kinetic and potential energy were analysed. Using the first mode shape as starting point to determine the dynamic behaviour gives an overall match for both the kinetic and potential energy.

- The determination of the kinetic energy with the EFA technique matches the kinetic energy extracted from FEM well, but larger differences were found compared with the case in which all needed data is used. A mean relative error of -11,15% is found between the EFA and FEM values.
- The underestimation of the kinetic energy derived with the EFA technique seems to be caused by the assumption that only the first bending mode shape is considered when predicting the dynamic behaviour of the system.
- Whether the EFA underestimates or overestimates the potential energy is hard to conclude from case 3. A part of the errors are caused by the assumption that only the first bending mode shape is considered when predicting the dynamic behaviour of the system. The period of the vibration varies, which indicates that multiple frequencies are present.
- Expressing the energy dissipation over time gives more insight in the identification of the energy dissipation over time. The identified energy dissipation shows large fluctuations over time. From the relative error it can be seen that the error reduces over time. Between 20 and 28 seconds the mean error value is 23.47%.
- The cause of the fluctuating differences might be caused by the lack of higher mode shapes when predicting the energies needed for the energy balance. To accommodate for the full dynamic behaviour of the system excited by an initial displacement, considering more modes might result in a higher accuracy of the identification of energy dissipation with the EFA method.

This approach of including analytical expressions for the mode shape does give information about the dynamic behaviour of the building, but this precise determination is not needed for identification of the soil energy dissipation. Case 4 has shown that solving the energy balance at the bottom of the building resulted in an accurate identification of the soil damper value. Solving the energy balance in the bottom part of the building is possible if the curvature, rotational velocity at the base and the soil stiffness are determined well. However, validation of these parameters can be done by determining the mode shapes belonging to the dynamic behaviour of the building. Therefore, the methodology of case 3 can be useful.

6.3 Assessment of the influence of lack of information on the wind load

This research has provided insight in the impact of reducing the amount of wind load information on the identification of the soil damping by using the EFA method. For this assessment case 5 and case 6 are used. With case 6 the amount of wind tunnel data is reduced. Only the top wind load series is introduced to the FEM model by using it on all the nodes.

It appears that a reduction on the wind data has no significant impact on the identification of the soil damping. In fact, compared with Case 4 (error of -0.60%), the error on the identified dissipated energy is slightly reduced. Although the comparison between case 4 and 6 shows a decreased relative error, the cause of reducing wind data has no significant impact. By using only the top pressure coefficients on all the nodes, the amount of external work induced to the system has a gentle propagation over time compared to a full wind data use.

With this case it is shown that applying the EFA method to identify the soil energy dissipation, an accurate knowledge of the wind load distribution over the building is not directly needed. The amount of energy that flows towards the soil is taken into account by the energy flux which implicitly involves the load that acts on the building. However, the distribution of the wind load is needed for accurately knowing what the structural energy dissipation distribution is in the building.

7 **Recommendations**

Based on current research recommendations for further research are:

- For future monitoring campaigns an accurate determination of the energy flux towards the foundation is important. The accuracy and its impact on the identification of soil damping could be evaluated by analysing a detailed 3D model of the bottom part of a building in FEM. The position of the sensors and their impact can be analysed. With this detailed model the impact of the structural damping in the bottom part of the structure should also be investigated.
- A better understanding of the structural damping is needed to increase the reliability of the identification process. This could be achieved by performing forced vibrations test on buildings and develop an analytical model that describes the behaviour of structural damping in Dutch buildings.
- For the purpose of this research only along wind response was considered. For further research it is recommended to investigate other responses, like across-wind and torsional responses as well and determine the accuracy of the EFA when multiple wind directions are considered. A more advanced FEM model can be made which incorporate spring and dashpots in multiple directions and a realistic wind load considered in multiple directions.
- For this research the choice was made to use only the rotational soil stiffness and damping to describe the soil structure interaction. The impact of the soil conditions can be further investigated by including also the horizontal stiffness and damping. Research is needed on expressing the dependence of these two components on each other.
- As shown during the cases, the error on the identified soil damping value fluctuated over time. For further research it is recommended to assess the impact of the duration of the simulation on identification of the damping with the EFA. This could be achieved by using a FEM model with a realistic wind load. The impact of the amplitude of the load can be investigated on the identification of damping with the EFA.
- Before the EFA based measurement technique can be applied successfully in future monitoring and measurement campaigns, the above uncertainties in this technique need to be assessed. Only then an accurate identification of the damping contribution of different building components is possible.

8 Bibliography

- [1] R. O. e. M. Ministerie Volkhuysvesting, „Structuurvisie Randstad 2040 - naar een duurzame en concurrerende Europese topregio,” 2008.
- [2] C. Geurts, C. van Bentum, S. Sanchez en S. van Dijk, „Damping hoogbouw voorspeld,” *Cement*, vol. 3, pp. 60-66, 2015.
- [3] S. Gomez, „Damping in high-rise buildings,” to be published, TU Delft, 2018.
- [4] „EN 1991-1-4 Eurocode 1: Actions on structures - Part 1-4: General actions - Wind actions,” CEN, 2011.
- [5] N. 3. 0. T. g. v. Bouwconstructies., „NEN 6702 (nl) - Technical principles for building structures, TGB 1990 - Loadings and deformations,” NEN, 2007.
- [6] A. P. Jeary, „Damping in tall buildings - a mechanism and a predictor,” *Earthquake Engineering and Structural Dynamics*, vol. 14, nr. HMSO, pp. 733-750, 1986.
- [7] A. Jeary, „Damping in structures,” *Journal of Wind Engineering and Industrial Aerodynamics*, vol. 72, nr. Elsevier, pp. 345-355, 1997.
- [8] A. P. Jeary, „The description and measurement of nonlinear damping in structures,” *Journal of Wind Engineering and Industrial Aerodynamics*, vol. 59, nr. Elsevier, pp. 103-114, 1996.
- [9] A. Jeary, *Designer's guide to the dynamic response of structures*, first ed., Cambridge: The University Press, 1997.
- [10] B. R. Ellis, „An assessment of the accuracy of predicting the fundamental natural frequencies of buildings and the implications concerning dynamic analysis of structures,” *Proc. inst. civil. eng.*, vol. part 2 69, pp. 763-776, 1980.
- [11] Y. Tamura, N. Satake, K. Suda, T. Arakawa en A. Sasaki, „Damping evaluation using full-scale data of buildings in Japan,” *Journal of Structural Engineering*, Vols. 1 van 2 vol. 129, no. 4, nr. ASCE, pp. 470-477, 2003.
- [12] A. Bronkhorst, C. van Bentum en S. Gomez, „TNO 2018 R10644: Wind-induced vibrations and damping in high-rise buildings,” TNO, Delft, 2018.
- [13] A. Chopra, *Dynamics of Structures* 3rd ed., New Jersey: Prentice Hall, 2007.
- [14] H. Cole Jr., „On-the-line analysis of random vibrations,” *AIAA/ASME 9th struct. dyn. materials conf.*, nr. Palm Springs, 1968.
- [15] A. Metrikine, *Dynamics, Slender Structures and an Introduction to Continuum Mechanics*, Delft: Delft University of Technology.
- [16] D. J. Inman, *Engineering Vibration*, New Jersey, United States of America: Prentice-Hall Inc., 2001.
- [17] Y. Lase, M. Ichchou en L. Jezequel, „Energy Flow Analysis of Bars and Beams: Theoretical formulations,” *Journal of Sound and Vibration*, vol. 192, nr. (1), pp. 281-305, 1996.
- [18] J. Wohlever en R. Bernhard, „Mechanical Energy Flow Models of Rods and Beams,” *Journal of Sound and Vibration*, vol. 153, nr. (1), pp. 1-19, 1992.
- [19] O. Bouthier en R. Bernhard, „Simple Models of the Energetics of Transversely Vibrating Plates,” *Journal of Sound and Vibration*, vol. 182, pp. 149-166, 1995.
- [20] P. Cho en R. Bernhard, „Energy Flow Analysis of Coupled Beams,” *Journal of Sound and Vibration*, vol. 211(4), pp. 593-605, 1998.

- [21] S. Gomez, A. Metrikine, B. Carboni en W. Lacarbonara, „Identification of Energy dissipation in structural joints by means of the energy flow analysis,” *J. Vib. Acoust*, vol. vol. 01, nr. ASME, pp. 1007-1-1007-8, 2018.
- [22] W. Wisman, H. Meijer en G. Bart, *Inleiding Thermodynamica*, Delft: VSSD, 2010.
- [23] S. Gómez en A. Metrikine, „The energy flow analysis as a tool for identification of damping in tall buildings subjected to wind: contribution of the foundation and the building structure,” *J. Vib. Acoust.*, vol. 141, 2019.
- [24] S. Gómez, A. Metrikine, B. Carboni en W. Lacarbonara, „Identification of Energy Dissipation in Structural Joints by Means of the Energy Flow Analysis,” *Journal of Vibration and Acoustics*, vol. 01, nr. ASME, pp. 1007-1-1007-8, 2018.
- [25] A. Davenport, „The application of statistical concepts to the wind loading of structures,” *Proceedings Institution of Civil Engineers*, vol. 19, pp. 449-472, 1961.
- [26] N. R. C. o. Italy, „Guide for the assessment of wind actions and effects on structures,” CNR-DT 207/2008, Italy, 2010.
- [27] J. Holmes, *Wind Loading of Structures.*, New York: Spon Press, 2001.
- [28] L. C. La Gasse, „Master Thesis: 'Structural reliability assessment of buildings subjected to wind loading',” Delft University of Technology, Delft, 2017.
- [29] J. Wolf, *Foundation vibration analysis using simple physical models*, Prentice Hall, 1995.
- [30] A. Bronkhorst, C. van Bentum en S. Gomez, „TNO report: 'Wind-induced vibrations and damping in high-rise buildings',” TNO, Delft, 2018.
- [31] S. de Graaf, I. Kalkman, C. Geurts en C. Van Bentum, „Drukvereffening beter begrepen (1),” *Cement*, vol. 5, pp. 46-49, 2013.
- [32] C. Geurts, *Wind-induced pressure fluctuations on building facades*, Eindhoven: Technische Universiteit Eindhoven, 1997.
- [33] S. Gómez en A. Metrikine, „Evaluation of the applicability of an energy method to calculate the damping in a lab-scale structure,” *Procedia Engineering*, nr. Elsevier Ltd., 2017.
- [34] Y. Tamura, K. Fuji, T. Ohtsuki, T. Wakahara en R. Kohsaka, „Effectiveness of tuned liquid dampers under wind excitation,” *Engineering Structures Vol. 17*, vol. 9, nr. Elsevier Science Ltd., pp. 609-621, 1995.
- [35] R. D. Ambrosini, „Material damping vs. radiation damping in soil-structure interaction analysis,” *Computers and Geotechnics*, vol. 33, nr. Elsevier, pp. 86-92, 2006.
- [36] A. Devin en P. Fanning, „Impact of nonstructural components on modal response and structural damping,” in *Topics on the Dynamics of Civil Structures, Vol. 1, Proceedings of the 30th IMAC, A Conference on Structural Dynamics*, Springer, 2012, pp. 412-421.
- [37] Y. Xu, „Parametric study of active mass dampers for wind-excited tall buildings,” in *Engineering Structures, Vol 18, No 1*, Elsevier Science Ltd, 1996, pp. pp 64-76.
- [38] M.-Y. Lui, W.-L. Chiang, J.-H. Hwang en C.-R. Chu, „Wind-induced vibration of high-rise building with tuned mass damper including soil-structure interaction,” *Journal of Wind Engineering and Industrial Aerodynamics*, vol. 96, nr. Elsevier, pp. 1092-1102, 2008.
- [39] X. Zhao, J. Ding en H. Sun, „Structural Design of Shanghai Tower for Wind Loads,” *The Twelfth East Asia-Pacific Conference on Structural Engineering and Construction ~ Procedia Engineering*, vol. 14, nr. Elsevier, pp. 1759-1767, 2011.

- [40] A. C. Webster en R. Vaicaitis, „Application of tuned mass dampers to control vibrations of composite floor systems,” *Engineering Journal / American Institute of Steel Construction*, pp. 116-124, 2003.
- [41] J. J. Connor, „Tuned Mass Damper Systems,” in *Introduction of Structural Motion Control*, MIT Prentice Hall, 2002, pp. 217-285.
- [42] C. Cruz en E. Miranda, „Evalutaion of the Rayleigh damping model for buildings,” *Engineering Structures*, vol. 138, nr. Elsevier, pp. 324-336, 2017.
- [43] NIST, „Soil-structure interaction for building structures,” U.S. Department of Commerce, Gaithersburg, MD 20899, 2012.
- [44] A. Tsouvalas, Lecture Notes CIE5260 Structural Response to Earthquakes Modules II & III, Delft: Delft University of Technology, 2018.
- [45] R. D. Blevins, *Formulas for natural frequency and mode shape*, New York: Robert E. Krieger Publishing co., inc., 1979.
- [46] L. Clive, P. Dym, F. ASCE en Harry E. Williams, „Estimating Fundamental Frequencies of Tall Buildings,” *Journal of Structural Engineering*, nr. ASCE, pp. 1-5, 2007.
- [47] J. P. Wolf en A. Deeks, *Foundation Vibration Analysis: A Strength of Materials Approach*, Elsevier Science, 2004.
- [48] T. Hughes, *The Finite Element Method - Linear Static and Dynamic Finite Element Analysis*, Englewood Cliffs NJ: Prentice- Hall, 1987.

Appendix A

Determine natural frequencies and mode shapes of continuous model for a flexible system

8.1.1 Boundary conditions Flexible system

The kinematic boundary conditions of a fixed-free system are stated as:

$$W|_{x=0} = 0 \quad (\text{A.3})$$

$$EI \frac{\partial^2 W}{\partial x^2} - k_r \frac{\partial W}{\partial x} \Big|_{x=0} = 0 \quad (\text{A.4})$$

The dynamic boundary conditions are stated as:

$$EI \frac{\partial^2 W}{\partial x^2} \Big|_{x=L} = 0 \quad (\text{A.5})$$

$$EI \frac{\partial^3 W}{\partial x^3} \Big|_{x=L} = 0 \quad (\text{A.6})$$

Substitution of the four boundary conditions into the expression for the eigenfunction $W(x)$, gives the following set homogeneous system of algebraic equations:

$$W|_{x=0} = 0 \rightarrow A + C = 0 \quad (\text{A.7})$$

$$EI \frac{\partial^2 W}{\partial x^2} - k_r \frac{\partial W}{\partial x} \Big|_{x=0} = 0 \rightarrow AEI\beta^2 - CEI\beta^2 - B\beta k_r - D\beta k_r = 0 \quad (\text{A.8})$$

$$EI \frac{\partial^2 W}{\partial x^2} \Big|_{x=L} = 0 \rightarrow EI\beta^2 \{A \cosh(\beta L) + B \sinh(\beta L) - C \cos(\beta L) - D \sin(\beta L)\} = 0 \quad (\text{A.9})$$

$$EI \frac{\partial^3 W}{\partial x^3} \Big|_{x=L} = 0 \rightarrow EI\beta^3 \{A \sinh(\beta L) + B \cosh(\beta L) + C \sin(\beta L) - D \cos(\beta L)\} = 0 \quad (\text{A.10})$$

Simplify eq. (A.8) by dividing by β :

$$EI \frac{\partial^2 W}{\partial x^2} - k_r \frac{\partial W}{\partial x} \Big|_{x=0} = 0 \rightarrow AEI\beta - CEI\beta - Bk_r - Dk_r = 0 \quad (\text{A.11})$$

Simplify eq. (A.9) by dividing by EI and β^2 :

$$EI \frac{\partial^2 W}{\partial x^2} \Big|_{x=L} = 0 \rightarrow A \cosh(\beta L) + B \sinh(\beta L) - C \cos(\beta L) - D \sin(\beta L) = 0 \quad (\text{A.12})$$

Simplify eq. (A.10) by dividing by EI and β^3 :

$$EI \frac{\partial^3 W}{\partial x^3} \Big|_{x=L} = 0 \rightarrow A \sinh(\beta L) + B \cosh(\beta L) + C \sin(\beta L) - D \cos(\beta L) = 0 \quad (\text{A.13})$$

The eq. (A.7), (A.11), (A.12) and (A.13) can be written as a coefficient matrix:

$$\begin{bmatrix} 1 & 0 & 1 & 0 \\ EI\beta & -k_r & -EI\beta & -k_r \\ \cosh(\beta L) & \sinh(\beta L) & -\cos(\beta L) & -\sin(\beta L) \\ \sinh(\beta L) & \cosh(\beta L) & \sin(\beta L) & -\cos(\beta L) \end{bmatrix} \begin{bmatrix} A \\ B \\ C \\ D \end{bmatrix} = 0 \quad (\text{A.14})$$

8.1.1.1 Natural Frequencies flexible system

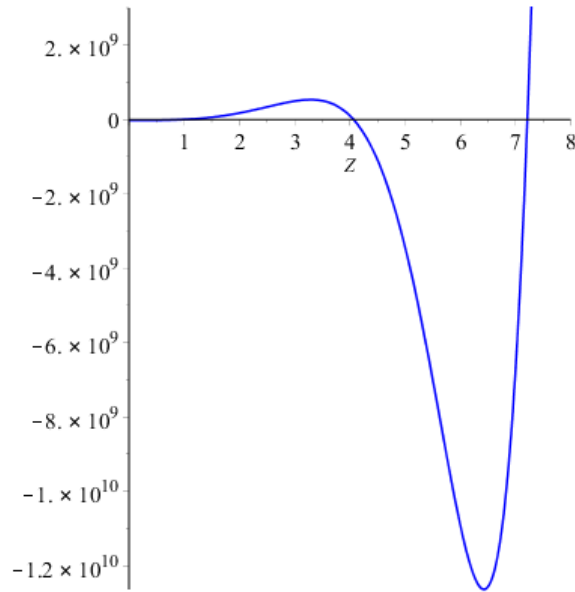
The homogeneous system shown at eq. (A.14) has a non-trivial solution if the determinant of the coefficient matrix is equal to zero. The determinant of this matrix gives an equation dependent on β . These β 's contain the natural frequencies of the system.

$$Det = -2EI \cos(\beta L) \sinh(\beta L) \beta + 2EI \sin(\beta L) \cosh(\beta L) \beta - 2kr - 2 \cos(\beta L) \cosh(\beta L) kr = 0 \quad (\text{A.15})$$

Maple is used to solve the frequency equation. The following parameters are used to involve the building stiffness and soil rotational stiffness.

$$\begin{aligned} k_r &= 5.94E + 06 \\ EI &= 2.08E + 09 \end{aligned} \quad (\text{A.16})$$

which results in the following graphical representation of the frequency equation.



The first 3 solutions of the frequency equation are:

$$\begin{aligned}
 \beta_1 L &\approx 1.846770557 \\
 \beta_2 L &\approx 4.665987825 \\
 \beta_3 L &\approx 7.826638635
 \end{aligned}
 \tag{A.17}$$

With these values of the weighted frequencies $\beta_n L$, the individual frequencies of vibration can be calculated as demonstrated at eq. (1.49).

8.1.1.2 Mode Shapes Flexible system

For the determination of the corresponding principal modes for the flexible system, the values of the weighted frequencies can be substituted into the earlier derived eigenfunction (1.55).

The derived mode shapes are checked with the tables from the book 'Formulas for natural frequency and mode shape' by Robert. D. Blevins PhD, 1979. In Figure 108 the first three normalized mode shapes of the flexible system are plotted.

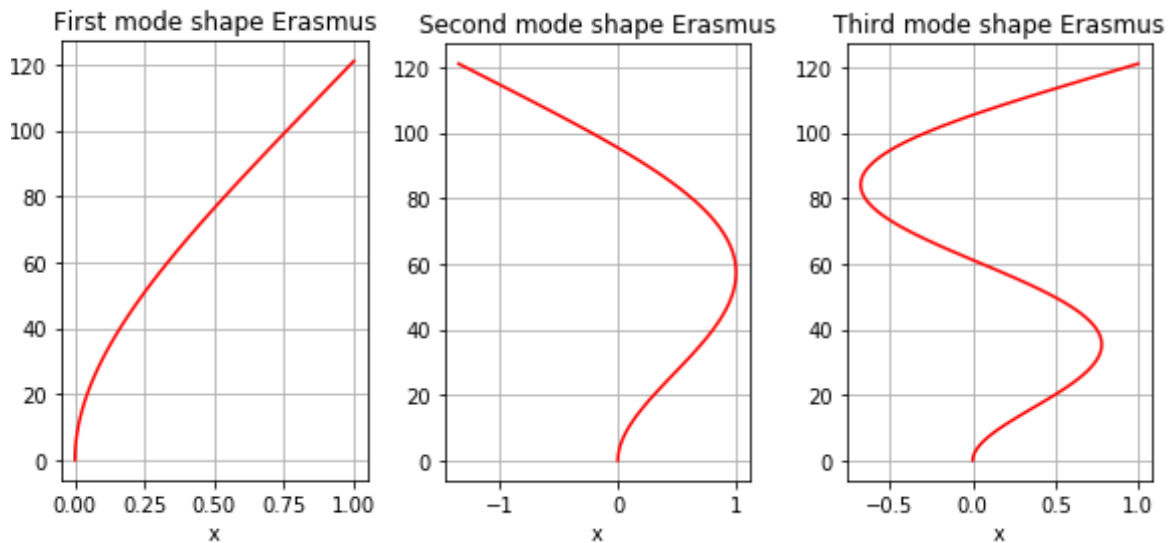


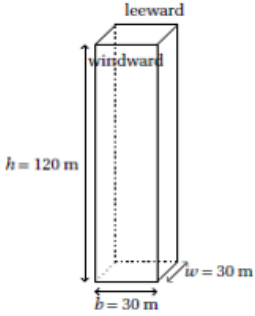
Figure 108 - first three mode shapes of a system influences by a rotational spring at the bottom

Appendix B

Wind load

Design wind velocity as specified in the National Annex to EN1991-1-4			
B	21	m	Full scale width of the building
D	45	m	Full scale depth of the building
H	120	m	Full scale length of the building
z	72	m	EN reference length
z ₀	0.5	m	Roughness length (een maat voor de ruwheid van het aardoppervlak. Hoe ruwer de aardoppervlak, des te groter de waarde voor z ₀)
R	1	Year	herhalingsjijd R in jaren
p	0.63	[-]	kans dat de extreme gemiddelde windsnelheid v(p) in een jaar wordt overschreden
K	0.234	[-]	vormparameter (Schiphol)
n	0.5	[-]	exponent NEN 1991-1-1-4 art. 4.2 aanbevolen waarde (Gumbel-verdeling voor windstuwdrukken).
C _{prob}	0.72	[-]	waarschijnlijkheidsfactor (bij een levensduur die afwijkt van de standaardperiode van 50 jaar hoort een andere waarde van de basisnelheid.
V _{b,0}	27	m/s	UGT, 50 jaar, windgebied II EN
k _r	0.22	[-]	Terrain factor depending on roughness length z ₀ (EC eq.4.5)
c _r	1.11	[-]	ruwheidsfactor hangt uitsluitend af van de hoogte z en de ruwheidslengte z ₀ .
c ₀	1	[-]	orography factor; influence of hills and cliffs can increase the mean wind velocity. With c ₀ this effect can be taken into account.
V _{m(50years)}	30.0	m/s	
V _{m(1 year)}	21.6568	m/s	V _{b,EN}

Dimensions Full Scale building (FS)			
L _{FS}	120	m	Full scale length of the building
B _{FS}	21	m	Full scale width of the building
W _{FS}	45	m	Full scale depth of the building



Dimensions Wind Tunnel model (WT)			
L _{FS}	0.48	m	Model Length
B _{FS}	0.12	m	Model width
W _{FS}	0.12	m	Model depth

Determine wind velocity at reference height EC			
V _{ref,h}	25.95	m/s	Full scale Wind velocity at reference height at the top of the building (EC eq.4.3)
k _r	0.2391	[-]	Terrain factor depending on roughness length z ₀ (EC eq.4.5)
z ₀	0.8	m	Roughness length in full scale, but consistent with the wind tunnel environment
z _{0,II}	0.03	m	Reference roughness length KNMI (ipv 0.05m EC, see mail)
V _{b,EN}	21.7	m/s	Design wind velocity as specified in the National Annex to EN1991-1-4

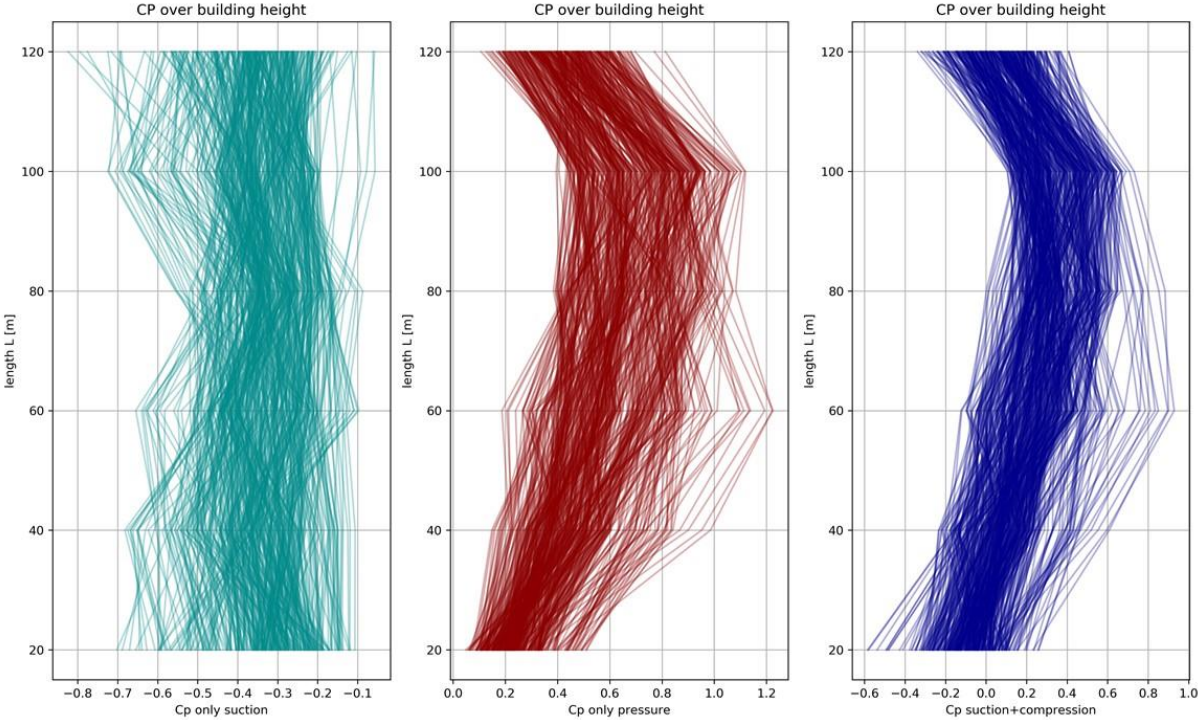
From Wind Tunnel to Full Scale			
Sam. freq.	400	Hz	sampling frequency
λ _g	1/250		Geometric scale
L _{WT}	0.48	m	Wind Tunnel length of the model
L _{FS}	120	m	Full scale length of the building
L _{WT} /L _{FS}	0.004		
V _{WT}	14.5	m/s	Wind velocity in Wind Tunnel
V _{FS}	25.95	m/s	Wind velocity at building hieght 120 [m] and terrain roughness 0.8 [m]
V _{FS} /V _{WT}	1.79		

Time scale			
t _{FS}	0.0025	sec	
t _{FS} /(L _{WT} /L _{FS})*(V _{FS} /V _{WT})	0.3493	sec	eq. 3.8 blz. 68 (Geurts 1997)

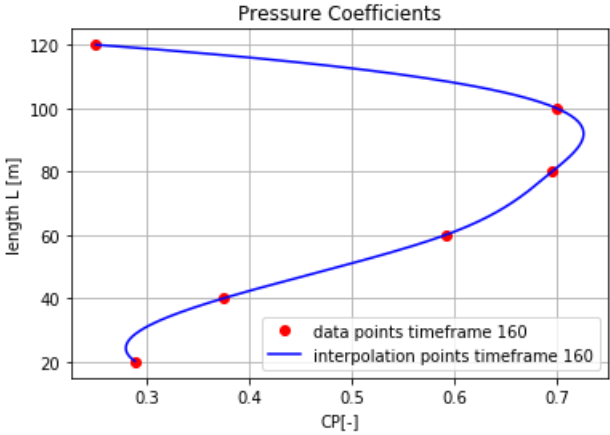
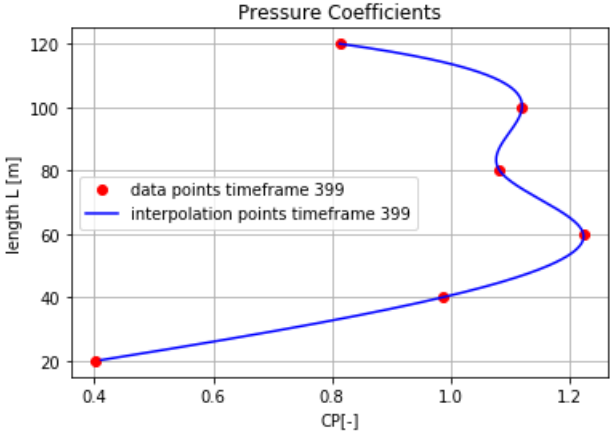
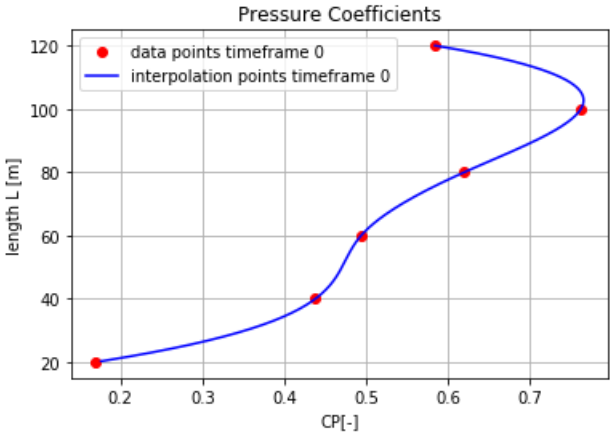
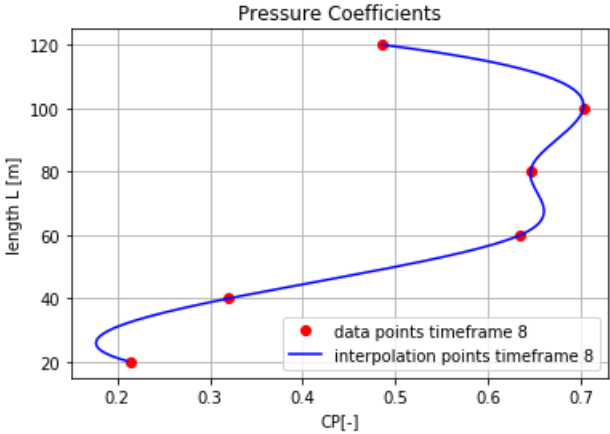
Frequency scale			
(L _{FS} /L _{WT})*(V _{WT} /V _{FS})	139.7172	Hz	eq. 3.9 blz. 68 (Geurts 1997)

Note that a small mistake has been made. The k_r factor has been applied twice. This resulted in a lower wind velocity.

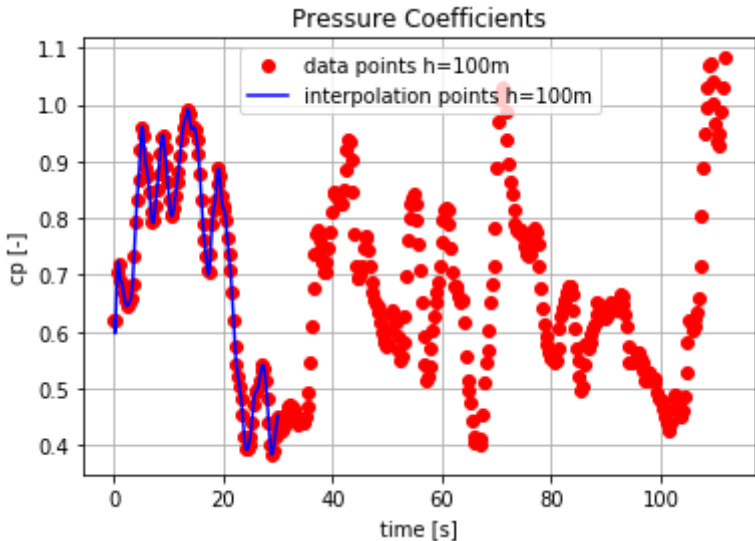
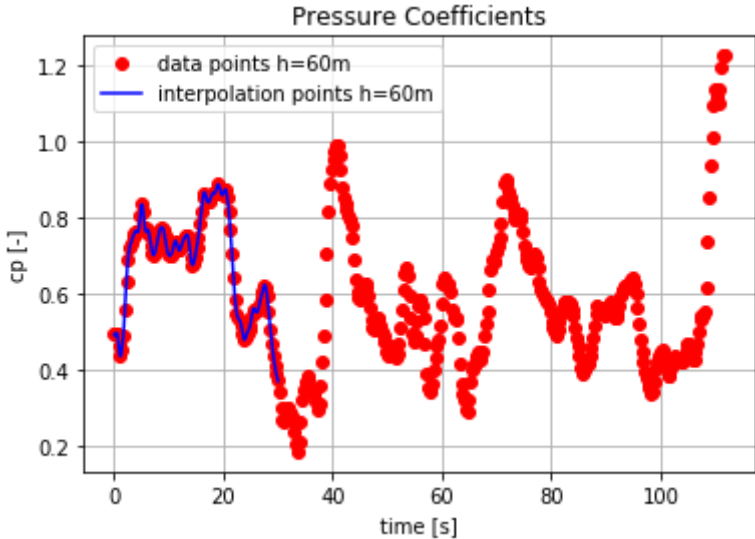
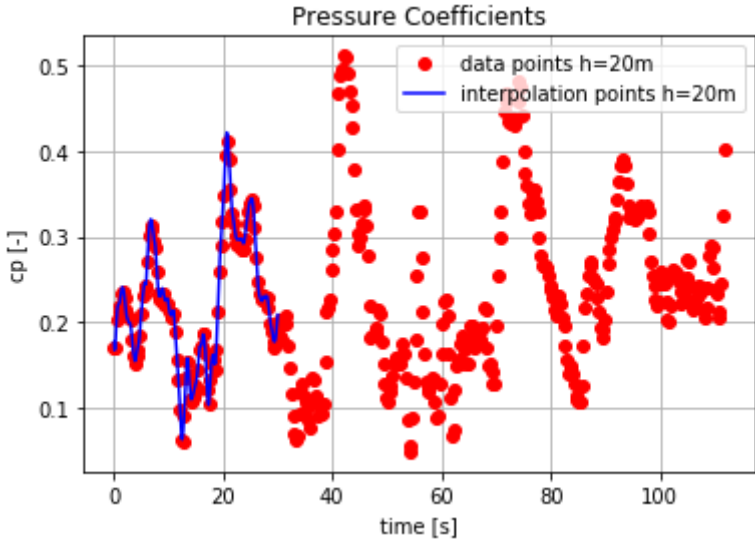
Figure X shows the suction and pressure distribution over height. The right plot in figure X shows a combination of the suction and pressure measured during the wind tunnel test.



Interpolation of the pressure coefficient over height



Pressure coefficients over time



Results Case 2 – Identification of soil damping in frequency domain

Another method of identification of the soil damper is by using the frequency domain instead of time domain. The frequency domain eliminates the zero values of the rotational velocity, see Figure 109. The fast Fourier transfer is used.

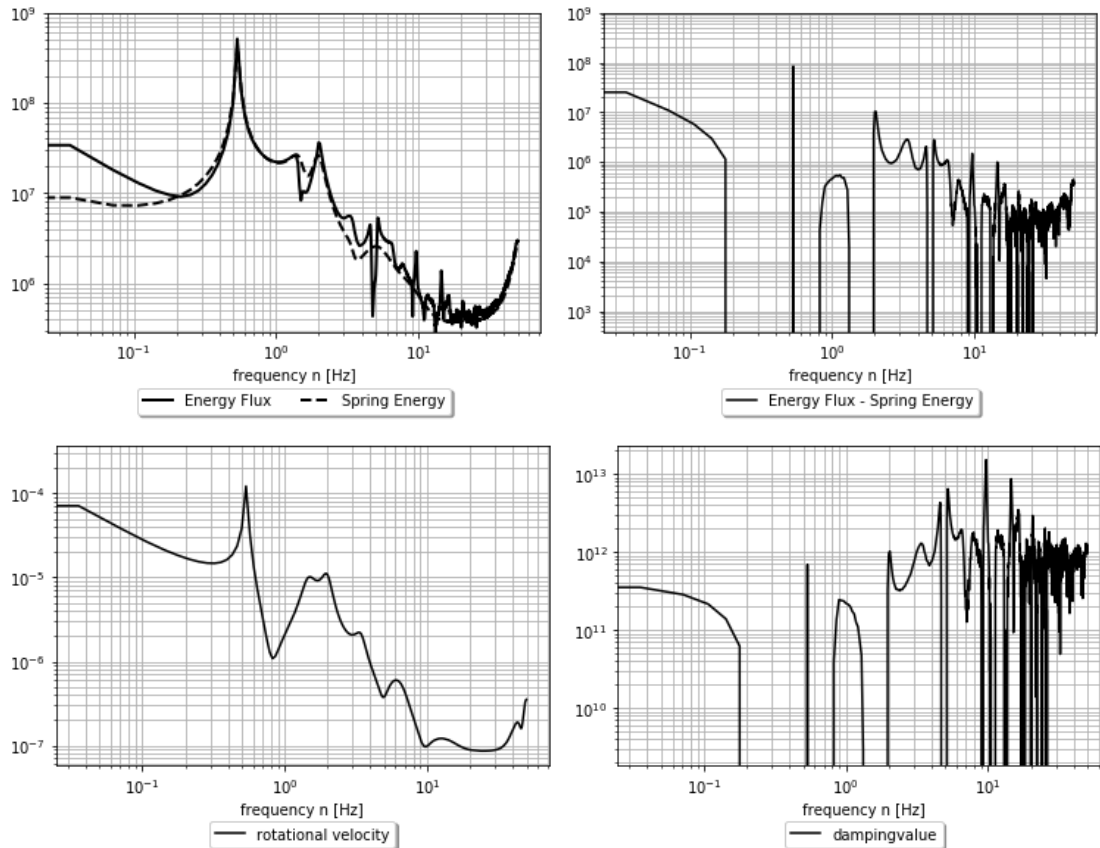


Figure 109 - Used data for calculating energy dissipation value in frequency domain. plot A. Energy flux and spring energy. Plot B. Difference between Energy flux and spring energy. Plot C. Rotational velocity bottom. Plot D. Determined sol damper

It can be observed that a large amount of energy is present in the first mode. The higher modes contain a small amount of energy. Therefore only the damping value found at the first frequency is valid. The damper values found at higher frequencies are not reliable since the Rayleigh damping is based on the first two eigen frequencies, and for that reason omitted from the analysis. The damping value is frequency dependent. Comparing the input value of the damping with the identified damping value in frequency domain results in an error of 4%.

Input Cr FEM	6.60E+11 Nms/rad
Spectra derived Cr EFA	6.88E+11 Nms/rad

Table 11 - Case (2) Soil damper values derived in frequency domain

